3D Acoustic Target Strength of Combinations of Geometric Shapes

Anthony Purcell
ANTHONY PURCELL CONSULTANTS

P.O. Box 1388
Lunenburg, Nova Scotia
B0J 2C0

Project Manager: M. Hazen, 902-426-3100 Ext. 176

Contract number: W7707-032345/001/HAL

Contract Scientific Authority: M. Hazen, 902-426-3100 Ext. 176

The scientific or technical validity of this Contract Report is entirely the responsibility of the contractor and the contents do not necessarily have the approval or endorsement of Defence R&D Canada

Defence R&D Canada – Atlantic

Contract Report

DRDC Atlantic CR 2003-150

January 2005

105-04533/

Author

A. Purcell

Approved by

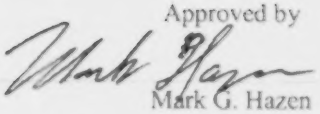

Mark G. Hazen

Contract Scientific Authority

Approved for release by

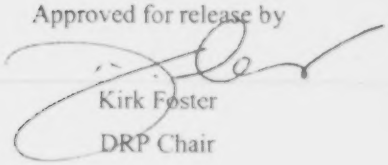

Kirk Foster

DRP Chair

© Her Majesty the Queen as represented by the Minister of National Defence, 2003

© Sa majesté la reine, représentée par le ministre de la Défense nationale, 2003

Abstract

This report is an investigation of the Kirchhoff approximation for the 3D acoustic target strength of simple geometric shapes and their combinations. In particular, it gives expressions for the out-of-plane bistatic scattering strengths of a variety of simple shapes, including the cylinder, the truncated cone and the ellipsoid. Previous investigations have given similar results for the in-plane bistatic case using the Bistatic Theorem to deduce bistatic formulae from monostatic results. The out-of-plane results given here do not depend upon the Bistatic Theorem, but require a detailed analysis of the viewed/illuminated area for each simple shape.

Résumé

Le présent rapport est une recherche sur l'approximation de Kirchhoff pour l'intensité des cibles acoustiques 3D constituées de formes géométriques simples et de leurs combinaisons. Plus précisément, il donne des expressions pour des forces de diffusion bistatiques et hors plan de diverses formes simples, y compris le cylindre, le cône tronqué et l'ellipsoïde. Des recherches antérieures ont donné des résultats similaires au moyen du théorème bistatique dans le cas de forces bistatiques dans le plan, afin de déduire des formules bistatiques à partir de résultats monostatiques. Les valeurs hors-plan résultantes données ici ne dépendent pas du théorème bistatique, mais nécessitent une analyse détaillée de la surface vue/illuminée pour chaque forme simple.

This page intentionally left blank.

Executive summary

Introduction
In the BASIS target strength model (Naval Research Laboratory Report NRL/FR-MM/7140-02-10,019) an interesting method was developed for approximating submarine target strengths by modelling the submarine as a collection of simple geometric shapes: a horizontal cylinder for the main hull, truncated cone and half-sphere for the stern, truncated ellipsoid or half sphere and cylinder for the bow, vertical elliptical cylinder for the sail, and flat plates for the fin plates. For frequencies high enough that wave-number times radius-of-curvature of the simple shape is large, the Helmholtz-Kirchhoff integral (HKI) gives a good approximation to the scattering strength of each simple shape and hence to the target strength as a coherent sum over the individual strengths.

In simple cases such as rectangular plates the analytic application of the HKI can produce exact expressions for target strength. For more complicated shapes such as the cone, in the monostatic case (source and receiver co-located) the application of saddle-point arguments to the Kirchhoff integral provides asymptotic approximations. By using the Bistatic Theorem the BASIS model deduced bistatic scattering strengths from monostatic results. This technique is applicable when the source and receiver view and illuminate the same areas of the simple shapes, and thus is limited to geometries where source and receiver lie in the symmetry plane of the object. For BASIS this limited it to the bistatic geometries in the horizontal plane and targets that were running level.

Results
This work investigates the use of the Helmholtz-Kirchhoff integral (HKI) for determining the scattering strengths of simple objects for out-of-plane geometries. It was found that saddle-point arguments can still be used to deduce expressions for scattering strengths. However, since the Bistatic Theorem cannot be used, detailed descriptions of the intersection of viewed and illuminated areas must be worked out. Expressions for these areas as a function of shape and source-receiver geometry were developed.

Using the expressions for the intersection areas, expressions for the out-of-plane scattering strengths of the simple shapes used by the BASIS model have been determined. These expressions require the use of a number of specialized functions. While the expressions are much more complex than those for the in-plane scattering case, they are still orders of magnitude more efficient to evaluate than conducting a direct numerical integration of the HKI. Mathematica notebooks have been developed for each of the BASIS shapes.

Significance
Bistatic target strength is a critical element in multistatic active sonar, and accurate descriptions are required for a wide range of applications, such as: hull design, sonar tactical development, and sonar performance prediction. BASIS provided a simple, fast code that has been used for operational and scientific research in multistatic sonar. However, in littoral waters with multipath propagation, or short detection ranges the in-plane restrictions have been problematic. These new scattering strength expressions will remove the in-plane restrictions and improve the fidelity multistatic sonar studies and research.

Future Plans
The out-of-plane expressions will be integrated into a BASIS-3D package and will replace the BASIS model for littoral warfare and medium-level fidelity modelling where execution speed is important.

Sommaire

Introduction
Sur le modèle BASIS d'intensité des cibles (rapport NRL/FR-MM/7140-02-10,019), une méthode intéressante avait été mise au point pour obtenir une approximation de l'intensité des cibles fournie par un sous-marin en modélisant ce dernier comme une collection de formes géométriques simples : un cylindre horizontal pour la coque, un cône tronqué et une demi-sphère pour l'arrière, une ellipsoïde tronquée ou une demi-sphère et un cylindre pour l'avant, un cylindre elliptique vertical pour le kiosque et des plaques planes pour les plaques de barres. Dans le cas des fréquences assez élevées pour que le nombre d'ondes multiplié par le rayon de courbure donne un chiffre élevé, l'intégrale de Helmholtz-Kirchhoff (HKI) donne une bonne approximation de la force de diffusion de chaque forme simple, et donc de la force cible titre de somme cohérente des forces individuelles.

Dans des cas simples comme des plaques rectangulaires, l'application analytique de l'intégrale HKI peut produire une expression exacte de l'intensité de la cible. Pour des formes plus complexes comme un cône, dans le cas monostatique (source et récepteur colocalisés), l'application de points-selles à l'intégrale de Kirchhoff donne des approximations asymptotiques. En ayant recours au théorème bistatique, le modèle BASIS a déduit les forces de diffusions bistatiques de valeurs monostatiques. Cette technique peut être utilisée lorsque la source et le récepteur voient et illuminent les mêmes endroits des formes simples : elle se limite donc aux géométries où la source et le récepteur se trouvent dans le plan de symétrie de l'objet. Dans le cas du modèle BASIS, une telle situation le limitait aux géométries bistatiques sur le plan horizontal et à des cibles qui étaient en trajectoire constante.

Résultats
Ces travaux examinent l'utilisation de l'intégrale de Helmholtz-Kirchhoff (HKI) pour déterminer les forces de diffusion d'objets simples pour des géométries hors-plan. On a constaté que des arguments de points-selles peuvent toujours servir à déduire des expressions de forces de diffusion. Par contre, comme on ne peut avoir recours au théorme bistatique, il faut élaborer des descriptions détaillées de l'intersection des zones vues et illuminées. Des expressions pour ces zones ont été développées en tant que fonction de la forme et de la géométrie de la source et du récepteur.

À l'aide des expressions des zones d'intersection, on a déterminé des expressions pour les forces de diffusion hors-plan des formes simples utilisées par le modèle BASIS. Ces expressions exigent l'utilisation d'un certain nombre de fonctions spécialisées. Bien que ces expressions sont beaucoup plus complexes que celles de diffusion en plan, leur efficacité est supérieure de plusieurs ordres de grandeur pour une évaluation comparativement à l'exécution d'une intégration numérique directe de l'intégrale HKI. Des guides mathématiques ont été mis au point pour chacune des formes de BASIS.

Portée des résultats
La force cible bistatique est un élément critique dans un sonar actif multistatique, et des descriptions exactes sont nécessaires pour une gamme étendue d'aplications, comme par exemple : forme de coque, développements tactiques sonar et prédiction du rendement d'un sonar. Le modèle BASIS a fourni un code simple et rapide qui a servi pour la recherche opérationnelle et scientifique dans le domaine du sonar multistatique. Toutefois, dans des eaux côtières à propagation par trajets multiples, ou à courtes portées de détection, les restrictions en plan ont posé des problèmes. Ces nouvelles expressions de force de diffusion élimineront les restrictions en plan et amélioreront la fidélité des études et des recherches sur les sonars multistatiques.

Recherches futures
Les expressions hors-plan seront intégrées dans un modèle BASIS 3D et remplaceront le modèle BASIS pour la guerre côtière et la modélisation à fidélité moyenne où la vitesse d'exécution est importante.

Contents

Abstract i

Résumé i

Executive summary iii

Sommaire iv

Contents vi

List of figures vii

1 Introduction 1

2 Preliminaries 2

3 The rectangular plate 5

4 The circular plate 8

5 The horizontal cylinder 11
5.1 The in-plane case . . . 11
5.2 The out-of-plane case . . . 13

6 The vertical cylinder 16
6.1 In-plane scattering for the vertical cylinder . . . 16
6.2 Out-of-plane scattering for the vertical cylinder . . . 20

7 The vertical elliptical cylinder 23
7.1 The bistatic case . . . 23

8 The sphere 26
8.1 Source/receiver in the x-y plane . . . 26
8.2 Out-of-plane scattering for the sphere . . . 30

9 The truncated cone 33
9.1 Introduction . . . 33
9.2 Special case: in-plane scattering . . . 35
9.2.1 The backscattering case . . . 35
9.2.2 In-plane scattering . . . 40
9.3 The general case: bistatic scattering . . . 46
9.4 Summary . . . 52

10 The ellipsoid 52
10.1 Parametrization of the ellipsoid . . . 52

11 Source/receiver in the x-y plane–monostatic case 52
11.1 Special cases–end-view $\theta = 0$, side-view $\theta = \pi/2$ . . . 55
11.2 General in-plane monostatic view . . . 55
11.3 Details . . . 56
11.4 Numerical results . . . 57
11.5 The half-ellipsoid . . . 57

12 Source/receiver in the x-y plane **59**
12.1 The in-plane bistatic case for the half-ellipsoid 63

13 The out-of-plane case **65**
13.1 Special case: out-of-plane monostatic case 67
13.2 General bistatic case 70

14 The out-of-plane half ellipsoid **73**

15 Scattering strength for the composite surface **75**

16 Summary **79**

A The incomplete Jacobi-Anger and Weber functions **80**

B Some elementary properties of Bessel, Weber and Struve functions **84**

C Some integrals of Bessel, Weber and Struve functions related to scattering from a cone **85**

D Integrals of Bessel, Weber and Struve functions in terms of incomplete Bessel functions **87**
D.1 Results 87
D.2 Proofs 89

References **92**

Distribution list **94**

List of Figures

1 The generic scattering geometry. . . . 3
2 The monostatic scattering geometry. . . . 3
3 The in-plane bistatic scattering geometry. . . . 4
4 The rectangular plate representing the generic starboard plates. . . . 6
5 Target strength for the fantail and sail plates. . . . 9
6 Target strength for the fantail and sail plates. . . . 10
7 The in-plane bistatic case for the horizontal cylinder. . . . 12
8 The out-of-plane bistatic case for the horizontal cylinder. . . . 14
9 Target strength for the horizontal cylinder. . . . 17
10 The in-plane bistatic case for the vertical cylinder. . . . 18
11 Target strength for the vertical cylinder. . . . 22
12 Target strength for the truncated vertical half-cylinder. . . . 23
13 The vertical elliptical cylinder. . . . 24
14 Target strength for the full and half vertical elliptical cylinder. . . . 27
15 The in-plane bistatic case for the sphere. . . . 28
16 The in-plane bistatic case for the sphere. . . . 31
17 The out-of-plane bow hemisphere. . . . 33
18 The horizontal truncated cone 34
19 The integration limits for the monostatic case for the truncated cone. . . . 36
20 The monostatic case for the cone. . . . 39
21 The monostatic case for the cone. . . . 39
22 The bistatic case for the cone. . . . 41
23 The bistatic case for the cone. . . . 43
24 The bistatic case for the cone. . . . 45
25 Exact results for the out-of-plane case for the cone. . . . 49
26 Approximate results for the out-of-plane case for the cone. . . . 51
27 The ellipsoid. . . . 53
28 The viewed/illuminated areas for the ellipsoid. . . . 54
29 Comparison of exact and approximate results for the ellipsoid. . . . 57
30 The viewed/illuminated areas for the half-ellipsoid. . . . 58
31 Comparison of exact and approximate results for the half-ellipsoid. . . . 60
32 The viewed/illuminated areas for the ellipsoid. . . . 61
33 The in-plane bistatic case for the ellipsoid. . . . 64
34 The in-plane bistatic case for the half-ellipsoid. . . . 66
35 The ellipsoid. . . . 67
36 Comparison of integral forms for the out-of-plane ellipsoid case. . . . 72
37 The out-of-plane bistatic case for the ellipsoid. . . . 74
38 The generic submarine model. . . . 75
39 The bistatic case for the composite surface. . . . 77
40 The bistatic case for the composite surface. . . . 78

1 Introduction

The essence of the contract requirement is to extend the BASIS-TS method (a coherent addition of Kirchhoff approximation scattering strengths for a few simple geometrical shapes) to include the possibility that the various scattering bodies do not necessarily lie in the source-receiver plane. This method is detailed in the Naval Research Laboratory Report, *The Bistatic Acoustic Simple Integrated Structure (BASIS) Target Strength Model*, by D.M. Drumheller, M.G. Hazen and L.E. Gilroy[1]. For (certain) scattering bodies whose symmetry plane coincides with the source-receiver plane, the Bistatic Theorem allows one to obtain the bistatic target strength from the monostatic case through a simple substitution argument $\theta \rightarrow \theta_B$ and $k \rightarrow k\cos(\beta/2)$, where θ_B is the bistatic aspect angle and β is the bistatic angle. The Bistatic Theorem assumes that the integration regions for the monostatic and bistatic cases are the same–i.e. that the source and receiver illuminate and view the same region of the scattering body. For flat scattering bodies this is obviously the case if the source and receiver lie on the same side; hence this case will present no difficulties and formulae are given in Secs. 3 and 4.

However, the Helmholtz-Kirchhoff integral for the scattering strengths is valid for any scattering geometries, and it is still possible to apply asymptotic arguments to deduce expressions for scattering strengths without the use of the Bistatic Theorem. The price to be paid for the failure of the Bistatic Theorem is that one must work out in detail the intersection of the viewed/illuminated areas and hence obtain the integration area(s) for the Kirchhoff integral. One may then apply asymptotic analysis to the Kirchhoff integral using this detailed knowledge of the relevant integration area and obtain expressions for the scattering strengths. The resulting expressions for the out-of-plane bistatic case for shapes such as the ellipsoid and truncated cone are quite complex, but are still orders of magnitude faster to compute than direct numerical integration of the Kirchhoff integral. The main result of this report is therefore to provide these out-of-plane expressions to allow an extension of the BASIS target strength method to source/receiver geometries that lie outside the symmetry plane of the model.

A simple case for which the Bistatic Theorem fails is the cylinder. For a cylinder that does not lie in the source-receiver plane, the source and receiver do not illuminate and view the same region of the cylinder. A portion of the cylinder will appear "dark" to the receiver. This bistatic illumination regime implies that the Kirchhoff integral for the reflected field involves the evaluation of "incomplete" cylinder functions. Therefore, on a mathematical level the problem is equivalent to finding asymptotic approximations (for high frequencies that is) for various cases of the "incomplete" cylinder functions. This problem has been analyzed fully by M.M. Agrest and M.S. Maksimov[2] in their text *Theory of Incomplete Cylindrical Functions and their Applications*. The use of their asymptotic results will be essential to analyzing this problem. Some details for the horizontal cylinder case are presented in Sec. 5.

Generally speaking, the Bistatic Theorem scattering strengths involve Bessel functions such as $J_1(kr_c) \equiv \pi^{-1}\int_0^\pi d\varphi \cos(\varphi - kr_c \sin\varphi)$, while for out-of-plane scattering one obtains a Bessel function contribution (the Bistatic Theorem prediction) plus an incomplete Bessel function $J_1(\beta, kr_c) \equiv \pi^{-1}\int_0^\beta d\varphi \cos(\varphi - kr_c \sin\varphi)$ contribution, where $\beta < \pi/2$ and r_c is the radius of curvature of the scattering surface. For large values of kr_c, the asymptotic evaluation of the Bessel function involves a saddle point analysis, which yields a contribution $J_1(kr_c) \propto 1/(kr_c)^{1/2}$. The incomplete Bessel function involves end-point contributions as well (rather than just saddle points) in the asymptotic analysis and one obtains $J_1(\beta, kr_c) \propto 1/(kr_c)$ for $\beta < \pi/2$. One could therefore argue that for high frequencies the Bistatic Theorem predictions will dominate. In effect, as long as the saddle point lies somewhere in the range of integration of the Kirchhoff integral for the scattering strength, ultimately the saddle point terms will dominate and one may use the high frequency limit of the Bistatic Theorem predictions. However, frequencies $(kr_c) >> 1$ large enough to satisfy the requirements of the Kirchhoff approximation, may still not be large enough to neglect the contributions of the incomplete Bessel functions which result from the failure of the Bistatic Theorem. Therefore one may regard the contribution of the incomplete Bessel functions as occurring in an intermediate range of frequencies, where terms of order $1/(kr_c)^{1/2}$ and $1/(kr_c)$ need to be simultaneously considered. One might foresee that the greatest deviations from the Bistatic Theorem predictions would occur for aspect and bistatic angle values which correspond to the greatest excursions of the source-receiver plane from the symmetry plane of the

scattering surface. For a horizontal cylinder this means the Bistatic Theorem predictions give the greatest error near the forward scattering direction $\beta \to \pi$.

For the remainder of the report, the contractor will extend the methods developed in Sec. 5 for the cylinder to other basic shapes including the sphere, the elliptical cylinder, the truncated cone and the ellipsoid. Due to the considerable body of work by M.M. Agrest and M.S. Maksimov[2], the case of the cylinder can be treated in some detail, including both saddle points and end-point contributions. The case of the ellipsoid and the truncated cone cannot be treated in the same detail, and will be approximated in terms of saddle point expansions alone. The contractor will implement these formulae into an extension (in the Mathematica language[3]) of the software given in Appendix C of the NRL report *The Bistatic Acoustic Simple Integrated Structure (BASIS) Target Strength Model*, by D.M. Drumheller, M.G. Hazen and L.E. Gilroy[1]. The use of Mathematica software to implement various ideas is for convenience, but the mathematical ideas could easily be written in MATLAB.

2 Preliminaries

The subject matter of this contract concerns the calculation of the field reflected from a finite body, assuming that the incident wavelength is small compared to the "radius of curvature" of the scattering body and the source/receiver distances and also that the size of the scattering body is small compared to the source/receiver distances. The first restriction implies the use of the Kirchhoff approximation is allowed, the second that the source can be treated as an incident plane wave and the scatterer is illuminated (and viewed) by a field of parallel rays (Fraunhofer diffraction). Supposing that the incident field is given by a point source, then

$$p_i(R_R) = \frac{P_S}{R_S} e^{-i\vec{k}_s \cdot (\vec{r} - \vec{R}_S)}, \tag{1}$$

where P_S is the source amplitude, R_S is the source/scatterer distance and $\vec{k}_S$ is the wavevector pointing from source to scatterer, see Fig. 1. By invoking Green's theorem and the Kirchhoff approximation[4],[5], [6] one finds for a rigid scattering surface that the refected field is given by

$$p_r(R_R) = -\frac{iP_s e^{-ik(R_S+R_R)}}{4\pi R_R R_S} \int_{\text{illum. area}} (\vec{k}_S + \vec{k}_R) \cdot \vec{n}\, e^{-i(\vec{k}_S+\vec{k}_R)\cdot\vec{r}} dS \tag{2}$$

where R_R is the receiver/scatterer distance, $\vec{k}_R$ is the wavevector pointing from receiver to scatterer, and $\vec{n}(\vec{r})$ is the outward surface normal to the infinitesimal surface area dS at the position $\vec{r}$.

The reflected field clearly depends on the source strength and source/receiver $R_{S/R}$ distances. To allow a more general discussion of the scattering process, the scattering function g is defined to eliminate the source amplitude P_S and the source/receiver $R_{S/R}$ distances to give a quantity which is characteristic of the scattering body rather than of the source or receiver. A standard choice is the definition

$$p_r(R_R) = -\frac{iP_s e^{-ik(R_S+R_R)}}{R_R R_S} g(\vec{k}_S, \vec{k}_R), \tag{3}$$

which yields the scattering function

$$g(\vec{k}_S, \vec{k}_R) = -\frac{1}{4\pi} \int_{\text{illum. area}} (\vec{k}_S + \vec{k}_R) \cdot \vec{n}\, e^{-i(\vec{k}_S+\vec{k}_R)\cdot\vec{r}} dS. \tag{4}$$

In a similar fashion the target strength is defined to characterize the reflected intensity from a scatterer without reference to the particular source or the source/receiver distance. A standard choice is

$$\text{Target Strength} \equiv |g(\vec{k}_S, \vec{k}_R)|^2. \tag{5}$$

In the special case where the source/receiver are the same position (the monostatic case–see Fig. 2) then

$$\vec{k}_S = \vec{k}_R = k(-\cos\theta, -\sin\theta). \tag{6}$$

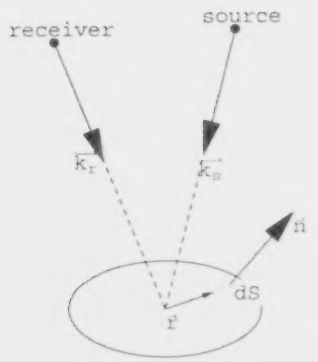

Figure 1: The generic scattering geometry.

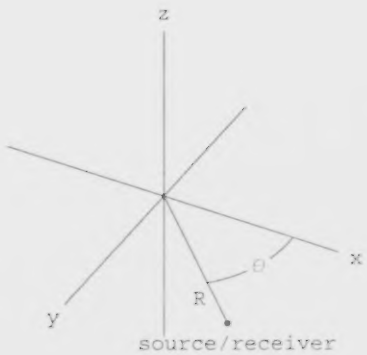

Figure 2: The monostatic scattering geometry.

This reduces the scattering strength to the form

$$g_{\text{monostatic}}(\theta, k) \equiv g(\vec{k}_S, \vec{k}_S) = -\frac{1}{2\pi} \int_{\text{illum. area}} \vec{k} \cdot \vec{n}\, e^{-i2\vec{k}\cdot\vec{r}}\, d\mathcal{S}. \tag{7}$$

Returning now to the more general case where the source/receiver do not coincide (the bistatic case–see Fig. 3) but lie in the same plane then

$$\begin{aligned} \vec{k}_s &= k(-\cos\theta_s, -\sin\theta_s, 0), \\ \vec{k}_r &= k(-\cos\theta_r, -\sin\theta_r, 0). \end{aligned} \tag{8}$$

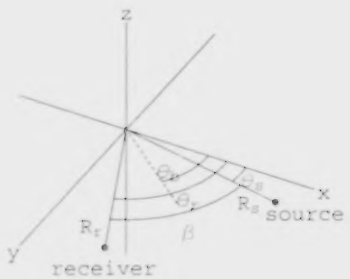

Figure 3: The in-plane bistatic scattering geometry.

If one now assumes that the integration regions in the monostatic case and the in-plane bistatic case coincide, then it immediately follows from simple substitution that

$$g(\vec{k}_S, \vec{k}_R) = g_{\text{monostatic}}(\theta_B, k\cos(\beta/2)) \tag{9}$$

where $\beta = \theta_S - \theta_R$ and $\theta_B = (\theta_S + \theta_R)/2$. This result is called the Bistatic Theorem and it relates the scattering strength calculated in the monostatic case to the bistatic case provided the source/receiver illuminate/view the same region of the scatterer as in the monostatic case.

For flat surfaces clearly the integration regions will be the same for the monostatic and bistatic cases provided the source and receiver lie on the same side of the scatterer. For other simple shapes such as the horizontal or vertical cylinder, the illuminated regions will be the same in the bistatic and monostatic cases only if the axis of symmetry of the scatterer and the source/receiver wavevectors lie in the same plane.

Most of the existing literature in the area of bistatic scattering cross section is related to radar applications. In fact, the very first radars deployed in the 1930's were bistatic. The development of the duplexer, which views and illuminates with the same antenna, in mid 1930's caused monostatic radar systems to dominate until the late 1950's. At that time bistatic radar was revived for "missile seekers" and has subsequently been employed for numerous applications. In any event, most of the applicable literature for bistatic cross

section can be found in the radar literature. A search of the word "bistatic" gives some 653 references since 1989 in the IEEE literature. The essential early references to the Bistatic Theorem are Kell[7]–"On the derivation of the bistatic RCS From Monostatic Measurements," J.W. Crispin and A.L. Maffett[8], "Radar Cross-Section Estimation for Simple Shapes,", and more recently Falconer[9]–"Extrapolation of Near-Field RCS Measurements to the Far Zone." Also notable is the 1955 paper by Siegel et. al.[10]–"Bistatic Radar Cross Sections of Surfaces of Revolution," and a recent review paper by Glaser[11]–"Some results in the Bistatic Radar Cross Section (RCS) of Complex Objects,". Some useful texts which touch on this subject include Crispin and Siegel[13], Bowman[14], Ruck et.al.[15], in particular Table 9.1 of Urick[16], Knott et.al.[17], Barton[18], Nicholas[19], and Willis[20]. The bistatic calculations in these references refer to in-plane bistatic scattering or equivalently to the Bistatic Theorem. Hence they are really just monostatic calculations of the scattering strength. The key point of view in most of these references in applying the Bistatic Theorem is to simplify the experimental analysis process, i.e. to find a simple way to analyze bistatic *data*. From the contractee's point of view the key issue is modelling, not data crunching. The use of the Bistatic Theorem is just a convenience, not essential for the applications intended in this contract. This is true, provided of course one can give expressions for the out-of-plane scattering strengths for the required simple shapes. To lend a concrete nature to this discussion, the case of the horizontal cylinder is considered in detail in Sec. 4 for in-plane and out-of-plane bistatic scattering.

In very general terms, the calculation of the scattering strength will involve the evaluation of integrals of the type

$$\int_{x_b}^{x_a} \varphi(x) e^{zh(x)} dx, \quad z >> 1.$$

If the limits of integration include the saddle point $h'(x_s) = 0$ then the integral is approximated with the formula

$$\int_{x_b}^{x_a} \varphi(x) e^{zh(x)} dx \approx \sqrt{\frac{-2\pi}{zh''(x_s)}} \varphi(x_s) e^{zh(x_s)} + \frac{\varphi(x_a)}{zh'(x_a)} e^{zh(x_a)} - \frac{\varphi(x_b)}{zh'(x_b)} e^{zh(x_b)}.$$

(1/2 of the first term if the saddle point is at an end point). If the limits of integration do not include a saddle point, then the integral is approximated with the end point contributions alone

$$\int_{x_b}^{x_a} \varphi(x) e^{zh(x)} dx \approx \frac{\varphi(x_a)}{zh'(x_a)} e^{zh(x_a)} - \frac{\varphi(x_b)}{zh'(x_b)} e^{zh(x_b)}.$$

See Felsen and Marcuvitz[22] for a general discussion or Sec. 9 of Chapter II of Maksimov for a specific discussion of incomplete cylinder functions. For out-of-plane scattering one typically finds that the scattering strength separates into the Bistatic Theorem result, whose asymptotic behavior is given by a saddle point contribution, plus an incomplete function, whose asymptotic behavior is determined by end point contributions.

As a simplified introduction to the generic problem, Sec. 3 will consider initially the rectangular plate

3 The rectangular plate

Consider the case of a rectangular plate as shown in Figure 4.

The outward normal, differential area and surface vector are given by

$$\begin{aligned} \vec{n} &= (-\sin f_a, \cos f_a, 0), \\ dA &= \frac{1}{\cos f_a} dx\, dz; \quad -\frac{W \cos f_a}{2} \le x \le -\frac{W \cos f_a}{2}, \quad -\frac{H}{2} \le z \le \frac{H}{2}, \\ \vec{r} &= (x, x \tan f_a, z). \end{aligned} \tag{10}$$

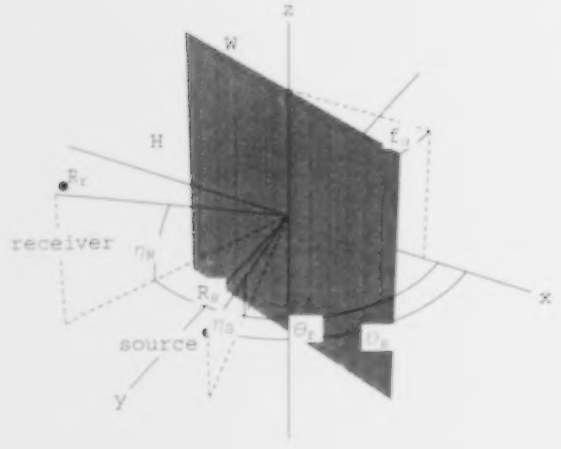

Figure 4: The rectangular plate representing the generic starboard plates.

The source/receiver wavevectors are

$$\begin{aligned}\vec{k}_s &= k(-\cos\eta_s\cos\theta_s, -\cos\eta_s\sin\theta_s, -\sin\eta_s),\\ \vec{k}_r &= k(-\cos\eta_r\cos\theta_r, -\cos\eta_r\sin\theta_r, -\sin\eta_r).\end{aligned} \tag{11}$$

This gives the result

$$\begin{aligned}(\vec{k}_s+\vec{k}_s)\cdot\vec{n} &= \\ &-k[-(\cos\eta_s\cos\theta_s+\cos\eta_r\cos\theta_r)\sin f_\alpha + (\cos\eta_s\sin\theta_s+\cos\eta_r\sin\theta_r)\cos f_\alpha].\\ (\vec{k}_s+\vec{k}_s)\cdot\vec{r} &= \\ &-k[(\cos\eta_s\cos\theta_s+\cos\eta_r\cos\theta_r)x + (\cos\eta_s\sin\theta_s+\cos\eta_r\sin\theta_r)x\tan f_\alpha + (\sin\eta_s+\sin\eta_r)z].\end{aligned} \tag{12}$$

In this case the scattering strength can be written as

$$\begin{aligned}-\frac{1}{4\pi}\int_{\text{illum. area}} &(\vec{k}_s+\vec{k}_s)\cdot\vec{n}\, e^{-i(\vec{k}_s+\vec{k}_s)\cdot\vec{r}}dS \;=\\ &\frac{k}{4\pi}\int_{-\frac{W}{2}\cos f_\alpha}^{\frac{W}{2}\cos f_\alpha} dx\int_{-\frac{H}{2}}^{\frac{H}{2}} dz[\cos\eta_s\sin(\theta_s-f_\alpha)+\cos\eta_r\sin(\theta_r-f_\alpha)]\times\\ &e^{ik[(\cos\eta_s\cos(\theta_s-f_\alpha)+\cos\eta_r\cos(\theta_r-f_\alpha))x/\cos f_\alpha+(\sin\eta_s+\sin\eta_r)z]}\\ &=\frac{kHW}{4\pi}[\cos\eta_s\sin(\theta_s-f_\alpha)+\cos\eta_r\sin(\theta_r-f_\alpha)]\times\\ &sa[\frac{1}{2}kW[(\cos\eta_s\cos(\theta_s-f_\alpha)+\cos\eta_r\cos(\theta_r-f_\alpha))]sa[\frac{1}{2}kH(\sin\eta_s+\sin\eta_r)].\end{aligned} \tag{13}$$

In the special case $\eta_{r/s}=0$ this would reduce to

$$g = \frac{kHW}{4\pi}[\sin(\theta_s-f_\alpha)+\sin(\theta_r-f_\alpha)]sa[\frac{1}{2}kW[(\cos(\theta_s-f_\alpha)+\cos(\theta_r-f_\alpha))]. \tag{14}$$

Now consider the port and starboard fin (or fantail) plates and sail plates of the diesel-electric submarine model (shown in Fig. 38) whose parameters are given in Table 1 of [1]. Note from Fig. 38 that the twin fantail plates shadow each other's inner surface, so one could choose to make the back of the plates acoustically inactive by multiplying by the function $\text{If}[\sin(\theta_s-f_\alpha)\geq 0 \&\& \sin(\theta_r-f_\alpha)\geq 0), 1, 0]$. If the origin of the fantail is shifted by a displacement

$$\vec{x}_{sfantail} = \{x_{10}, y_{10}, z_{10}\} = \{F_L + (F_W - L)/2 - T_W, (F_W/2)\sin(F_\alpha), 0\}$$

then there is an additional multiplicative factor of

$$e^{-i(\vec{k}_s+\vec{k}_s)\cdot\vec{x}_{sfantail}}.$$

Hence for the starboard fantail of width $W = F_W^{'} = F_W/\cos[f_\alpha]$ and total height $H = 2F_H$

$$\begin{aligned}g_{sfantail} &= \\ \frac{k(2F_H)F_W^{'}}{4\pi}&\left\{[\cos\eta_s\sin(\theta_s-F_\alpha)+\cos\eta_r\sin(\theta_r-F_\alpha)]sa[\frac{1}{2}kF_W^{'}[(\cos\eta_s\cos(\theta_s-F_\alpha)+\cos\eta_r\cos(\theta_r-F_\alpha))]\times\right.\\ &\left. sa[\frac{1}{2}k(2F_H)(\sin\eta_s+\sin\eta_r)]\right\}\text{If}[\sin(\theta_s-F_\alpha)\geq 0 \&\& \sin(\theta_r-F_\alpha)\geq 0, 1, 0]e^{-i(\vec{k}_s+\vec{k}_s)\cdot\vec{x}_{sfantail}}.\end{aligned} \tag{15}$$

In a similar fashion for the port fantail, starboard sail, and port sail

$$\begin{aligned}
\vec{x}_{pfantail} &= \{x_{11}, y_{11}, z_{11}\} = \{F_L + (F_W - L)/2 - T_W, -(F_W/2)\sin(F_\alpha), 0\}, \\
g_{pfantail} &= \\
&-\frac{k(2F_H)F_W^{'}}{4\pi}\left\{[\cos\eta_s \sin(\theta_s + F_\alpha) + \cos\eta_r \sin(\theta_r + F_\alpha)]sa[\frac{1}{2}kF_W^{'}[(\cos\eta_s\cos(\theta_s + F_\alpha) + \cos\eta_r\cos(\theta_r + F_\alpha))]\times\right. \\
&\left. sa[\frac{1}{2}k(2F_H)(\sin\eta_s + \sin\eta_r)]\right\} \mathrm{If}[\sin(\theta_s + F_\alpha) \le 0 \&\& \sin(\theta_r + F_\alpha) \le 0, 1, 0] e^{-i(\vec{k}_s + \vec{k}_r)\cdot\vec{x}_{pfantail}},
\end{aligned} \tag{16}$$

$$\begin{aligned}
\vec{x}_{ssail} &= \{x_6, y_6, z_6\} = \{S_L + (S_W - L)/2, (S_W/2)\tan(S_\alpha), R_1 + S_H/2\}, \\
g_{ssail} &= \\
&\frac{kS_HS_W^{'}}{4\pi}\left\{[\cos\eta_s \sin(\theta_s - S_\alpha) + \cos\eta_r \sin(\theta_r - S_\alpha)]sa[\frac{1}{2}kS_W^{'}[(\cos\eta_s\cos(\theta_s - S_\alpha) + \cos\eta_r\cos(\theta_r - S_\alpha))]\times\right. \\
&\left. sa[\frac{1}{2}kS_H(\sin\eta_s + \sin\eta_r)]\right\} \mathrm{If}[\sin(\theta_s - S_\alpha) \ge 0 \&\& \sin(\theta_r - S_\alpha) \ge 0, 1, 0] e^{-i(\vec{k}_s + \vec{k}_r)\cdot\vec{x}_{ssail}},
\end{aligned} \tag{17}$$

$$\begin{aligned}
\vec{x}_{psail} &= \{x_7, y_7, z_7\} = \{S_L + (S_W - L)/2, -(S_W/2)\tan(S_\alpha), R_1 + S_H/2\}, \\
g_{psail} &= \\
&-\frac{k(S_H)S_W^{'}}{4\pi}\left\{[\cos\eta_s \sin(\theta_s + S_\alpha) + \cos\eta_r \sin(\theta_r + S_\alpha)]sa[\frac{1}{2}kS_W^{'}[(\cos\eta_s\cos(\theta_s + S_\alpha) + \cos\eta_r\cos(\theta_r + S_\alpha))]\times\right. \\
&\left. sa[\frac{1}{2}kS_H(\sin\eta_s + \sin\eta_r)]\right\} \mathrm{If}[\sin(\theta_s + S_\alpha) \le 0 \&\& \sin(\theta_r + S_\alpha) \le 0, 1, 0] e^{-i(\vec{k}_s + \vec{k}_r)\cdot\vec{x}_{psail}}
\end{aligned} \tag{18}$$

The cumulative effect of the starboard/port sail and fantail plates is just the sum of the scattering strengths $g(\eta_s, \eta_r, \theta_s, \theta_r) = g_{sfantail} + g_{pfantail} + g_{ssail} + g_{psail}$.

Some numerical examples are shown in Figs. 5, 6, with the parameters given in Table 1 of [1]. These figures give the coherent sum of the scattering strengths for the port and starboard fantail and sail plates, where the scattering plots are shown in the $\theta_R - \theta_S$ plane. Alternatively, one could display the scattering strength in the $\beta - \theta_B$ (bistatic-aspect angle) plane, this is equivalent to rotating the $\theta_R - \theta_S$ plots 45 degrees clockwise. One notes that the monostatic case is the diagonal in the $\theta_R - \theta_S$ plot. Figs. 1 and 2 compare the in-plane and very out-of-plane cases; for these cases moving source and receiver out-of-plane gives results similar to those obtained by decreasing the frequency.

4 The circular plate

Consider a circular plate of radius a, lying in the $y - z$ plane and centered at the origin. The outward normal, differential area and surface vector are given by

$$\begin{aligned}
\vec{n} &= (1, 0, 0), \\
d\vec{A} &= r\,dr\,d\varphi, \quad 0 \le r \le a, \quad 0 \le \varphi \le 2\pi, \\
\vec{r} &= (0, r\cos\varphi, r\sin\phi).
\end{aligned} \tag{19}$$

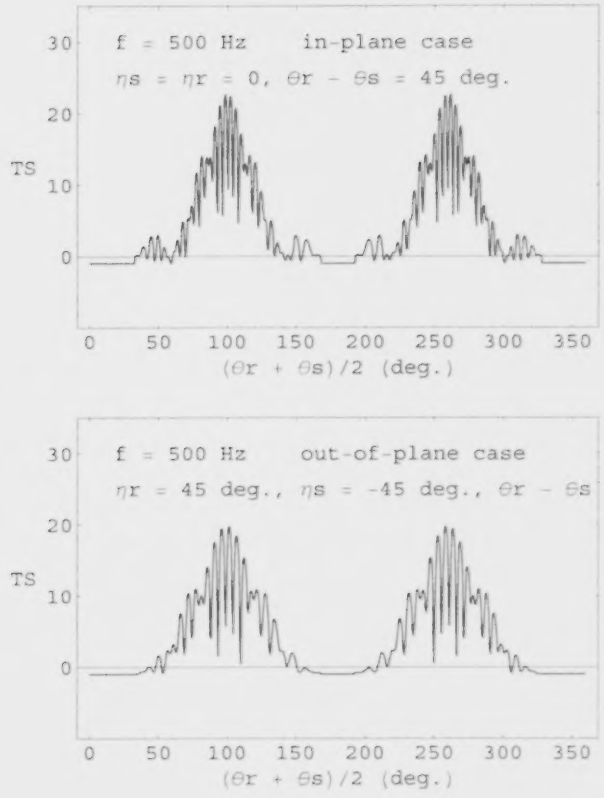

Figure 5: A plot of $10\log(10^{-1/10} + \text{target strength})$ for the fantail and sail plates for the diesel-electric submarine shown in Fig. 38. The frequency = 500 Hz, from Table 1 of [1]: $\{S_H, S_W, F_H, F_W, f_a\} = \{3.7 \text{ m}, 7.0 \text{ m}, 3.5 \text{ m}, 2.6 \text{ m}, 10^o\}$ and the angular parameters are given by $\{\eta_s, \eta_r, \theta_s, \theta_r\} = \{\eta_s, \eta_r, \theta_B + 45^o/2, \theta_B - 45^o/2\}$ where $(\theta_r + \theta_s)/2 \equiv \theta_B$.

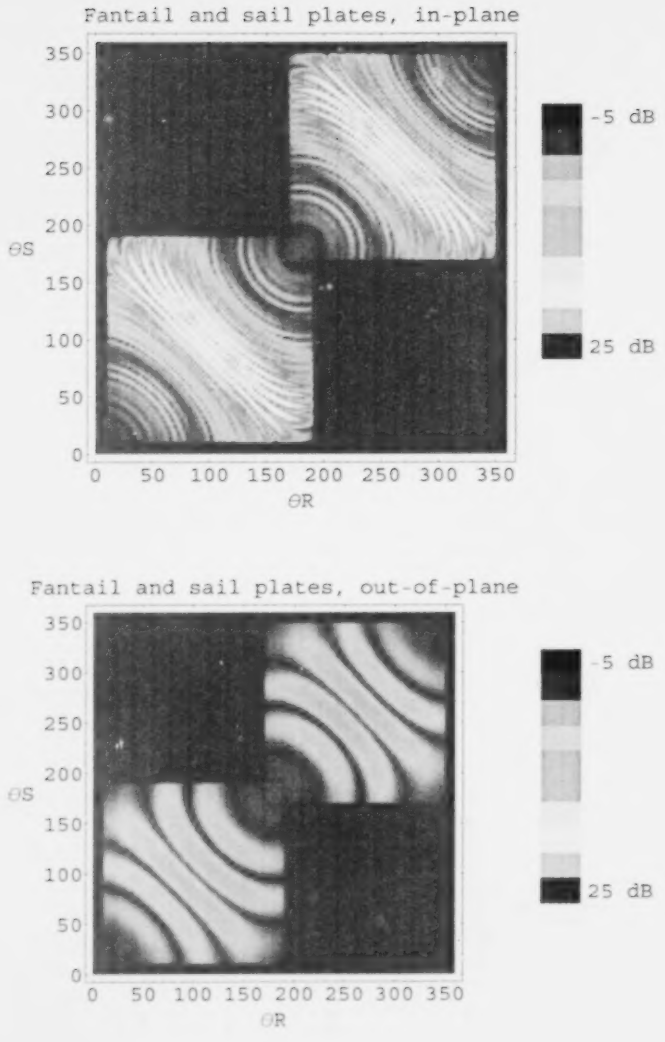

Figure 6: A plot of $10\log(10^{-1/10} + \text{target strength})$ for the fantail and sail plates for the diesel-electric submarine shown in Fig. 38. The frequency = 500 Hz. from Table 1 of [1]: $\{S_H, S_W, F_H, F_W, f_\alpha\} = \{3.7\text{ m}, 7.0\text{ m}, 3.5\text{ m}, 2.6\text{ m}, 10^\circ\}$. For the upper plot the angular parameters are given by $\{\eta_s, \eta_r, \theta_s, \theta_r\} = \{0, 0, \theta_r, \theta_s\}$: for the lower plot $\{\eta_s, \eta_r, \theta_s, \theta_r\} = \{80^\circ, -80^\circ, \theta_r, \theta_s\}$.

The source/receiver wavevectors are

$$\begin{aligned}\vec{k}_s &= k(-\cos\eta_s\cos\theta_s, -\cos\eta_s\sin\theta_s, -\sin\eta_s),\\ \vec{k}_r &= k(-\cos\eta_r\cos\theta_r, -\cos\eta_r\sin\theta_r, -\sin\eta_r).\end{aligned} \tag{20}$$

This gives the result

$$\begin{aligned}(\vec{k}_r+\vec{k}_s)\cdot\vec{n} &= -k[\cos\eta_s\cos\theta_s+\cos\eta_r\cos\theta_r],\\ (\vec{k}_r+\vec{k}_s)\cdot\vec{r} &= -k[(\cos\eta_s\sin\theta_s+\cos\eta_r\sin\theta_r)r\cos\varphi+(\sin\eta_s+\sin\eta_r)r\sin\varphi].\end{aligned} \tag{21}$$

For shorthand define the auxiliary function

$$\lambda=\sqrt{(\cos\eta_s\sin\theta_s+\cos\eta_r\sin\theta_r)^2+(\sin\eta_s+\sin\eta_r)^2}. \tag{22}$$

In this case the scattering strength can be written as

$$\begin{aligned}g &= -\frac{1}{4\pi}\int_{\text{illum. area}}(\vec{k}_s+\vec{k}_s)\cdot\vec{n}\,e^{-i(\vec{k}_s+\vec{k}_s)\cdot\vec{r}}dS\\ &= \frac{k[\cos\eta_s\cos\theta_s+\cos\eta_r\cos\theta_r]}{4\pi}\int_0^a dr\,r\int_0^{2\pi}d\varphi e^{ikr\{(\cos\eta_s\sin\theta_s+\cos\eta_r\sin\theta_r)\cos\varphi+(\sin\eta_s+\sin\eta_r)\sin\varphi\}}\\ &= \frac{k[\cos\eta_s\cos\theta_s+\cos\eta_r\cos\theta_r]}{4\pi}\int_0^a dr\,r\int_0^{2\pi}d\varphi e^{ik\lambda r\cos\varphi}\\ &= \frac{k[\cos\eta_s\cos\theta_s+\cos\eta_r\cos\theta_r]}{4\pi(k\lambda)^2}\int_0^{2\pi}\frac{d\varphi}{\cos^2\varphi}\left\{-1+(1-ik\lambda a\cos\varphi)e^{ik\lambda a\cos\varphi}\right\}\\ &= \frac{k[\cos\eta_s\cos\theta_s+\cos\eta_r\cos\theta_r]}{4\pi(k\lambda)^2}[2\pi k\lambda a J_1(k\lambda a)]\\ &= \frac{k}{2\pi}\pi a^2\frac{[\cos\eta_s\cos\theta_s+\cos\eta_r\cos\theta_r]}{2}\frac{2J_1(k\lambda a)}{(k\lambda a)}.\end{aligned} \tag{23}$$

This result will prove useful in modelling the finite cone.

This previous result is valid for the acoustically active side facing the positive x-axis and hence $-\pi/2\le\theta_{s/r}\le\pi$. For the acoustically active side facing the negative x-axis then the outward normal changes sign and one obtains the same result as above except with a multiplication by -1 and $\pi/2\le\theta_{s/r}\le 3\pi/2$.

5 The horizontal cylinder

5.1 The in-plane case

Now consider the case of the horizontal cylinder, whose geometry is shown in Figure 7. The unit normal to the surface, differential area and displacement are given by

$$\begin{aligned}\vec{n} &= (0,\cos\varphi,\sin\varphi),\\ dA &= r\,d\varphi dr,\\ \vec{r} &= (x, r\cos\varphi, r\sin\varphi).\end{aligned} \tag{24}$$

For the case of a source and receiver in the same plane

$$\begin{aligned}\vec{k}_s &= k(-\cos\theta_s, -\sin\theta_s, 0),\\ \vec{k}_r &= k(-\cos\theta_r, -\sin\theta_r, 0).\end{aligned} \tag{25}$$

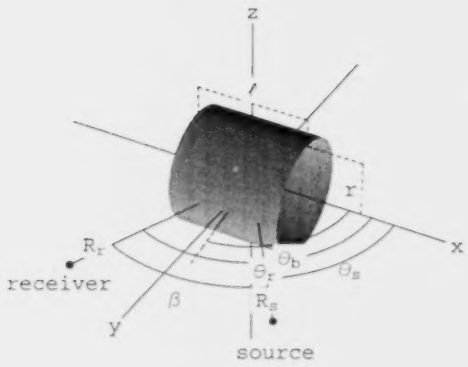

Figure 7: The in-plane bistatic case for the horizontal cylinder.

This gives the result

$$\begin{aligned}(\vec{k}_s+\vec{k}_s)\cdot\vec{n} &= -k(\sin\theta_s+\sin\theta_r)\cos\varphi = -2k\cos(\beta/2)\sin\theta_B\cos\varphi,\\ (\vec{k}_s+\vec{k}_s)\cdot\vec{r} &= -k(\cos\theta_s+\cos\theta_r)x - k(\sin\theta_s+\sin\theta_r)r\cos\varphi\\ &= -2k\cos(\beta/2)\cos\theta_B x - 2k\cos(\beta/2)\sin\theta_B r\cos\varphi. \end{aligned} \tag{26}$$

In this case the scattering strength can be written as

$$\begin{aligned}-\frac{1}{4\pi}\int_{\text{illum. area}}(\vec{k}_s+\vec{k}_s)\cdot\vec{n}\,e^{-i(\vec{k}_s+\vec{k}_s)\cdot\vec{r}}dS &=\\ \frac{kr}{2\pi}\cos(\beta/2)\sin\theta_B\int_{-l/2}^{l/2}dx\int_{-\pi/2}^{\pi/2}d\varphi\cos\varphi e^{i2k\cos(\beta/2)[\cos\theta_B x+\sin\theta_B r\cos\varphi]}&\\ = \frac{r}{2\pi}\tan\theta_B\sin(kl\cos(\beta/2)\cos\theta_B)\int_{-\pi/2}^{\pi/2}d\varphi\cos\varphi e^{i2k\cos(\beta/2)\sin\theta_B r\cos\varphi}&\\ = \frac{r}{2}\tan\theta_B\sin(kl\cos(\beta/2)\cos\theta_B)\frac{2}{\pi}\int_0^{\pi/2}d\varphi\cos\varphi e^{i2kr\cos(\beta/2)\sin\theta_B\cos\varphi}&\end{aligned}$$

$$= \frac{r}{2}\cos(\beta/2)\tan\theta_B\sin(kl\cos(\beta/2)\cos\theta_B)[i\,J_1(2kr\cos(\beta/2)\sin\theta_B)+E_1(2kr\cos(\beta/2)\sin\theta_B)]. \tag{27}$$

At this point, one can invoke the asymptotic approximations for the Bessel and Weber functions (Eq. (2.19)) to obtain

$$\begin{aligned}-\frac{1}{4\pi}\int_{\text{illum. area}}(\vec{k}_s+\vec{k}_s)\cdot\vec{n}\,e^{-i(\vec{k}_s+\vec{k}_s)\cdot\vec{r}}dS &=\\ \frac{r}{2}\tan\theta_B\sin(kl\cos(\beta/2)\cos\theta_B)\sqrt{\frac{1}{\pi kr\cos(\beta/2)\sin\theta_B}}e^{i2kr\cos(\beta/2)\sin\theta_B-i\pi/4}.&\end{aligned} \tag{28}$$

This is just the Bistatic Theorem result.

The key point in the preceding is that since the source and receiver lie in the same plane the cylinder is illuminated and observed over the limits $-\pi/2\le\varphi\le\pi/2$. This in turn gives the factor

$$[i\,J_1(k(\sin\theta_s+\sin\theta_r)r)+E_1(k(\sin\theta_s+\sin\theta_r)r)]\approx\sqrt{\frac{2}{\pi k(\sin\theta_s+\sin\theta_r)r}}e^{ik(\sin\theta_s+\sin\theta_r)r-i\pi/4},$$

(valid for $k(\sin\theta_s+\sin\theta_r)r >> 1$) whose asymptotic behavior has been carefully studied (see [21] for example). A further point to observe is that the asymptotic approximation for the Bessel functions breaks down as $k(\sin\theta_s+\sin\theta_r)r\to 0$, however since the Bessel functions are multiplied by a factor of $(\sin\theta_s+\sin\theta_r)$, this problem can be safely ignored.

Also note that the previous results hold for $\sin\theta_{r/s}$ positive. For $(\sin\theta_s+\sin\theta_r)<0$ then the asymptotic formula above is multiplied by -1 and $(\sin\theta_s+\sin\theta_r)$ is replaced by $|(\sin\theta_s+\sin\theta_r)|$ throughout.

5.2 The out-of-plane case

Now consider the case in which the receiver does not lie in the same plane as the source, as shown in Fig. 8. In this case one obtains

$$\begin{aligned}\vec{k}_s &= k(-\cos\eta_s\cos\theta_s, -\cos\eta_s\sin\theta_s, -\sin\eta_s),\\ \vec{k}_r &= k(-\cos\eta_r\cos\theta_r, -\cos\eta_r\sin\theta_r, -\sin\eta_r).\end{aligned} \tag{29}$$

This gives the result

$$\begin{aligned}(\vec{k}_s+\vec{k}_s)\cdot\vec{n} &= -k[(\sin\theta_s\cos\eta_s+\cos\eta_r\sin\theta_r)\cos\varphi+\sin\varphi(\sin\eta_s+\sin\eta_r)],\\ (\vec{k}_r+\vec{k}_s)\cdot\vec{r} &= -k[(\cos\theta_s\cos\eta_s+\cos\eta_r\cos\theta_r)x+\\ &\quad[(\sin\theta_s\cos\eta_s+\cos\eta_r\sin\theta_r)\cos\varphi+\sin\varphi(\sin\eta_s+\sin\eta_r)]r.\end{aligned} \tag{30}$$

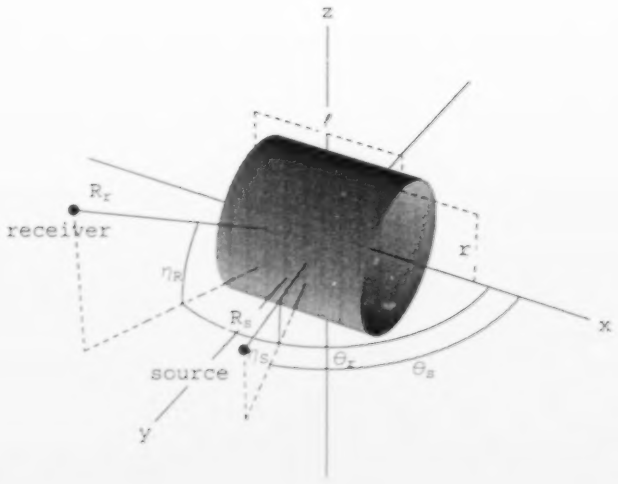

Figure 8: The out-of-plane bistatic case for the horizontal cylinder.

Since the source/receiver plane does not coincide with the symmetry plane of the cylinder, there are no particular simplifications that result from a different choice of angular parameter such as aspect angle or bistatic angle.

The viewed/illuminated areas are determined by solving the multiple-valued equations

$$\vec{k}_{r/s} \cdot \vec{n} \;=\; 0. \tag{31}$$

This gives

$$\tan[\varphi] \;=\; -\cot[\eta_{r/s}]\sin[\theta_{r/s}]. \tag{32}$$

This can be solved in the form

$$\begin{aligned}
\varphi_{Ru} &= \pi + \arctan[\sin\eta_r, -\cos\eta_r \sin\theta_r],\\
\varphi_{Rl} &= \arctan[\sin\eta_r, -\cos\eta_r \sin\theta_r],\\
\varphi_{Su} &= \pi + \arctan[\sin\eta_s, -\cos\eta_s \sin\theta_s],\\
\varphi_{Sl} &= \arctan[\sin\eta_s, -\cos\eta_s \sin\theta_s],
\end{aligned} \tag{33}$$

where $\arctan[x,y]$ is in the same quadrant as the point (x,y); in Mathematica language $\arctan[x,y] \equiv ArcTan[x,y]$. This means that the illuminated area is spanned by the angles $\varphi_{Sl} \le \varphi \le \varphi_{Su}$ and the viewed area by $\varphi_{Rl} \le \varphi \le \varphi_{Ru}$. The integration area for the Kirchhoff integral is then the intersection of these areas.

If one defines the auxiliary angles

$$\begin{aligned}
\varphi_{upper} &= Minimum[\varphi_{Ru}, \varphi_{Su}],\\
\varphi_{lower} &= Maximum[\varphi_{Rl}, \varphi_{Sl}],
\end{aligned} \tag{34}$$

then the integration area for the Kirchhoff integral can be written as $\varphi_{lower} \le \varphi \le \varphi_{upper}$.

The scattering strength can be written as

$$\begin{aligned}
g = -\frac{1}{4\pi}\int_{\text{illum. area}} (\vec{k}_r + \vec{k}_s)\cdot\vec{n}\, e^{-i(\vec{k}_r+\vec{k}_s)\cdot\vec{r}}\, dS \;=\;\\
\frac{kr}{4\pi}\int_{-l/2}^{l/2} dx \int_{\varphi_{upper}}^{\varphi_{upper}} d\varphi [(\sin\theta_s\cos\eta_s + \cos\eta_r\sin\theta_r)\cos\varphi + \sin\varphi(\sin\eta_s+\sin\eta_r)] \times\\
e^{ik[(\cos\theta_s\cos\eta_s+\cos\eta_r\cos\theta_r)x + [(\sin\theta_s\cos\eta_s+\cos\eta_r\sin\theta_r)\cos\varphi+\sin\varphi(\sin\eta_s+\sin\eta_r)]r}\\
= \frac{r\sin(\frac{kl}{2}(\cos\theta_s\cos\eta_s+\cos\eta_r\cos\theta_r))}{2\pi(\cos\theta_s\cos\eta_s+\cos\eta_r\cos\theta_r)} \int_{\varphi_{lower}}^{\varphi_{upper}} d\varphi \times\\
[(\sin\theta_s\cos\eta_s+\cos\eta_r\sin\theta_r)\cos\varphi+\sin\varphi(\sin\eta_s+\sin\eta_r)]e^{ik[(\sin\theta_s\cos\eta_s+\cos\eta_r\sin\theta_r)\cos\varphi+\sin\varphi(\sin\eta_s+\sin\eta_r)]r}
\end{aligned} \tag{35}$$

Now define the auxiliary variables

$$\begin{aligned}
\omega &= \arctan[(\sin\eta_r+\sin\eta_s),(\cos\eta_r\sin\theta_r+\cos\eta_s\sin\theta_s)]\\
\lambda &= \sqrt{(\cos\eta_r\sin\theta_r+\cos\eta_s\sin\theta_s)^2+(\sin\eta_r+\sin\eta_s)^2}.
\end{aligned} \tag{36}$$

The scattering strength becomes

$$g \;=\; \frac{r\lambda\sin(\frac{kl}{2}(\cos\theta_s\cos\eta_s+\cos\eta_r\cos\theta_r))}{2\pi(\cos\theta_s\cos\eta_s+\cos\eta_r\cos\theta_r)} \int_{\varphi_{lower}+\omega}^{\varphi_{upper}+\omega} d\varphi \sin\varphi e^{ikr\lambda\sin\varphi} \tag{37}$$

Now in terms of the incomplete Bessel functions defined in the Appendices, one has

$$\begin{aligned}
g \;=\; &\frac{1}{4} r\, k\, l\lambda\; sa[\frac{kl}{2}(\cos\theta_s\cos\eta_s+\cos\eta_r\cos\theta_r))] \times\\
&\left\{\left(ie_1(\varphi_{upper}+\omega, k\,r\lambda) + \frac{sin[\varphi_{upper}+\omega]}{\pi} ea[k\,r\lambda sin[\varphi_{upper}+\omega]]\right) -\right.\\
&\left.\left(ie_1(\varphi_{lower}+\omega, k\,r\lambda) + \frac{sin[\varphi_{lower}+\omega]}{\pi} ea[k\,r\lambda sin[\varphi_{lower}+\omega]]\right)\right\}.
\end{aligned} \tag{38}$$

where

$$
\begin{aligned}
sa[x] &= \frac{\sin[x]}{x}, \\
ea[x] &= \frac{(1-e^{ix})}{x}, \\
\epsilon_1(\beta,z) &\equiv A_1(\beta,z) - iB_1(\beta,z) = \frac{1}{\pi}\int_0^{\beta} \sin\varphi e^{iz\sin\varphi}.
\end{aligned} \tag{39}
$$

The function $\epsilon_1(\beta,z)$ is evaluated in the software using various expansions.

The values for the functions $A_{\pm 1}$, $B_{\pm 1}$ can then be found from the accompanying Mathematica notebooks, which incorporates the fairly complicated asymptotic expressions for these functions. Because the asymptotic behavior of $A_{\pm}1(\beta,x)$, $B_{\pm}1(\beta,x)$ depends on the particular angular regime β (see Appendix A), one would not attempt to write these formulae out explicitly everytime these functions are used, but instead develop these expressions systematically in the software. The expansions used to approximate these functions are given in Appendix A. The asymptotic value of factors such as $E_1(x)+iJ_1(x)) \approx \sqrt{\frac{2}{\pi x}}e^{i(x-\pi/4)}$ is sufficiently simple to write out explicitly everywhere where it occurs, but this is not the case for the general case of the incomplete versions of these functions.

One must also observe the following inconvenient feature about out-of-plane scattering: the function $xJ_1(x) \approx x\sqrt{2/(\pi x)}\cos(x-3\pi/4) \to 0$ as $x \to 0$, however the incomplete functions $A_1(\beta,x) \propto 1/x$ as $x \to \infty$. Hence one may not use asymptotic results for $A_1(\beta,x)$ for x small i.e. near forward scattering. For accurate results, one must evaluate the functions $A_1(\beta,x)$ for small x, a time consuming procedure, given in the software. However for the special case $z >> 1$ and $-\frac{\pi}{2} + \arcsin(\frac{1}{z}) \le \beta \le \frac{\pi}{2} - \arcsin(\frac{1}{z})$ one has

$$
B_n(\beta,z) + iA_n(\beta,z) \approx \frac{1}{\pi z}\left[\frac{e^{i(z\sin\beta - n\beta)}}{\cos\beta} - 1\right], \quad -\frac{\pi}{2} + \arcsin(\frac{1}{z}) \le \beta \le \frac{\pi}{2} - \arcsin(\frac{1}{z}). \tag{40}
$$

Four numerical examples are shown in Fig 9–including the source/receiver in-plane case, source/receiver both 20 degrees above the symmetry plane, source 20 degrees below and receiver 20 degrees above the symmetry plane, and the asymmetric case, receiver 20 degrees above and source in-plane. The key feature of out-of-plane scattering emerges by comparing the in-plane case and the source/receiver 20 degrees above the symmetry plane case. As well as the bright areas correponding to broadside scattering ($\theta_R \approx \theta_S \approx 90^o, 270^o$), there are additional bright areas corresponging to scattering from the top of the cylinder in the forward direction ($\theta_R \approx \theta_S \pm 180^o$).

The drawback of this approach, namely evaluating the incomplete Bessel functions with this degree of accuracy, is the loss of computing speed. The advantage is that the scattering in forward directions for such cases such as $\eta_r = \eta_s = 20$ degrees will be accurately computed. The use of saddle point terms alone would overestimate the scattering in forward directions, where quantities such as $k\lambda$ take on their smallest values in the $\theta_r - \theta_s$ plane.

6 The vertical cylinder

6.1 In-plane scattering for the vertical cylinder

Consider the vertical cylinder, whose scattering geometry is shown in Figure 10. The unit normal to the surface, differential area and displacement are given by

$$
\begin{aligned}
\vec{n} &= (\cos\varphi, \sin\varphi, 0), \\
dA &= a d\varphi dz, \\
\vec{r} &= (a\cos\varphi, a\sin\varphi, z).
\end{aligned} \tag{41}
$$

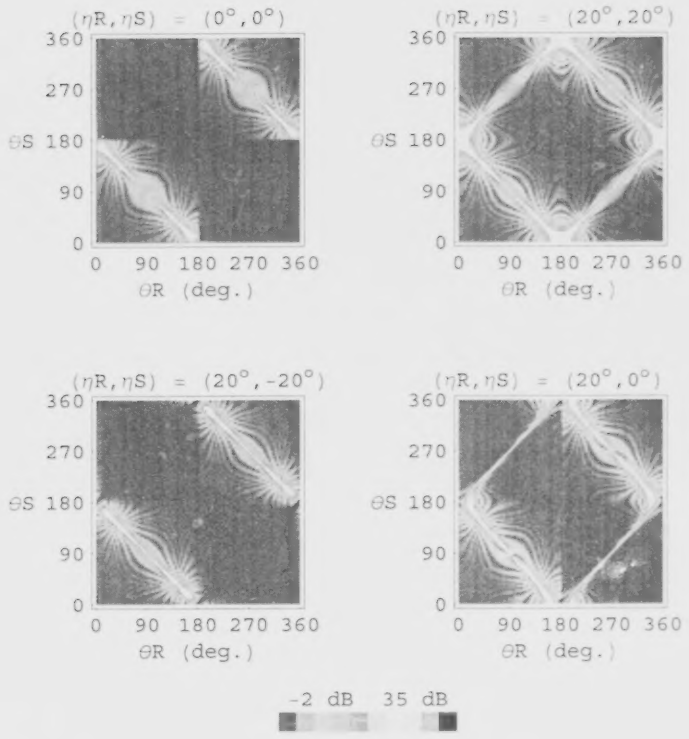

Figure 9: A plot of T.S. $= 10\log(10^{-2/10} + |g(\eta_r, \eta_s, \theta_r, \theta_s|^2)$ for the horizontal cylinder of radius $a = 2.8$ m, $l = 46.2$ m, frequency $f = 500$ Hz. The principal feature of out-of-plane scattering is the appearance of additional scattering surfaces, corresponding to additional bright areas in the $\theta_r - \theta_s$ plane. In the case $\eta_r = \eta_s = 20$ degrees, this corresponds to a 40 degree wide viewed/illuminated strip (for $\theta_r = 90$ degrees, $\theta_s = 270$ degrees say) on the top of the cylinder, in addition to scattering from the sides of the cylinder.

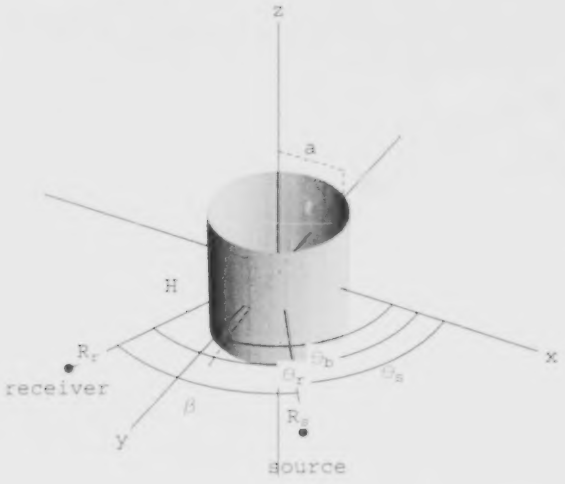

Figure 10: The in-plane bistatic case for the vertical cylinder of radius a and height H.

For the case of a source and receiver in the same plane

$$\begin{aligned}\vec{k}_s &= k(-\cos\theta_s, -\sin\theta_s, 0),\\ \vec{k}_r &= k(-\cos\theta_r, -\sin\theta_r, 0).\end{aligned} \tag{42}$$

As always, it is convenient to introduce the notation

$$\begin{aligned}\beta &= \theta_S - \theta_R,\\ \theta_B &= (\theta_S + \theta_R)/2.\end{aligned} \tag{43}$$

This gives the result

$$\begin{aligned}(\vec{k}_s + \vec{k}_r)\cdot\vec{n} &= -k\left[(\cos\theta_s + \cos\theta_r)\cos\varphi + (\sin\theta_s + \sin\theta_r)\sin\varphi\right] = -2k\cos(\beta/2)\cos(\varphi - \theta_B),\\ (\vec{k}_s + \vec{k}_r)\cdot\vec{r} &= -2ka\cos(\beta/2)\cos(\varphi - \theta_B).\end{aligned} \tag{44}$$

The viewed/illuminated areas are given by

$$\vec{k}_{s/r}\cdot\vec{n} = 0. \tag{45}$$

This gives

$$\begin{aligned}\cos\theta_r\cos\varphi + \sin\theta_r\sin\varphi &= 0,\\ \cos\theta_s\cos\varphi + \sin\theta_s\sin\varphi &= 0.\end{aligned} \tag{46}$$

This can be solved as

$$\begin{aligned}\varphi_{Ru} &= \pi/2 + \theta_r,\\ \varphi_{Rl} &= -\pi/2 + \theta_r,\\ \varphi_{Su} &= \pi/2 + \theta_s,\\ \varphi_{Sl} &= -\pi/2 + \theta_s.\end{aligned} \tag{47}$$

The integration region is the intersection of the ranges $\varphi_{Rl} \le \varphi \le \varphi_{Ru}$ and $\varphi_{Sl} \le \varphi \le \varphi_{Su}$. Again define the extra functions

$$\begin{aligned}\varphi_{upper} &= Min[\varphi_{Ru}, \varphi_{Su}],\\ \varphi_{lower} &= Max[\varphi_{Rl}, \varphi_{Sl}]\end{aligned} \tag{48}$$

This means that the integration region is $\varphi_{lower} \le \varphi \le \varphi_{upper}$.

The scattering strength becomes

$$\begin{aligned}g &= -\frac{1}{4\pi}\int_{\text{illum. area}} (\vec{k}_s + \vec{k}_r)\cdot\vec{n}\, e^{-i(\vec{k}_s + \vec{k}_r)\cdot\vec{r}}\, dS\\ &= \frac{ka}{4\pi}\int_{-H/2}^{H/2} dz \int_{\varphi_{lower}}^{\varphi_{upper}} d\varphi \left[(\cos\theta_s + \cos\theta_r)\cos\varphi + (\sin\theta_s + \sin\theta_r)\sin\varphi\right] \times\\ &\qquad e^{ika[(\cos\theta_s + \cos\theta_r)\cos\varphi + (\sin\theta_s + \sin\theta_r)\sin\varphi]}\end{aligned} \tag{49}$$

Now define

$$\begin{aligned}\omega &= \arctan[(\sin\theta_s + \sin\theta_r), (\cos\theta_s + \cos\theta_r)],\\ \lambda &= \sqrt{(\sin\theta_s + \sin\theta_r)^2 + (\cos\theta_s + \cos\theta_r)^2}.\end{aligned} \tag{50}$$

The scattering strength reduces to

$$\begin{aligned}g &= \frac{kaH\lambda}{4\pi}\int_{\varphi_{lower}}^{\varphi_{upper}} d\varphi \sin(\varphi + \omega) e^{ika\lambda\sin(\varphi + \omega)}\\ &= \frac{kaH\lambda}{4\pi}\int_{\varphi_{lower}+\omega}^{\varphi_{upper}+\omega} d\varphi \sin\varphi\, e^{ika\lambda\sin\varphi}\end{aligned} \tag{51}$$

Again, using the incomplete Bessel functions introduced in the previously, one obtains

$$
\begin{aligned}
g &= \frac{kaH\lambda}{4\pi}\int_{\varphi_{lower}}^{\varphi_{upper}} d\varphi \sin(\varphi+\omega)e^{ika\lambda\sin(\varphi+\omega)} \\
&= \frac{kaH\lambda}{4}\left\{\left(ie_1(\varphi_{upper}+\omega,ka\lambda)+\frac{\sin[\varphi_{upper}+\omega]}{\pi}ea(ka\lambda\sin[\varphi_{upper}+\omega])\right)-\right. \\
&\left.\left(ie_1(\varphi_{lower}+\omega,ka\lambda)+\frac{\sin[\varphi_{lower}+\omega]}{\pi}ea(ka\lambda\sin[\varphi_{lower}+\omega])\right)\right\}. \qquad (52)
\end{aligned}
$$

At this point one can see that the Bistatic Theorem will not apply here even for the in-plane case since the integration regions for the monostatic case and bistatic case are different.

6.2 Out-of-plane scattering for the vertical cylinder

Now consider the case in which the source and receiver do not necessarily lie in the $x-y$ plane:

In this case one obtains

$$
\begin{aligned}
\vec{k}_s &= k(-\cos\eta_s\cos\theta_s,-\cos\eta_s\sin\theta_s,-\sin\eta_s), \\
\vec{k}_r &= k(-\cos\eta_r\cos\theta_r,-\cos\eta_r\sin\theta_r,-\sin\eta_r). \qquad (53)
\end{aligned}
$$

The unit normal to the surface, differential area and displacement are given by

$$
\begin{aligned}
\vec{n} &= (\cos\varphi,\sin\varphi,0), \\
d\Lambda &= ad\varphi dz, \\
\vec{r} &= (a\cos\varphi,a\sin\varphi,z). \qquad (54)
\end{aligned}
$$

This gives the result

$$
\begin{aligned}
(\vec{k}_s+\vec{k}_s)\cdot\vec{n} &= -k\left[(\cos\eta_s\cos\theta_s+\cos\eta_r\cos\theta_r)\cos\varphi+(\cos\eta_s\sin\theta_s+\cos\eta_r\sin\theta_r)\sin\varphi\right], \\
(\vec{k}_s+\vec{k}_s)\cdot\vec{r} &= \\
&-k\left[a(\cos\eta_s\cos\theta_s+\cos\eta_r\cos\theta_r)\cos\varphi+a(\cos\eta_s\sin\theta_s+\cos\eta_r\sin\theta_r)\sin\varphi+(\sin\eta_s+\sin\eta_r)z\right]. \qquad (55)
\end{aligned}
$$

The viewed/illuminated areas are given by

$$
\vec{k}_{s/r}\cdot\vec{n}=0. \qquad (56)
$$

This gives

$$
\begin{aligned}
\cos\eta_r\cos\theta_r\cos\varphi+\cos\eta_r\sin\theta_r\sin\varphi &= 0, \\
\cos\eta_s\cos\theta_s\cos\varphi+\cos\eta_s\sin\theta_s\sin\varphi &= 0 \qquad (57)
\end{aligned}
$$

This can be solved in the form

$$
\begin{aligned}
\varphi_{upper} &= \frac{\pi}{2}+\frac{1}{2}[(\theta_r+\theta_s)-|(\theta_r-\theta_s)|], \quad |\theta_r-\theta_s|<\pi, \\
\varphi_{lower} &= -\frac{\pi}{2}+\frac{1}{2}[(\theta_r+\theta_s)+|(\theta_r-\theta_s)|] \quad |\theta_r-\theta_s|<\pi, \\
\varphi_{upper} &= \frac{\pi}{2}+\frac{1}{2}[(\theta_r+\theta_s)+|(\theta_r-\theta_s)|], \quad |\theta_r-\theta_s|>\pi \\
\varphi_{lower} &= \frac{3\pi}{2}+\frac{1}{2}[(\theta_r+\theta_s)-|(\theta_r-\theta_s)|] \quad |\theta_r-\theta_s|>\pi. \qquad (58)
\end{aligned}
$$

This means that the integration region is $\varphi_{lower}\le\varphi\le\varphi_{upper}$.

The scattering strength can be written as

$$
\begin{aligned}
g &= -\frac{1}{4\pi}\int_{\text{illum. area}} (\vec{k}_s + \vec{k}_s)\cdot\vec{n}\, e^{-i(\vec{k}_s+\vec{k}_s)\cdot\vec{r}}dS \\
&= \frac{ka}{4\pi}\int_{-H/2}^{H/2} dz \int_{\varphi_{lower}}^{\varphi_{upper}} d\varphi\,[(\cos\eta_s\cos\theta_s + \cos\eta_r\cos\theta_r)\cos\varphi + (\cos\eta_s\sin\theta_s + \cos\eta_r\sin\theta_r)\sin\varphi]\times \\
&\quad e^{ik|a(\cos\eta_s\cos\theta_s+\cos\eta_r\cos\theta_r)\cos\varphi + a(\cos\eta_s\sin\theta_s+\cos\eta_r\sin\theta_r)\sin\varphi + (\sin\eta_s+\sin\eta_r)z|} \\
&= \frac{kaH\ sa[\frac{1}{2}kH(\sin\eta_s+\sin\eta_r)]}{4\pi}\int_{\varphi_{lower}}^{\varphi_{upper}} d\varphi\,[(\cos\eta_s\cos\theta_s + \cos\eta_r\cos\theta_r)\cos\varphi + \\
&\quad (\cos\eta_s\sin\theta_s + \cos\eta_r\sin\theta_r)\sin\varphi]\, e^{ika[(\cos\eta_s\cos\theta_s+\cos\eta_r\cos\theta_r)\cos\varphi + (\cos\eta_s\sin\theta_s+\cos\eta_r\sin\theta_r)\sin\varphi]}. \qquad (59)
\end{aligned}
$$

Now define the auxiliary functions

$$
\begin{aligned}
\omega &= \arctan[(\cos\eta_s\sin\theta_s + \cos\eta_r\sin\theta_r), (\cos\eta_s\cos\theta_s + \cos\eta_r\cos\theta_r)], \\
\lambda &= \sqrt{(\cos\eta_s\sin\theta_s + \cos\eta_r\sin\theta_r)^2 + (\cos\eta_s\cos\theta_s + \cos\eta_r\cos\theta_r)^2}. \qquad (60)
\end{aligned}
$$

This gives

$$
\begin{aligned}
g &= \frac{kaH\lambda\ sa[\frac{1}{2}kH(\sin\eta_s+\sin\eta_r)]}{4\pi}\int_{\varphi_{lower}+\omega}^{\varphi_{upper}+\omega} d\varphi\,\sin\varphi e^{ika\lambda\sin\varphi} \\
&= \frac{kaH\lambda\ sa[\frac{1}{2}kH(\sin\eta_s+\sin\eta_r)]}{4}\left\{\left(ie_1(\varphi_{upper}+\omega, ka\lambda) + \frac{\sin[\varphi_{upper}+\omega]}{\pi}ea(ka\lambda\sin[\varphi_{upper}+\omega])\right) - \right. \\
&\quad \left.\left(ie_1(\varphi_{lower}+\omega, ka\lambda) + \frac{\sin[\varphi_{lower}+\omega]}{\pi}ea(ka\lambda\sin[\varphi_{lower}+\omega])\right)\right\}. \qquad (61)
\end{aligned}
$$

A numerical example for the full vertical cylinder is shown in Fig 11, which shows the effect of changing the view angle as the source/receiver moves out-of-plane.

For the truncated vertical cylinder facing the positive x-axis, the integration region consists of the intersection of the intervals $-\pi/2 \le \varphi \le \pi/2$ and $\varphi_{lower} \le \varphi \le \varphi_{upper}$. By construction $\varphi_{upper} > \varphi_{lower}$ and $\pi/2 \le \varphi_{upper} \le 5\pi/2$, $-\pi/2 \le \varphi_{lower} \le 5\pi/2$. This means that the integration limits for the half vertical cylinder can be defined as

$$
\begin{aligned}
\varphi_{halfupper} &= \begin{cases} \pi/2, & \pi/2 \le \varphi_{upper} \le 3\pi/2,\ \pi/2 \le \varphi_{lower} \le 3\pi/2, \\ \pi/2, & \pi/2 \le \varphi_{upper} \le 3\pi/2,\ \varphi_{lower} \le \pi/2, \\ \varphi_{upper}, & 3\pi/2 \le \varphi_{upper} \le 5\pi/2, \varphi_{lower} \le 3\pi/2 \end{cases} \\
\varphi_{halflower} &= \begin{cases} \pi/2, & \pi/2 \le \varphi_{upper} \le 3\pi/2,\ \pi/2 \le \varphi_{lower} \le 3\pi/2 \\ \varphi_{lower}, & \pi/2 \le \varphi_{upper} \le 3\pi/2,\ \varphi_{lower} \le \pi/2 \\ 3\pi/2, & 3\pi/2 \le \varphi_{upper} \le 5\pi/2,\ \varphi_{lower} \le 3\pi/2, \\ \varphi_{lower}, & 3\pi/2 \le \varphi_{upper} \le 5\pi/2,\ \varphi_{lower} > 3\pi/2 \end{cases}
\end{aligned}
\qquad (62)
$$

Now just replace $\{\varphi_{upper}, \varphi_{lower}\} \to \{\varphi_{halfupper}, \varphi_{halflower}\}$ in the previous result for g. A numerical example for the bow cylinder, which consists of a truncated vertical cylinder facing the positive x-direction, is shown in Figure 12. Apart from some interesting edge effects, the main effect of moving from the full vertical cylinder to the half-cylinder is to remove the center part (90 degrees < aspect angle < 270 degrees) of the full vertical cylinder plot. Note that the truncated result is larger at the aspect angle near 90°, than at 0°, even though less of the surface is illuminated/viewed. This is due to the oscillatory nature of the integrand and the relatively modest frequencies; for larger frequencies the scattering strength will more closely follow the size of the illuminated/viewed areas.

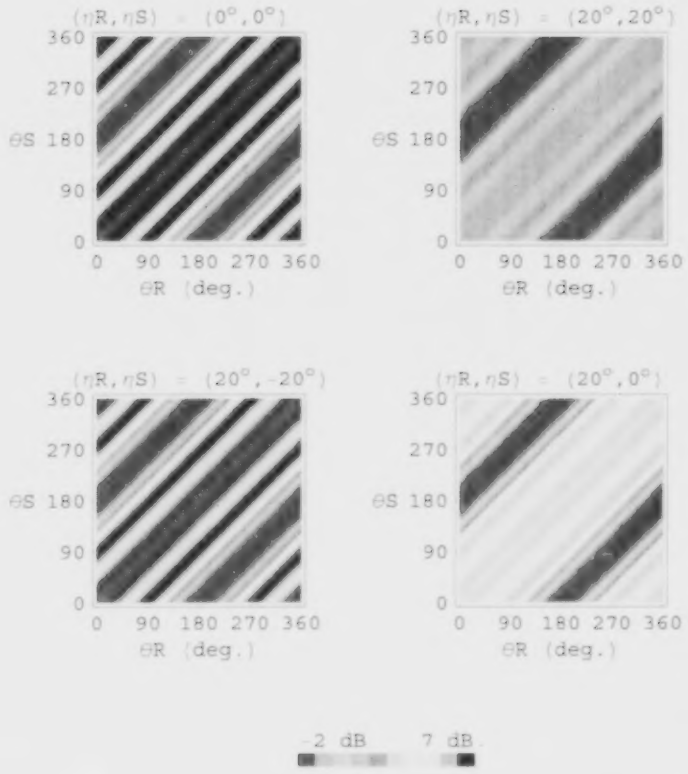

Figure 11: A plot of T.S. $= 10\log(10^{-2/10} + |g(\eta_r, \eta_s, \theta_r, \theta_s|^2)$ for the full vertical cylinder of radius $a = 2.8$ m. $H = 2.8$ m. frequency $f = 500$ Hz for various out-of-plane cases.

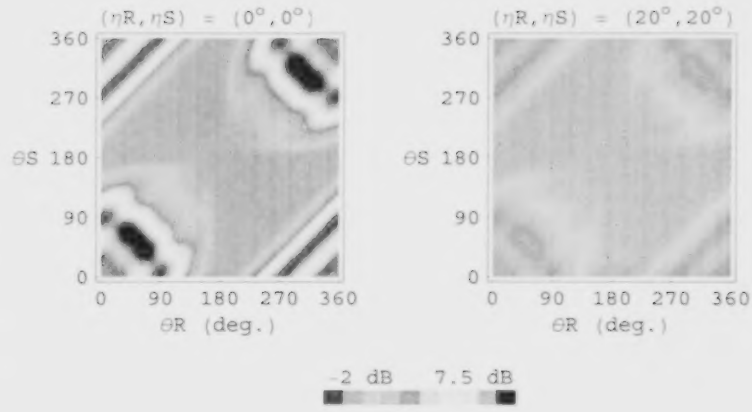

Figure 12: A plot of T.S. $= 10\log(10^{-1/10} + |g(\eta_r, \eta_s, \theta_r, \theta_s|^2)$ for the truncated vertical half-cylinder facing the positive x-direction (bow cylinder of Sub model) of radius $a = 2.8$ m, $H = 2.8$ m, frequency $f = 500$ Hz for the in-plane case $\{\eta_r, \eta_s, \theta_r, \theta_s\} = \{0, 0, \theta_r, \theta_s\}$ and the out-of-plane case $\{\eta_r, \eta_s, \theta_r, \theta_s\} = \{20°, 20°, \theta_r, \theta_s\}$. This provides a model for the bow cylinder for the sub model.

7 The vertical elliptical cylinder

7.1 The bistatic case

Consider the vertical elliptical cylinder, as shown in Figure 13. The bistatic case follows the same pattern as the monostatic case. In this case one obtains

$$\begin{aligned} \vec{k}_s &= k(-\cos\eta_s\cos\theta_s, -\cos\eta_s\sin\theta_s, -\sin\eta_s), \\ \vec{k}_r &= k(-\cos\eta_r\cos\theta_r, -\cos\eta_r\sin\theta_r, -\sin\eta_r). \end{aligned} \tag{63}$$

The unit normal to the surface, differential area and displacement are given by

$$\begin{aligned} \vec{n} &= \frac{1}{\sqrt{a^2\sin^2\varphi + b^2\cos^2\varphi}}(b\cos\varphi, a\sin\varphi, 0), \\ dA &= \sqrt{a^2\sin^2\varphi + b^2\cos^2\varphi}\,d\varphi dz, \\ \vec{r} &= (a\cos\varphi, b\sin\varphi, z). \end{aligned} \tag{64}$$

Then one obtains

$$\begin{aligned} (\vec{k}_s + \vec{k}_s)\cdot\vec{n} &= \\ &-\frac{k}{\sqrt{a^2\sin^2\varphi + b^2\cos^2\varphi}}\left\{b\cos\varphi(\cos\eta_r\cos\theta_r + \cos\eta_s\cos\theta_s) + a\sin\varphi(\cos\eta_r\sin\theta_r + \cos\eta_s\sin\theta_s)\right\}, \\ (\vec{k}_s + \vec{k}_s)\cdot\vec{r} &= \\ &-k\left\{a\cos\varphi(\cos\eta_r\cos\theta_r + \cos\eta_s\cos\theta_s) + b\sin\varphi(\cos\eta_r\sin\theta_r + \cos\eta_s\sin\theta_s) + z(\sin\eta_r + \sin\eta_s)\right\} \end{aligned} \tag{65}$$

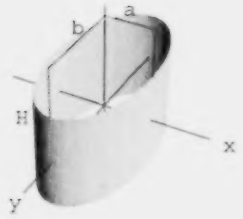

Figure 13: The vertical elliptical cylinder of radius along the x-axis a, radius along the y-axis b, and height H.

The integration region is determined by the intersection of the viewed/illuminated areas determined by solving the constraints $\vec{k}_{s/r} \cdot \vec{n} = 0$ which give

$$\begin{aligned} b\cos\varphi\cos\theta_r + a\sin\varphi\sin\theta_r &= 0, \\ b\cos\varphi\cos\theta_s + a\sin\varphi\sin\theta_s &= 0. \end{aligned} \tag{66}$$

If one defines the functions

$$\begin{aligned} \varepsilon_{1r} &= \begin{cases} \arctan[b\cos\theta_r, a\sin\theta_r] & 0 \le \theta_r \le \pi, \\ 2\pi + \arctan[b\cos\theta_r, a\sin\theta_r] & \pi < \theta_r \le 2\pi, \end{cases} \\ \varepsilon_{1s} &= \begin{cases} \arctan[b\cos\theta_s, a\sin\theta_s] & 0 \le \theta_s \le \pi, \\ 2\pi + \arctan[b\cos\theta_s, a\sin\theta_s] & \pi < \theta_s \le 2\pi, \end{cases} \end{aligned} \tag{67}$$

Then the integration limits are given by

$$\begin{aligned} \varphi_{upper} &= \frac{\pi}{2} + \frac{1}{2}[(\varepsilon_{1r} + \varepsilon_{1s}) - |(\varepsilon_{1r} - \varepsilon_{1s})|], \quad |\varepsilon_{1r} - \varepsilon_{1s}| < \pi, \\ \varphi_{lower} &= -\frac{\pi}{2} + \frac{1}{2}[(\varepsilon_{1r} + \varepsilon_{1s}) + |(\varepsilon_{1r} - \varepsilon_{1s})|] \quad |\varepsilon_{1r} - \varepsilon_{1s}| < \pi, \\ \varphi_{upper} &= \frac{\pi}{2} + \frac{1}{2}[(\varepsilon_{1r} + \varepsilon_{1s}) + |(\varepsilon_{1r} - \varepsilon_{1s})|], \quad |\varepsilon_{1r} - \varepsilon_{1s}| > \pi \\ \varphi_{lower} &= \frac{3\pi}{2} + \frac{1}{2}[(\varepsilon_{1r} + \varepsilon_{1s}) - |(\varepsilon_{1r} - \varepsilon_{1s})|] \quad |\varepsilon_{1r} - \varepsilon_{1s}| > \pi. \end{aligned} \tag{68}$$

This means that the integration region is $\varphi_{lower} \le \varphi \le \varphi_{upper}$.

This gives the bistatic scattering strength

$$\begin{aligned} g &= -\frac{1}{4\pi}\int_{\text{illum. area}} (\vec{k}_s + \vec{k}_s)\cdot\vec{n}\, e^{-i(\vec{k}_r + \vec{k}_s)\cdot\vec{r}}\, d\mathcal{S} \\ &= \frac{k}{4\pi}\int_{-H/2}^{H/2} dz \int_{\varphi_{lower}}^{\varphi_{upper}} d\varphi \left\{ b\cos\varphi(\cos\eta_r\cos\theta_r + \cos\eta_s\cos\theta_s) + a\sin\varphi(\cos\eta_r\sin\theta_r + \cos\eta_s\sin\theta_s) \right\} \times \\ &\quad e^{ik\{a\cos\varphi(\cos\eta_r\cos\theta_r + \cos\eta_s\cos\theta_s) + b\sin\varphi(\cos\eta_r\sin\theta_r + \cos\eta_s\sin\theta_s) + z(\sin\eta_r + \sin\eta_s)\}} \end{aligned}$$

$$= \frac{kHsa[\frac{kH}{2}(\sin\eta_r+\sin\eta_s)]}{4\pi}\int_{\varphi_{lower}}^{\varphi_{upper}} d\varphi \times$$
$$\{b\cos\varphi(\cos\eta_r\cos\theta_r+\cos\eta_s\cos\theta_s)+a\sin\varphi(\cos\eta_r\sin\theta_r+\cos\eta_s\sin\theta_s)\}\times$$
$$e^{ik\{a\cos\varphi(\cos\eta_r\cos\theta_r+\cos\eta_s\cos\theta_s)+b\sin\varphi(\cos\eta_r\sin\theta_r+\cos\eta_s\sin\theta_s)\}} \tag{69}$$

Now define the shorthands

$$\begin{aligned}
\omega_1 &= \arctan[b(\cos\eta_r\sin\theta_r+\cos\eta_s\sin\theta_s), a(\cos\eta_r\cos\theta_r+\cos\eta_s\cos\theta_s)],\\
\omega_2 &= \arctan[a\sin\varphi(\cos\eta_r\sin\theta_r+\cos\eta_s\sin\theta_s), b\cos\varphi(\cos\eta_r\cos\theta_r+\cos\eta_s\cos\theta_s)],\\
\lambda_1 &= \sqrt{(b(\cos\eta_r\sin\theta_r+\cos\eta_s\sin\theta_s))^2+(a(\cos\eta_r\cos\theta_r+\cos\eta_s\cos\theta_s))^2}\\
\lambda_2 &= \sqrt{(a(\cos\eta_r\sin\theta_r+\cos\eta_s\sin\theta_s))^2+(b(\cos\eta_r\cos\theta_r+\cos\eta_s\cos\theta_s))^2}.
\end{aligned} \tag{70}$$

This reduces the scattering strength to

$$\begin{aligned}
g &= \frac{kH\lambda_2 sa[\frac{kH}{2}(\sin\eta_r+\sin\eta_s)]}{4\pi}\int_{\varphi_{lower}}^{\varphi_{upper}} d\varphi\sin(\varphi+\omega_2)e^{ik\lambda_1\sin(\varphi+\omega_1)}\\
&= \frac{kH\lambda_2 sa[\frac{kH}{2}(\sin\eta_r+\sin\eta_s)]}{4\pi}\int_{\varphi_{lower}+\omega_1}^{\varphi_{upper}+\omega_1} d\varphi\sin(\varphi+\omega_2-\omega_1)e^{ik\lambda_1\sin\varphi}\\
&= \frac{kH\lambda_2 sa[\frac{kH}{2}(\sin\eta_r+\sin\eta_s)]}{4\pi}\left\{\sin(\omega_2-\omega_1)\int_{\varphi_{lower}+\omega_1}^{\varphi_{upper}+\omega_1} d\varphi\cos\varphi e^{ik\lambda_1\sin\varphi}+\right.\\
&\qquad \left.\cos(\omega_2-\omega_1)\int_{\varphi_{lower}+\omega_1}^{\varphi_{upper}+\omega_1} d\varphi\sin\varphi e^{ik\lambda_1\sin\varphi}\right\}\\
&= \frac{kH\lambda_2 sa[\frac{kH}{2}(\sin\eta_r+\sin\eta_s)]}{4\pi}\left\{\frac{\sin(\omega_2-\omega_1)}{ik\lambda_1}\left[e^{ik\lambda_1\sin[\varphi_{upper}+\omega_1]}-e^{ik\lambda_1\sin[\varphi_{lower}+\omega_1]}\right]+\right.\\
&\qquad \left.\cos(\omega_2-\omega_1)\int_{\varphi_{lower}+\omega_1}^{\varphi_{upper}+\omega_1} d\varphi\sin\varphi e^{ik\lambda_1\sin\varphi}\right\}
\end{aligned} \tag{71}$$

In terms of the incomplete functions introduced in the appendix, this gives:

$$\begin{aligned}
g &= \frac{kH\lambda_2 sa[\frac{kH}{2}(\sin\eta_r+\sin\eta_s)]}{4}\times\\
&\{\frac{1}{\pi}e^{i(\omega_2-\omega_1)}\left[\sin(\varphi_{upper}+\omega_1)ca[k\lambda_1\sin(\varphi_{upper}+\omega_1)]-\sin(\varphi_{lower}+\omega_1)ca[k\lambda_1\sin(\varphi_{lower}+\omega_1)]\right]+\\
&i\cos(\omega_2-\omega_1)[\epsilon_1(\varphi_{upper}+\omega_1,k\lambda_1)-\epsilon_1(\varphi_{lower}+\omega_1,k\lambda_1)]\}.
\end{aligned} \tag{72}$$

For the truncated vertical elliptical cylinder facing the positive x-axis, the integration region consists of the intersection of the intervals $-\pi/2\le\varphi\le\pi/2$ and $\varphi_{lower}\le\varphi\le\varphi_{upper}$. By construction $\varphi_{upper}\ge\varphi_{lower}$ and $\pi/2\le\varphi_{upper}\le 5\pi/2$, $-\pi/2\le\varphi_{lower}\le 5\pi/2$. This means that the integration limits for the half vertical elliptical cylinder can be defined as

$$\varphi_{halfupper} = \begin{cases}
\pi/2, & \pi/2\le\varphi_{upper}\le 3\pi/2,\ \pi/2\le\varphi_{lower}\le 3\pi/2,\\
\pi/2, & \pi/2\le\varphi_{upper}\le 3\pi/2,\ \varphi_{lower}\le\pi/2,\\
\varphi_{upper}, & 3\pi/2\le\varphi_{upper}\le 5\pi/2, \varphi_{lower}\le 3\pi/2
\end{cases}$$

$$\varphi_{halflower} = \begin{cases}
\pi/2, & \pi/2\le\varphi_{upper}\le 3\pi/2,\ \pi/2\le\varphi_{lower}\le 3\pi/2\\
\varphi_{lower}, & \pi/2\le\varphi_{upper}\le 3\pi/2,\ \varphi_{lower}\le\pi/2\\
3\pi/2, & 3\pi/2\le\varphi_{upper}\le 5\pi/2,\ \varphi_{lower}\le 3\pi/2,\\
\varphi_{lower}, & 3\pi/2\le\varphi_{upper}\le 5\pi/2,\ \varphi_{lower}>3\pi/2
\end{cases} \tag{73}$$

Now just replace $\{\varphi_{upper}, \varphi_{lower}\} \rightarrow \{\varphi_{halfupper}, \varphi_{halflower}\}$ in the previous result for g. Some numerical examples for the full and truncated vertical elliptical cylinder are shown in Figure 14. The top row of graphs gives the in-plane case, the bottom row gives the out-of-plane case. The right column of graphs gives a model for the truncated elliptical sail front for the Sub model. As in the vertical cylinder case, apart from edge effects, the main effect of moving from the full vertical elliptical cylinder to the half elliptical cylinder is to remove the center part (90 degrees < aspect angle < 270 degrees) of the full vertical cylinder plot. One also notes that the broad part of the elliptical cylinder ($a = 3$ m, $b = 1.23$ m) is facing the y-axes, so the bright regions of the plot correspond to broadside scattering ($\theta_R \approx \theta_S \approx 90^o, 270^o$).

8 The sphere

8.1 Source/receiver in the x-y plane

Consider the sphere, whose scattering geometry is shown in Figure 15. The unit normal to the surface, differential area and displacement are given by

$$\begin{aligned} \vec{n} &= (\cos\varphi\cos\phi, \cos\varphi\sin\phi, \sin\varphi), \\ d\Lambda &= a^2\cos\varphi\, d\varphi\, d\phi, \\ \vec{r} &= a(\cos\varphi\cos\phi, \cos\varphi\sin\phi, \sin\varphi). \end{aligned} \tag{74}$$

For the case of a source and receiver in the same plane

$$\begin{aligned} \vec{k}_s &= k(-\cos\theta_s, -\sin\theta_s, 0), \\ \vec{k}_r &= k(-\cos\theta_r, -\sin\theta_r, 0). \end{aligned} \tag{75}$$

It is convenient to introduce the notation

$$\begin{aligned} \beta &= \theta_S - \theta_R, \\ \theta_B &= (\theta_S + \theta_R)/2. \end{aligned} \tag{76}$$

This gives the result

$$\begin{aligned} (\vec{k}_s + \vec{k}_s)\cdot\vec{n} &= -2k\cos(\beta/2)\cos(\phi - \theta_B)\cos\varphi, \\ (\vec{k}_s + \vec{k}_s)\cdot\vec{r} &= -2ka\cos(\beta/2)\cos(\phi - \theta_B)\cos\varphi. \end{aligned} \tag{77}$$

For source/receiver in the $x - y$ plane the illumination problem consists of two cases. The φ variable is integrated over the limits $-\pi/2 \le \varphi \le \pi/2$. The ϕ integration has the following two cases:

The illumination problem consists of two cases:
(1). $|\theta_r - \theta_s| < \pi$, $\quad -\frac{\pi}{2} + \frac{1}{2}[(\theta_r + \theta_s) + |(\theta_r - \theta_s)|] \le \phi \le \frac{\pi}{2} + \frac{1}{2}[(\theta_r + \theta_s) - |(\theta_r - \theta_s)|]$,
(2). $|\theta_r - \theta_s| > \pi$, $\quad \frac{3\pi}{2} + \frac{1}{2}[(\theta_r + \theta_s) - |(\theta_r - \theta_s)|] \le \phi \le \frac{\pi}{2} + \frac{1}{2}[(\theta_r + \theta_s) + |(\theta_r - \theta_s)|]$. Case (2). can be transformed into case (1) by replacing $|(\theta_r - \theta_s)| \rightarrow 2\pi - |(\theta_r - \theta_s)|$.

In case (1). the scattering strength can be written as

$$\begin{aligned} g &= -\frac{1}{4\pi}\int_{\text{illum. area}} (\vec{k}_s + \vec{k}_s)\cdot\vec{n}\; e^{-i(\vec{k}_s + \vec{k}_s)\cdot\vec{r}} dS \\ &= \frac{ka^2\cos(\beta/2)}{2\pi}\int_{-\frac{\pi}{2}+\frac{1}{2}\{(\theta_r+\theta_s)+|\theta_r-\theta_s|\}}^{\frac{\pi}{2}+\frac{1}{2}\{(\theta_r+\theta_s)-|\theta_r-\theta_s|\}} d\phi \int_{-\pi/2}^{\pi/2} d\varphi\cos^2\varphi\cos(\phi-\theta_B)e^{i2ka\cos(\beta/2)\cos(\phi-\theta_B)\cos\varphi} \\ &= \frac{ka^2\cos(\beta/2)}{2\pi}\int_{-\pi/2+|\beta|/2}^{\pi/2-|\beta|/2} d\phi \int_{-\pi/2}^{\pi/2} d\varphi\cos^2\varphi\cos\phi e^{i2ka\cos(\beta/2)\cos\phi\cos\varphi} \end{aligned}$$

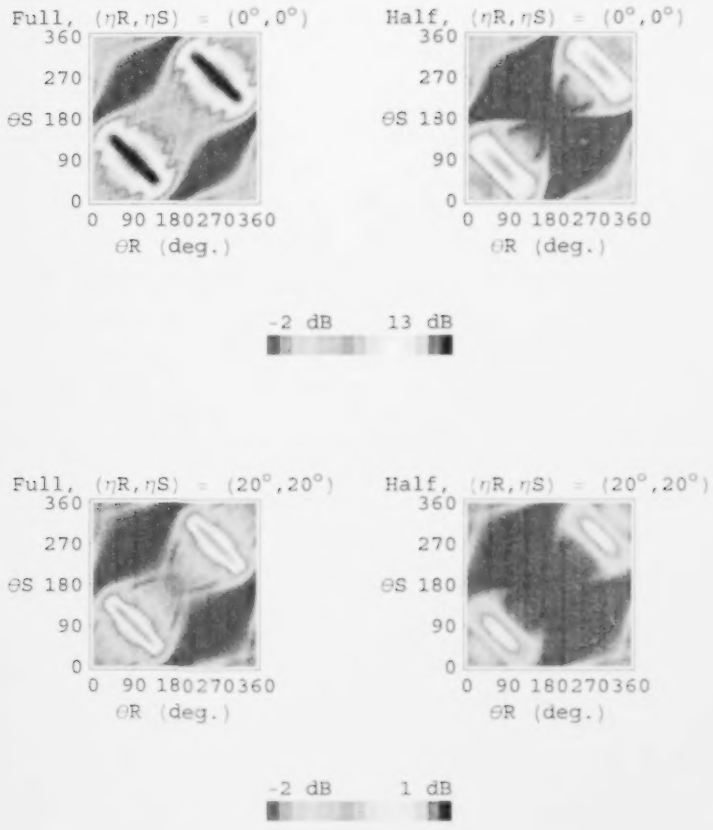

Figure 14: A plot of T.S. $= 10\log(10^{-2/10} + |g(\eta_r, \eta_s, \theta_r, \theta_s)|^2)$ for the full and half vertical elliptical cylinder, where the half elliptical cylinder faces the positive x-direction. The radii of the elliptical cylinder are $a = 3.0$ m, $b = 7.0\tan[10.0^o]$ m ≈ 1.23 m, the height $H = 3.7$ m, and the frequency $f = 500$ Hz. The top graphs show the in-plane case $\{\eta_r, \eta_s, \theta_r, \theta_s\} = \{0, 0, \theta_r, \theta_s\}$, the bottom graphs show the out-of-plane case $\{\eta_r, \eta_s, \theta_r, \theta_s\} = \{20^o, 20^o, \theta_r, \theta_s\}$. The two graphs in the right column give a model for the truncated elliptical sail front.

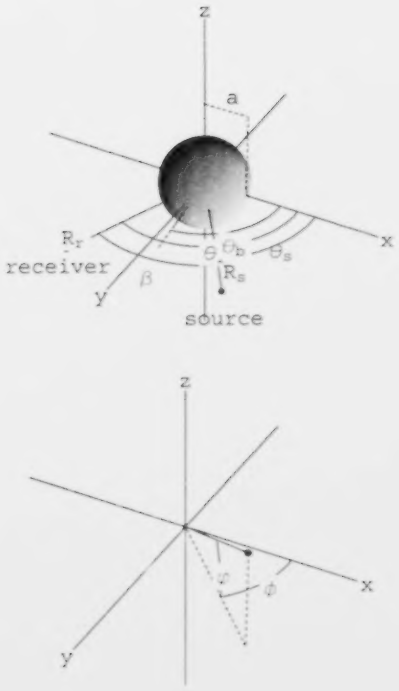

Figure 15: The in-plane bistatic case for the sphere of radius a.

$$
\begin{aligned}
&= \frac{2ka^2\cos(\beta/2)}{\pi}\int_0^{\pi/2-|\beta|/2} d\phi \int_0^{\pi/2} d\varphi \cos^2\varphi \cos\phi e^{i2ka\cos(\beta/2)\cos\phi\cos\varphi} \\
&= \frac{2ka^2\cos(\beta/2)}{\pi}\int_0^{\pi/2} d\phi \int_0^{\pi/2} d\varphi \cos^2\varphi \cos(\phi) e^{i2ka\cos(\beta/2)\cos\phi\cos\varphi} + \\
&\frac{2ka^2\cos(\beta/2)}{\pi}\int_{\pi/2}^{\pi/2-|\beta|/2} d\phi \int_0^{\pi/2} d\varphi \cos^2\varphi \cos\phi e^{i2ka\cos(\beta/2)\cos\phi\cos\varphi} \\
&= \frac{ia}{2}[e^{ika\cos(\beta/2)}\frac{\sin[ka\cos(\beta/2)]}{ka\cos(\beta/2)} - e^{2ika\cos(\beta/2)}] + \\
&\frac{2ka^2\cos(\beta/2)}{\pi}\int_{\pi/2}^{\pi/2-|\beta|/2} d\phi \int_0^{\pi/2} d\varphi \cos^2\varphi \cos\phi e^{i2ka\cos(\beta/2)\cos\phi\cos\varphi} \\
&= \frac{ia}{2}[e^{ika\cos(\beta/2)}\frac{\sin[ka\cos(\beta/2)]}{ka\cos(\beta/2)} - e^{2ika\cos(\beta/2)}] - \\
&\frac{2ka^2\cos(\beta/2)}{\pi}\int_0^{|\beta|/2} d\phi \int_0^{\pi/2} d\varphi \cos^2\varphi \sin\phi e^{i2ka\cos(\beta/2)\sin\phi\cos\varphi}.
\end{aligned}
\tag{78}
$$

The first term above is just the bistatic prediction

$$
g_{\text{bistatic}} = \frac{ia}{2}[e^{ika\cos(\beta/2)}\frac{\sin[ka\cos(\beta/2)]}{ka\cos(\beta/2)} - e^{2ika\cos(\beta/2)}], \tag{79}
$$

while the second term can be written as

$$
g - g_{\text{bistatic}} = -\frac{2ka^2\cos(\beta/2)}{\pi}\int_0^{|\beta|/2} d\phi \int_0^{\pi/2} d\varphi \cos^2\varphi \sin\phi e^{i2ka\cos(\beta/2)\sin\phi\cos\varphi}. \tag{80}
$$

For the case $2ka\cos(\beta/2) >> 1$, the ϕ integration can be approximated with a integration by parts method to give the end-point contribution:

$$
\int_0^{|\beta|/2} d\phi \sin\phi e^{i2ka\cos(\beta/2)\sin\phi\cos\varphi} \approx \frac{\sin(|\beta|/2)}{i2ka\cos^2(\beta/2)\cos\varphi} e^{i2ka\cos(\beta/2)\sin(|\beta|/2)\cos\varphi}. \tag{81}
$$

This gives

$$
\begin{aligned}
g - g_{\text{bistatic}} &= -\frac{a}{\pi}\frac{\sin(|\beta|/2)}{i\cos(\beta/2)}\int_0^{\pi/2} d\varphi \cos\varphi e^{ika\sin(|\beta|)\cos\varphi} \\
&\approx \frac{ia}{2}\frac{\sin(|\beta|/2)}{\cos(\beta/2)}\{E_1(ka\sin(|\beta|)) + iJ_1(ka\sin(|\beta|))\}, \quad 2ka\cos(\beta/2) >> 1.
\end{aligned}
\tag{82}
$$

If one substitutes the asymptotic representation for the Bessel functions one obtains

$$
g - g_{\text{bistatic}} \approx \frac{ia}{2}\frac{\sin(|\beta|/2)}{\cos(\beta/2)}\sqrt{\frac{2}{\pi ka\sin(|\beta|)}} e^{ika\sin(|\beta|)-i\pi/4}, \quad 2ka\cos(\beta/2) >> 1. \tag{83}
$$

This representation fails as $\beta/2 \to \pi/2$. By expanding the exponential in Eq. (80) one obtains the series representation

$$
g - g_{\text{bistatic}} = -\frac{ka^2\cos(\beta/2)}{\sqrt{\pi}}\sum_{n=0}^{\infty}\frac{a_n(i2ka\cos(\beta/2))^n}{n!}, \quad 2ka\cos(\beta/2) << 1. \tag{84}
$$

where

$$
a_n = \frac{\Gamma[\frac{3+n}{2}]}{\Gamma[2+\frac{n}{2}]}\int_0^{|\beta|/2} d\phi \sin^{n+1}\phi. \tag{85}
$$

The a_n obey the recurrence relation

$$\begin{aligned} a_n &= \frac{n}{n+2}a_{n-2} - \frac{\Gamma[\frac{3+n}{2}]}{(n+1)\Gamma[2+\frac{n}{2}]}\sin^n(|\beta|/2)\cos(|\beta|/2), \\ a_0 &= \sqrt{\pi}\sin^2(|\beta|/4), \\ a_1 &= \frac{1}{3\sqrt{\pi}}(|\beta| - \sin(|\beta|)), \\ a_1 &= \frac{1}{2}\sqrt{\pi}(2+\cos(|\beta|/2))\sin^4(|\beta|/4)). \end{aligned} \tag{86}$$

which is useful in the numerical evaluation of Eq. (84). To lowest order one obtains

$$g - g_{\text{bistatic}} = -ka^2\cos(\beta/2)\sin^2(|\beta|/4), \quad 2ka\cos(\beta/2) << 1, \tag{87}$$

The two representations given in Eqs. (82), (84) can be meshed together to give an approximation for the scattering strength over all angles for $ka >> 1$. Some numerical examples are shown in Fig. 16. The previous results are valid for $|\beta| < \pi$, otherwise replace $|\beta| \to 2\pi - |\beta|$.

In evaluating the bistatic term, use has been made of the intermediate results

$$\int_0^{\pi/2} d\phi \int_0^{\pi/2} d\varphi \cos^2\varphi \cos\phi\, e^{i2x\cos\phi\cos\varphi} = \frac{i\pi}{8x}\{e^{ix}\frac{\sin x}{x} - e^{2ix}\} \tag{88}$$

$$\int_0^{\pi/2} d\varphi \cos^2\varphi\, e^{ix\cos\varphi} = \frac{\pi}{4}\{[J_0(x) - J_2(x)] - i[E_0(x) - E_2(x)]\} \tag{89}$$

8.2 Out-of-plane scattering for the sphere

For the out-of-plane case

$$\begin{aligned} \vec{n} &= (\cos\varphi\cos\phi, \cos\varphi\sin\phi, \sin\varphi), \\ dA &= a^2\cos\varphi\, d\varphi\, d\phi, \\ \vec{r} &= a(\cos\varphi\cos\phi, \cos\varphi\sin\phi, \sin\varphi). \end{aligned} \tag{90}$$

and

$$\begin{aligned} \vec{k}_s &= k(-\cos\eta_s\cos\theta_s, -\cos\eta_s\sin\theta_s, -\sin\eta_s), \\ \vec{k}_r &= k(-\cos\eta_r\cos\theta_r, -\cos\eta_r\sin\theta_r, -\sin\eta_r). \end{aligned} \tag{91}$$

This gives the result

$$\begin{aligned} &(\vec{k}_s + \vec{k}_s)\cdot\vec{n} = \\ &-k[(\cos\eta_s\cos\theta_s + \cos\eta_r\cos\theta_r)\cos\varphi\cos\phi + (\cos\eta_s\sin\theta_s + \cos\eta_r\sin\theta_r)\cos\varphi\sin\phi + (\sin\eta_s + \sin\eta_r)\sin\varphi], \\ &(\vec{k}_s + \vec{k}_s)\cdot\vec{r} = \\ &-ka[(\cos\eta_s\cos\theta_s + \cos\eta_r\cos\theta_r)\cos\varphi\cos\phi + (\cos\eta_s\sin\theta_s + \cos\eta_r\sin\theta_r)\cos\varphi\sin\phi + (\sin\eta_s + \sin\eta_r)\sin\varphi]. \end{aligned} \tag{92}$$

Because of the symmetry of the sphere, the out-of-plane case can be obtained from the results of the previous section by re-expressing the angular coordinates $\beta = \beta(\eta_r, \eta_s, \theta_r, \theta_s)$ and by setting $g'(\eta_r, \eta_s, \theta_r, \theta_s) = g(\beta(\eta_r, \eta_s, \theta_r, \theta_s))$, where g' is the out-of-plane scattering strength and $g(\beta)$ is the scattering strength for the in plane case given in the previous section. Hence we have to re-express the bistatic angle β in terms of the coordinates $\{\eta_r, \eta_s, \theta_r, \theta_s\}$. From Eq. (91),

$$\beta = \arccos[\vec{k}_s\cdot\vec{k}_r/k^2] = \arccos[(\cos\eta_s\cos\theta_s\cos\eta_r\cos\theta_r + \cos\eta_s\sin\theta_s\cos\eta_r\sin\theta_r + \sin\eta_s\sin\eta_r)]. \tag{93}$$

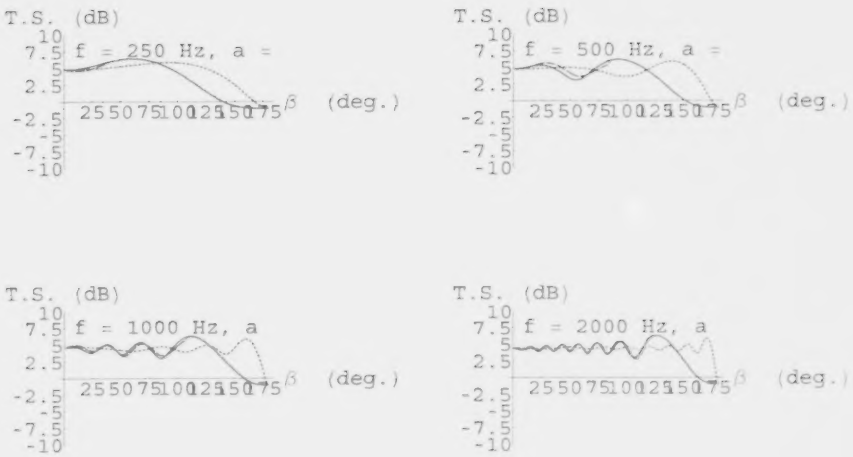

Figure 16: Comparison of target strength formulae for the in-plane bistatic case for the sphere of radius $a = 2.8$ m and frequencies $f = 250,\ 500,\ 1000,\ 2000$ Hz. The short dashed line gives the Bistatic Theorem prediction in Eq. (79)(plus a constant term) Target Strength $= 10\log[10^{-1/10} + |g_{\text{bistatic}}|^2]$, the long dashed line gives the asymptotic model given by Eqs. (82, (84), while the solid line gives the exact result Target Strength $= 10\log[10^{-1/10} + |g|^2]$ given by Eq. (78). The maximum difference between the exact result and the Bistatic Theorem result could amount to ≈ 5 dB as β approaches 180 degrees, depending on the size of the constant term. Note that the maximum target strength does not occur at the monostatic case $\beta = 0$ due to the oscillatory nature of the integrand in Eq. (4).

In the special case $\eta_s = \eta_r = 0$ this reduces to the usual result $|\beta| = |\theta_r - \theta_s|$.

If one identifies the bisector of $\vec{k}_s$ and $\vec{k}_r$ as $\vec{k}_B$, then

$$\begin{aligned}\vec{k}_B &= -k(\cos\eta_B\cos\theta_B, \cos\eta_B\sin\theta_B, \sin\eta_B) = \frac{1}{2}\{\vec{k}_s + \vec{k}_r\} \\ &= -\frac{k}{2}(\cos\eta_s\cos\theta_s + \cos\eta_r\cos\theta_r, \cos\eta_s\sin\theta_s + \cos\eta_r\sin\theta_r, \sin\eta_s + \sin\eta_r). \end{aligned} \tag{94}$$

In keeping with the method used in the Drumheller, Hazen, and Gilroy the effect of truncating the sphere to a hemisphere facing the +x-axis can be modelled by multiplying the scattering strength for the full sphere by the windowing function

$$\mathrm{If}[\cos\eta_s\cos\theta_s + \cos\eta_r\cos\theta_r \geq 0, 1, 0] = \begin{cases} 1, & \text{if } \cos\eta_s\cos\theta_s + \cos\eta_r\cos\theta_r \geq 0, \\ 0, & \text{if } \cos\eta_s\cos\theta_s + \cos\eta_r\cos\theta_r \leq 0. \end{cases} \tag{95}$$

Hence for the hemisphere facing the ±x-axis the scattering strength is

$$\begin{aligned} g &\approx \left\{ \frac{ia}{2}[e^{ika\cos(\beta/2)}\frac{\sin[ka\cos(\beta/2)]}{ka\cos(\beta/2)} - e^{2ika\cos(\beta/2)}] + \right. \\ &\left. \frac{ia}{2}\frac{\sin(|\beta|/2)}{\cos(\beta/2)}\{E_1(ka\sin(|\beta|)) + \imath J_1(ka\sin(|\beta|))\}\right\} \mathrm{If}[\cos\eta_s\cos\theta_s + \cos\eta_r\cos\theta_r \overset{\geq}{\leq} 0, 1, 0], \quad 2ka\cos(\beta/2) >> 1, \\ &\approx \left\{ \frac{ia}{2}[e^{ika\cos(\beta/2)}\frac{\sin[ka\cos(\beta/2)]}{ka\cos(\beta/2)} - e^{2ika\cos(\beta/2)}] - \right. \\ &\left. ka^2\cos(\beta/2)\sin^2(|\beta|/4)\right\} \mathrm{If}[\cos\eta_s\cos\theta_s + \cos\eta_r\cos\theta_r \overset{>}{<} 0, 1, 0], \quad 2ka\cos(\beta/2) << 1; \\ &\beta = \arccos[(\cos\eta_s\cos\theta_s\cos\eta_r\cos\theta_r + \cos\eta_s\sin\theta_s\cos\eta_r\sin\theta_r + \sin\eta_s\sin\eta_r)]. \end{aligned} \tag{96}$$

For the bow hemisphere of radius r_1 one obtains

$$\begin{aligned} x_{bowhemisphere} &= \{L/2, 0, 0\}, \\ y_{bowhemisphere} &\approx \left\{ \frac{ir_1}{2}[e^{ikr_1\cos(\beta/2)}\frac{\sin[kr_1\cos(\beta/2)]}{kr_1\cos(\beta/2)} - e^{2ikr_1\cos(\beta/2)}] + \right. \\ &\left. \frac{ir_1}{2}\frac{\sin(|\beta|/2)}{\cos(\beta/2)}\{E_1(kr_1\sin(|\beta|)) + \imath J_1(kr_1\sin(|\beta|))\}\right\} \\ &\mathrm{If}[\cos\eta_s\cos\theta_s + \cos\eta_r\cos\theta_r > 0, 1, 0]e^{-\imath(\vec{k}_s+\vec{k}_r)\cdot\vec{x}_{bowhemisphere}}, \quad 2kr_1\cos(\beta/2) >> 1, \\ &\approx \left\{ \frac{ir_1}{2}[e^{ikr_1\cos(\beta/2)}\frac{\sin[kr_1\cos(\beta/2)]}{kr_1\cos(\beta/2)} - e^{2ikr_1\cos(\beta/2)}] - kr_1^2\cos(\beta/2)\sin^2(|\beta|/4)\right\} \\ &\mathrm{If}[\cos\eta_s\cos\theta_s + \cos\eta_r\cos\theta_r > 0, 1, 0]e^{-\imath(\vec{k}_s+\vec{k}_r)\cdot\vec{x}_{bowhemisphere}}, \quad 2kr_1\cos(\beta/2) << 1; \\ &\beta = \arccos[(\cos\eta_s\cos\theta_s\cos\eta_r\cos\theta_r + \cos\eta_s\sin\theta_s\cos\eta_r\sin\theta_r + \sin\eta_s\sin\eta_r)]. \end{aligned} \tag{97}$$

For a stern hemisphere of radius r_1 one obtains

$$\begin{aligned} x_{sternhemisphere} &= \{-L/2, 0, 0\}, \\ y_{sternhemisphere} &\approx \left\{ \frac{ir_1}{2}[e^{ikr_1\cos(\beta/2)}\frac{\sin[kr_1\cos(\beta/2)]}{kr_1\cos(\beta/2)} - e^{2ikr_1\cos(\beta/2)}] + \right. \\ &\left. \frac{ir_1}{2}\frac{\sin(|\beta|/2)}{\cos(\beta/2)}\{E_1(kr_1\sin(|\beta|)) + \imath J_1(kr_1\sin(|\beta|))\}\right\} \\ &\mathrm{If}[\cos\eta_s\cos\theta_s + \cos\eta_r\cos\theta_r \leq 0, 1, 0]e^{-\imath(\vec{k}_s+\vec{k}_r)\cdot\vec{x}_{sternhemisphere}}, \quad 2kr_1\cos(\beta/2) >> 1, \\ &\approx \left\{ \frac{ir_1}{2}[e^{ikr_1\cos(\beta/2)}\frac{\sin[kr_1\cos(\beta/2)]}{kr_1\cos(\beta/2)} - e^{2ikr_1\cos(\beta/2)}] - kr_1^2\cos(\beta/2)\sin^2(|\beta|/4)\right\} \\ &\mathrm{If}[\cos\eta_s\cos\theta_s + \cos\eta_r\cos\theta_r \leq 0, 1, 0]e^{-\imath(\vec{k}_s+\vec{k}_r)\cdot\vec{x}_{sternhemisphere}}, \quad 2kr_1\cos(\beta/2) << 1; \\ &\beta = \arccos[(\cos\eta_s\cos\theta_s\cos\eta_r\cos\theta_r + \cos\eta_s\sin\theta_s\cos\eta_r\sin\theta_r + \sin\eta_s\sin\eta_r)]. \end{aligned} \tag{98}$$

The previous results are valid for $|\beta| < \pi$, otherwise replace $|\beta| \to 2\pi - |\beta|$. A numerical example is shown in Fig. 17. Again as in Fig. 16, the maximum target strength does not occur in the monostatic case $\theta_r = \theta_s$, due to the oscillatory nature of the integrand in the Kirchhoff/Fraunhofer integral Eq. (4) for the scattering strength. Note that this fairly crude truncation method (one simply cuts out a region of the full sphere plot) could be improved, see comments in the Summary.

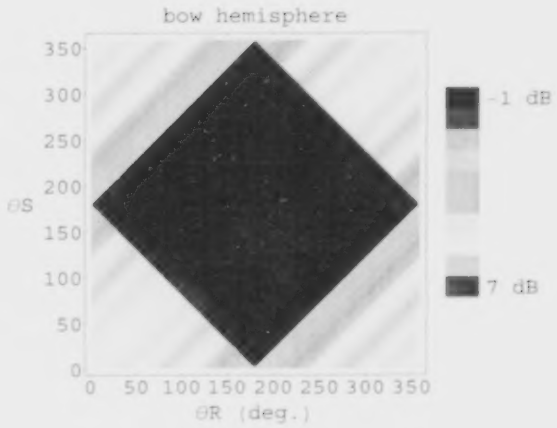

Figure 17: A plot of Target Strength $= 10\log[10^{-1/10} + |\eta_{\text{bowhemisphere}}|^2]$, for the hemisphere of radius $a = 2.8$ m and frequency $f = 500$ Hz. The angular parameters are given by $\{\eta_r, \eta_s, \theta_r, \theta_s\} = \{40°, 40°, \theta_r, \theta_s\}$, so the source/receiver lies 40 degrees above the $x - y$ plane. As in Fig. 16, the maximum target strength does not occur in the monostatic case, due to the oscillatory nature of the integrand in the Kirchhoff integral.

9 The truncated cone

9.1 Introduction

Consider the truncated horizontal cone, whose surface is given in parametric form by

$$\vec{r} = \{x, (\rho_0 + x\tan\alpha)\cos\varphi, (\rho_0 + x\tan\alpha)\sin\varphi\}, \tag{99}$$

where $-L/2 \le x \le L/2$, $-\pi \le \varphi \le \pi$. The abbreviations $\rho_0 = (\rho_1 + \rho_2)/2$, $\rho_1 = \rho_0 - L\tan(\alpha)/2$, $\rho_2 = \rho_0 + L\tan(\alpha)/2$ will prove useful. A sketch of a representative cone is shown in Fig. 18

The unit normal and the differential area are given by

$$\begin{aligned} \vec{n} &= \{-\sin\alpha, \cos\alpha\cos\varphi, \cos\alpha\sin\varphi\} \\ \vec{n}dS &= -\vec{r}_x \times \vec{r}_\varphi \, dx\, d\varphi \\ &= \rho\{-\tan\alpha, \cos\varphi, \sin\varphi\}\, dx\, d\varphi, \end{aligned} \tag{100}$$

where $\rho(x) = (\rho_0 + x\tan\alpha)$.

The viewed/illuminated areas are given formally by the conditions $\vec{k}_{R/S} \cdot \vec{n} = 0$ which gives

$$-\sin\alpha\cos\eta_{R/S}\cos\theta_{R/S} + \cos\alpha\cos\varphi\cos\eta_{R/S}\sin\theta_{R/S} + \cos\alpha\sin\varphi\sin\eta_{R/S} = 0. \tag{101}$$

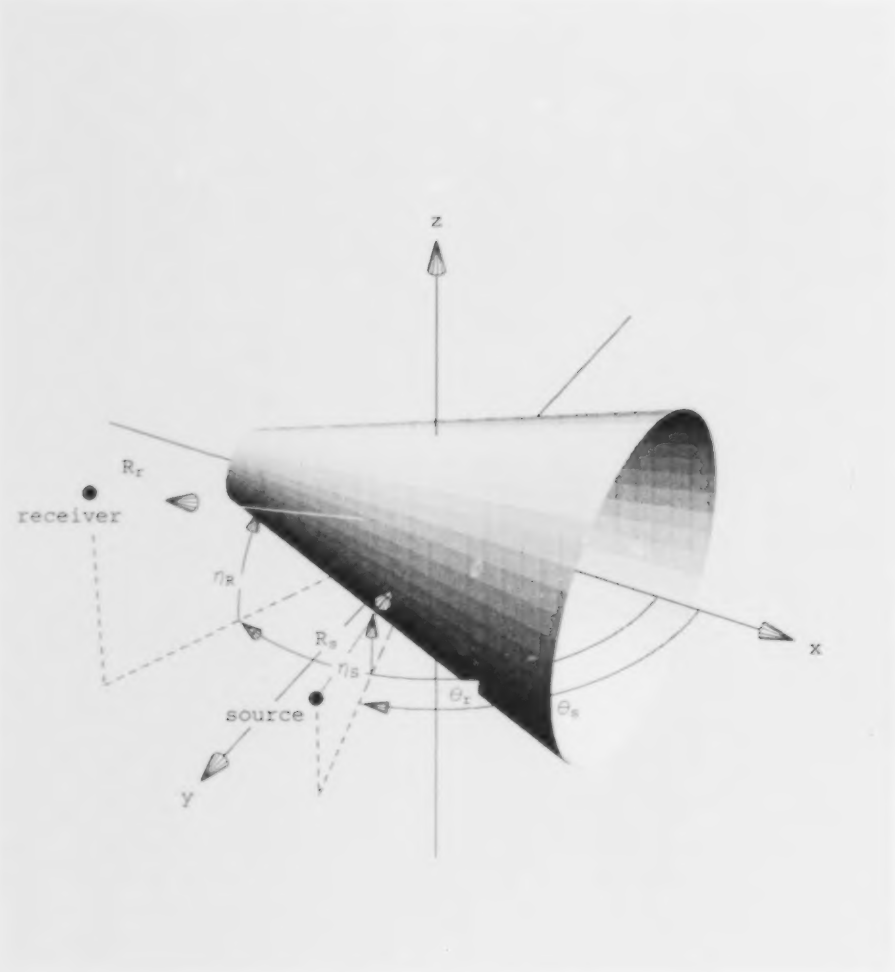

Figure 18: The horizontal truncated cone.

This can be rewritten as

$$\cos\alpha\sqrt{(\cos\eta_{R/S}\sin\theta_{R/S})^2+(\sin\eta_{R/S})^2}\cos(\varphi-\omega)=\sin\alpha\cos\eta_{R/S}\cos\theta_{R/S}. \tag{102}$$

where $\omega=\arctan[\sin\eta_{R/S}/(\cos\eta_{R/S}\sin\theta_{R/S})]$.

9.2 Special case: in-plane scattering

9.2.1 The backscattering case

In the special case of monostatic $\theta_{R/S}=\theta$ in-plane scattering $\eta_{R/S}=0$

$$\cos\varphi=\tan\alpha\cot\theta. \tag{103}$$

One obtains the solution for the upper integration limit (if arccos is the principal branch)

$$\begin{aligned}
\varphi_{upper}(\theta) &= 0, \quad 0\le\theta\le\alpha,\\
\varphi_{upper}(\theta) &= \arccos(\cot\theta\tan\alpha), \quad \alpha<\theta<\pi-\alpha,\\
\varphi_{upper}(\pi/2) &= \pi/2,\\
\varphi_{upper}(\theta) &= \pi, \quad \pi-\alpha\le\theta\le\pi,\\
\varphi_{upper}(\theta) &= \pi+\varphi_{upper}(2\pi-\theta), \quad \pi\le\theta\le 2\pi.
\end{aligned} \tag{104}$$

and for the lower limit

$$\begin{aligned}
\varphi_{lower}(\theta) &= 0, \quad 0\le\theta\le\alpha,\\
\varphi_{lower}(\theta) &= -\arccos(\cot\theta\tan\alpha), \quad \alpha<\theta<\pi-\alpha,\\
\varphi_{lower}(\pi/2) &= -\pi/2,\\
\varphi_{lower}(\theta) &= -\pi, \quad \pi-\alpha\le\theta\le\pi,\\
\varphi_{lower}(\theta) &= \pi+\varphi_{lower}(2\pi-\theta), \quad \pi\le\theta\le 2\pi+\alpha.
\end{aligned} \tag{105}$$

This choice of integration limits ensures that $g(\theta)=g(2\pi-\theta)$. The integration limits are shown below in Fig. 19.

For $0\le\theta\le\pi$ the scattering strength becomes

$$\begin{aligned}
g &= -\frac{1}{4\pi}\int_{\text{illum. area}}(\vec{k}_s+\vec{k}_s)\cdot\vec{n}\,e^{-i(\vec{k}_s+\vec{k}_s)\cdot\vec{r}}dS=\\
&= \frac{k}{2\pi\cos\alpha}\int_{-L/2}^{L/2}dx\int_{\varphi_{lower}}^{\varphi_{upper}}d\varphi(\rho_0+x\tan\alpha)[-\cos\theta\sin\alpha+\sin\theta\cos\alpha\cos\varphi]\times\\
&\quad e^{2ik[x\cos\theta+(\rho_0+x\tan\alpha)\sin\theta\cos\varphi]}.
\end{aligned} \tag{106}$$

For $\pi\le\theta\le 2\pi$, then is easy to show that $g(\theta)=g(2\pi-\theta)$ using the integration limits shown in Fig. 19.

Now one can examine the various interesting sub-cases:

$$g(0\le\theta\le\alpha) = 0, \tag{107}$$

$$\begin{aligned}
g(\theta=\pi) &= k\tan\alpha\int_{-L/2}^{L/2}dx(\rho_0+x\tan\alpha)e^{-2ikx}\\
&= k\tan\alpha\left[\rho_0\frac{e^{-2ikx}}{(-2ik)}+\tan\alpha\{xe^{-2ikx}+\frac{e^{-2ikx}}{(-2ik)^2}\}\right]_{-L/2}^{L/2}\\
&= kL\tan\alpha\left[\rho_0\frac{\sin(kL)}{kL}+\tan\alpha\{\cos(kL)+\frac{\sin(kL)}{kL(-2ik)}\}\right], \text{ the exact pointy end-view}
\end{aligned} \tag{108}$$

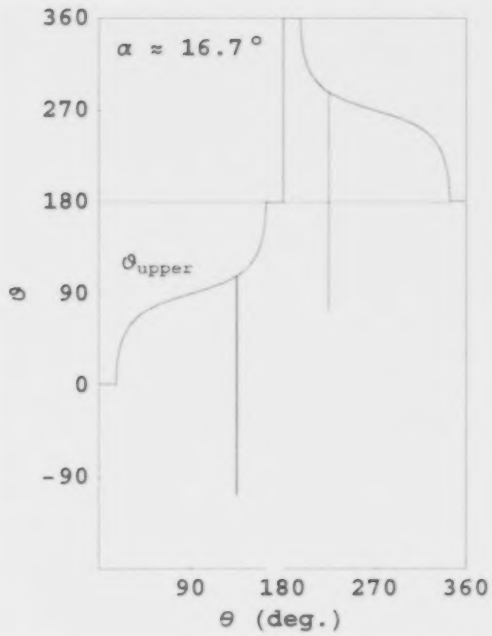

Figure 19: Integration limits for the monostatic case for the truncated cone. For the convention that $0 \leq \theta \leq 2\pi$, the integration region is given by $\varphi_{lower} \leq \varphi \leq \varphi_{upper}$. For $0 \leq \theta \leq \pi$, this is the vertical black line, for $\pi < \theta \leq 2\pi$ the vertical brown line.

$$
\begin{aligned}
g[\pi-\alpha\le\theta\le\pi] \;=\;& \\
&\frac{k}{2\pi\cos\alpha}\int_{-L/2}^{L/2}dx\int_{-\pi}^{\pi}d\varphi(\rho_0+x\tan\alpha)[-\cos\theta\sin\alpha+\sin\theta\cos\alpha\cos\varphi]e^{2ik[x\cos\theta+(\rho_0+x\tan\alpha)\sin\theta\cos\varphi]} \\
&=\frac{ke^{-2ik\rho_0\cos\theta\cot\alpha}}{\pi\sin\alpha}\int_{\rho_1}^{\rho_2}d\rho\,\rho\int_0^{\pi}d\varphi[-\cos\theta\sin\alpha+\sin\theta\cos\alpha\cos\varphi]e^{2ik\rho[\cos\theta\cot\alpha+\sin\theta\cos\varphi]} \\
&=\frac{e^{-2ik\rho_0\cos\theta\cot\alpha}}{4k\sin^2\theta\sin\alpha}\int_{2k\rho_1\sin\theta}^{2k\rho_2\sin\theta}dt\;t\,e^{it\cot\theta\cot\alpha}[-\cos\theta\sin\alpha J_0(t)+i\sin\theta\cos\alpha J_1(t)],
\end{aligned}
$$

the general pointy end-view. (109)

Now observe that the factor $\cot\theta\cot\alpha >> 1$ within the pointy end-view so an integration by parts works very well.

$$
\begin{aligned}
g[\pi-\alpha\le\theta\le\pi] \;\approx\;& \\
&\frac{e^{-2ik\rho_0\cos\theta\cot\alpha}}{2i\cos\theta\cos\alpha}\left\{\rho_2\,e^{2ik\rho_2\cos\theta\cot\alpha}[-\cos\theta\sin\alpha J_0(2k\rho_2\sin\theta)+i\sin\theta\cos\alpha J_1(2k\rho_2\sin\theta)]\;-\right. \\
&\left.\rho_1\,e^{2ik\rho_1\cos\theta\cot\alpha}[-\cos\theta\sin\alpha J_0(2k\rho_1\sin\theta)+i\sin\theta\cos\alpha J_1(2k\rho_1\sin\theta)]\right\}.
\end{aligned}
$$

the general pointy end-view. (110)

$$
\begin{aligned}
g(\theta=\pi/2) \;&=\; \frac{k}{2\pi}\int_{-L/2}^{L/2}dx\int_{-\pi/2}^{\pi/2}d\varphi(\rho_0+x\tan\alpha)\cos\varphi e^{2ik(\rho_0+x\tan\alpha)\cos\varphi} \\
&=\; \frac{k}{\pi\tan\alpha}\int_{\rho_1}^{\rho_2}d\rho\int_0^{\pi/2}d\varphi\rho\cos\varphi e^{2ik\rho\cos\varphi} \\
&=\; \frac{ik}{2\tan\alpha}\int_{\rho_1}^{\rho_2}d\rho\,\rho\{J_1(2k\rho)-iE_1(2k\rho)\} \\
&=\; \frac{i}{8k\tan\alpha}\int_{2k\rho_1}^{2k\rho_2}dt\,t\{J_1(t)-iE_1(t)\} \\
&=\; \frac{1}{4i\pi\tan\alpha}[-\pi\rho_1J_0(2k\rho_1)+\pi\rho_2J_0(2k\rho_2)-i\pi\rho_1H_0(2k\rho_1)+i\pi\rho_2H_0(2k\rho_2)\;+ \\
&\quad \pi\rho_1\,{}_1F_2(\tfrac{1}{2};1,\tfrac{3}{2};-k^2\rho_1^2)]-\pi\rho_2\,{}_1F_2(\tfrac{1}{2};1,\tfrac{3}{2};-k^2\rho_2^2)]\;+ \\
&\quad 2ik\rho_1^2\,{}_2F_3(1,1;\tfrac{3}{2},\tfrac{3}{2},2;-k^2\rho_1^2)]-2ik\rho_2^2\,{}_2F_3(1,1;\tfrac{3}{2},\tfrac{3}{2},2;-k^2\rho_2^2)\Big],\ \text{the exact side-view.}
\end{aligned}
\tag{111}
$$

$$
\begin{aligned}
g[\pi-\alpha\le\theta\le\alpha] =& \\
&\frac{k}{2\pi\cos\alpha}\int_{-L/2}^{L/2}dx\int_{\varphi_{1}(x)}^{\varphi_{2}(x)}d\varphi(\rho_0+x\tan\alpha)[-\cos\theta\sin\alpha+\sin\theta\cos\alpha\cos\varphi]e^{2ik[x\cos\theta+(\rho_0+x\tan\alpha)\sin\theta\cos\varphi]} \\
&\approx\frac{ke^{-2ik\rho_0\cos\theta\cot\alpha}}{2\pi\sin\alpha}\int_{\rho_1}^{\rho_2}d\rho\,\rho\int_{-\pi/2}^{\pi/2}d\varphi[-\cos\theta\sin\alpha+\sin\theta\cos\alpha\cos\varphi]e^{2ik\rho[\cos\theta\cot\alpha+\sin\theta\cos\varphi]} \\
&\approx\frac{ke^{-2ik\rho_0\cos\theta\cot\alpha}}{2\sin\alpha}\int_{\rho_1}^{\rho_2}d\rho\,\rho\,e^{2ik\rho\cos\theta\cot\alpha}[-\cos\theta\sin\alpha\{J_0(2k\rho\sin\theta)-iE_0(2k\rho\sin\theta)\}+
\end{aligned}
$$

$$
\begin{aligned}
& i\sin\theta\cos\alpha\{J_1(2k\rho\sin\theta) - iE_1(2k\rho\sin\theta)\}] \\
\approx \frac{e^{-2ik\rho_0\cos\theta\cot\alpha}}{8k\sin^2\theta\sin\alpha} \int_{2k\rho_1\sin\theta}^{2k\rho_2\sin\theta} & dt\ t\ e^{it\cot\theta\cot\alpha}[-\cos\theta\sin\alpha\{J_0(t) - iE_0(t)\} + \\
& i\sin\theta\cos\alpha\{J_1(t) - iE_1(t)\}], \quad \text{the general side-view.} \qquad (112)
\end{aligned}
$$

At this point there are two possibilities: one could perform these integrals in terms of more general functions (see Appendix C), or one could substitute the asymptotic approximations for the Bessel functions given in Appendix B, assuming $2k\rho_{1,2}\sin\theta >> 1$. One notes that in the general side-view $\sin\theta$ never gets smaller than $\sin\alpha$. From the Appendix B

$$
J_0(x) - iE_0(x) \approx iJ_1(x) + E_1(x) \approx \sqrt{2/(\pi x)}e^{i(x-\pi/4)},
$$

this gives

$$
\begin{aligned}
& g[\pi - \alpha \le \theta \le \alpha] \\
& \quad \approx \frac{\sqrt{2}\sin(\theta-\alpha)e^{-2ik\rho_0\cos\theta\cot\alpha - i\pi/4}}{\sqrt{\pi}8k\sin^2\theta\sin\alpha} \int_{2k\rho_1\sin\theta}^{2k\rho_2\sin\theta} dt\ \sqrt{t}\ e^{it[1+\cot\theta\cot\alpha]}, \quad \text{the general side-view.} \qquad (113)
\end{aligned}
$$

Now consider the result

$$
\int_0^z dt\ \sqrt{t}\ e^{ita} = -i\sqrt{z}\frac{e^{iaz}}{a} - \frac{(-1)^{\frac{1}{4}}\sqrt{\pi}\,\mathrm{Erf}[(-1)^{\frac{3}{4}}\sqrt{a}\sqrt{z}]}{2a^{\frac{3}{2}}},
$$

valid for any real a or z provided one uses principal values for all multiple valued roots and $\mathrm{Erf}[x] = (2/\pi)\int_0^z \exp[-t^2]dt$ is the error function. This yields the approximation

$$
\begin{aligned}
& g[\pi - \alpha \le \theta \le \alpha] \\
& \approx \frac{\sqrt{2}\sin(\theta-\alpha)e^{-2ik\rho_0\cos\theta\cot\alpha - i\pi/4}}{\sqrt{\pi}8k\sin^2\theta\sin\alpha} \left\{ -i\frac{\sin\theta\sin\alpha\sqrt{2k\sin\theta}}{\cos(\theta-\alpha)}[\sqrt{\rho_2}e^{i2k\rho_2\cos(\theta-\alpha)/\sin\alpha} - \sqrt{\rho_1}e^{i2k\rho_1\cos(\theta-\alpha)/\sin\alpha}] - \right. \\
& \left. \frac{i(-1)^{\frac{1}{4}}\sqrt{\pi}(\sin\theta\sin\alpha)^{3/2}}{2(\cos[\theta-\alpha])^{\frac{3}{2}}}\{\mathrm{Erf}[(-1)^{\frac{1}{4}}\sqrt{2k\rho_2\cos(\theta-\alpha)/\sin\alpha}] - \mathrm{Erf}[(-1)^{\frac{3}{4}}\sqrt{2k\rho_1\cos(\theta-\alpha)/\sin\alpha}]\} \right\}, \\
& \qquad\qquad \text{the general side-view.} \qquad (114)
\end{aligned}
$$

The Hazen, Gilroy, Drumheller (HGD) side-view model is just an expansion of the error functions above. By joining together the end-view and the side-view approximation one obtains a very accurate model of the monostatic scattering strength as shown in Fig. 20.

Hazen/Gilroy/Drumheller model [HGD] have produced a similar model for the side-view for monostatic scattering, with a different model for the end-view. Details of the HGD model are given in the accompanying software. A comparison of an exact numerical calculation and the HGD model is shown in Figs. 21.

Conclusion: the HGD model can be easily improved near the pointy-end-view by using their side-view expression for $\alpha < \theta < \pi - \alpha$ and then adjoining on Eq. (110) for the end view for $\pi - \alpha < \theta < \pi$. The side-view and Eq. (110) match up very closely at $\theta = \pi - \alpha$ so there is no need to introduce any smoothing functions near $\theta = \pi - \alpha$, or cut-offs.

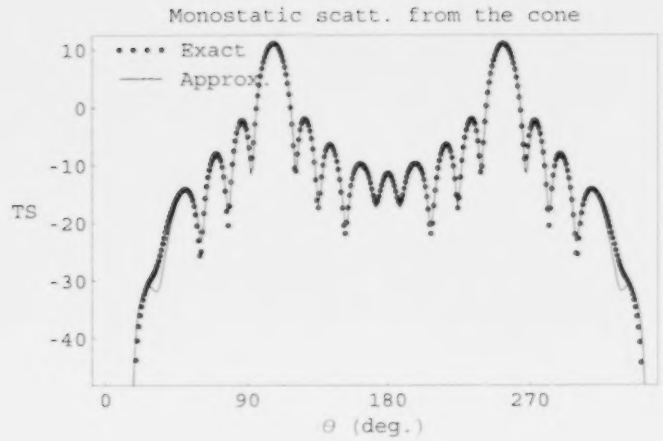

Figure 20: Target strength for the monostatic case for the cone with frequency $f = 500$ Hz, $\rho_2 = 2.8$ m, $\rho_1 = 1.0$, $L = 6.0$ m and cone half-angle $\alpha \approx 16.7$ degrees. The data points give the full Kirchhoff result Target Strength $= 10\log[|g(\theta)|^2]$, the solid line gives Target Strength $= 10\log[|g_{approx.}(\theta)|^2]$ given by Eqs. (110) and (114).

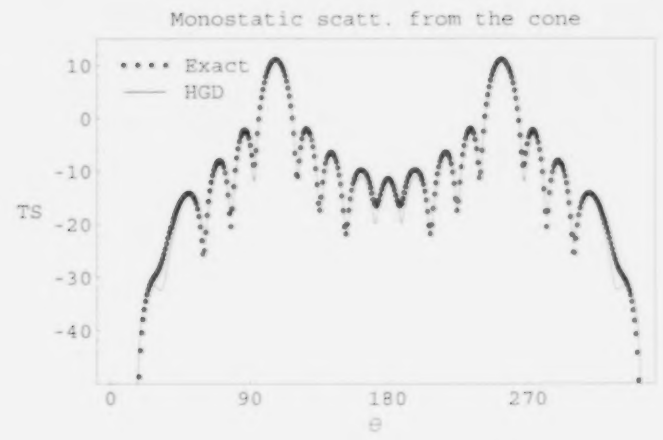

Figure 21: Target strength for the monostatic case for the cone with frequency $f = 500$ Hz, $\rho_2 = 2.0$ m, $\rho_1 = 1.0$, $L = 6.0$ m and cone half-angle $\alpha \approx 16.7$ degrees. The data points give the full Kirchhoff result Target Strength $= 10\log[|g(\theta)|^2]$, the solid line gives the Hazen/Gilroy/Drumheller model Target Strength $= 10\log[|g_{cone}(\theta)|^2]$. Note a small discrepancy near $\theta \approx \pi \pm \alpha$. This size of this error depends on the particular frequency.

Summary of monostatic formulae:

$$
\begin{aligned}
g(\theta) &= 0, \ 0 \le \theta \le \alpha; \\
g(\theta) &\approx \\
&\frac{\sqrt{2}\sin(\theta-\alpha)e^{-2ik\rho_0\cos\theta\cot\alpha-i\pi/4}}{\sqrt{\pi}8k\sin^2\theta\sin\alpha}\left\{-i\frac{\sin\theta\sin\alpha\sqrt{2k\sin\theta}}{\cos(\theta-\alpha)}[\sqrt{\rho_2}e^{i2k\rho_2\cos(\theta-\alpha)/\sin\alpha}-\sqrt{\rho_1}e^{i2k\rho_1\cos(\theta-\alpha)/\sin\alpha}]-\right. \\
&\left.\frac{i(-1)^{\frac{1}{2}}\sqrt{\pi}(\sin\theta\sin\alpha)^{3/2}}{2(\cos[\theta-\alpha])^{\frac{1}{2}}}\{\mathrm{Erf}[(-1)^{\frac{3}{4}}\sqrt{2k\rho_2\cos(\theta-\alpha)/\sin\alpha}]-\mathrm{Erf}[(-1)^{\frac{3}{4}}\sqrt{2k\rho_1\cos(\theta-\alpha)/\sin\alpha}]\}\right\}, \\
&\qquad\qquad \pi-\alpha \le \theta \le \alpha; \\
g(\theta) &\approx \frac{e^{-2ik\rho_0\cos\theta\cot\alpha}}{2i\cos\theta\cos\alpha}\left\{\rho_2\, e^{2ik\rho_2\cos\theta\cot\alpha}[-\cos\theta\sin\alpha J_0(2k\rho_2\sin\theta)+i\sin\theta\cos\alpha J_1(2k\rho_2\sin\theta)]-\right. \\
&\left.\rho_1\, e^{2ik\rho_1\cos\theta\cot\alpha}[-\cos\theta\sin\alpha J_0(2k\rho_1\sin\theta)+i\sin\theta\cos\alpha J_1(2k\rho_1\sin\theta)]\right\}, \pi-\alpha \le \theta \le \pi; \\
g(\theta) &= g(2\pi-\theta), \ \pi < \theta \le 2\pi; \\
g(\theta) &= g(Mod[\theta, 2\pi]), \text{ all other values of } \theta.
\end{aligned}
$$

9.2.2 In-plane scattering

In the more general case of in-plane scattering $\eta_{R/S} = 0$

$$\cos\varphi_{R/S} = \tan\alpha\cot\theta_{R/S}. \tag{115}$$

To define the integration areas for the Kirchhoff integral (if arccos is the principal branch) for the illuminated and viewed areas one must define the functions

$$
\begin{aligned}
\varphi_{Ru}(\theta) &= 0, \quad 0 \le \theta_R \le \alpha, \\
\varphi_{Ru}(\theta) &= \arccos(\cot\theta_R\tan\alpha), \quad \alpha < \theta_R < \pi-\alpha, \\
\varphi_{Ru}(\pi/2) &= \pi/2, \\
\varphi_{Ru}(\theta) &= \pi, \quad \pi-\alpha \le \theta_R \le \pi, \\
\varphi_{Ru}(\theta) &= \pi + \varphi_{Ru}(2\pi-\theta), \quad \pi \le \theta_R \le 2\pi,
\end{aligned} \tag{116}
$$

$$
\begin{aligned}
\varphi_{Rl}(\theta) &= 0, \quad 0 \le \theta_R \le \alpha, \\
\varphi_{Rl}(\theta) &= -\arccos(\cot\theta_R\tan\alpha), \quad \alpha < \theta_R < \pi-\alpha, \\
\varphi_{Rl}(\pi/2) &= -\pi/2, \\
\varphi_{Rl}(\theta) &= -\pi, \quad \pi-\alpha \le \theta_R \le \pi, \\
\varphi_{Rl}(\theta) &= \pi + \varphi_{Rl}(2\pi-\theta), \quad \pi \le \theta_R \le 2\pi,
\end{aligned} \tag{117}
$$

$$
\begin{aligned}
\varphi_{Su}(\theta) &= 0, \quad 0 \le \theta_S \le \alpha, \\
\varphi_{Su}(\theta) &= \arccos(\cot\theta_S\tan\alpha), \quad \alpha < \theta_S < \pi-\alpha, \\
\varphi_{Su}(\pi/2) &= \pi/2, \\
\varphi_{Su}(\theta) &= \pi, \quad \pi-\alpha \le \theta_S \le \pi, \\
\varphi_{Su}(\theta) &= \pi + \varphi_{su}(2\pi-\theta), \quad \pi \le \theta_R \le 2\pi,
\end{aligned} \tag{118}
$$

$$
\begin{aligned}
\varphi_{Sl}(\theta) &= 0, \quad 0 \le \theta_S \le \alpha, \\
\varphi_{Sl}(\theta) &= -\arccos(\cot\theta_S\tan\alpha), \quad \alpha < \theta_S < \pi-\alpha, \\
\varphi_{Sl}(\pi/2) &= -\pi/2, \\
\varphi_{Sl}(\theta) &= -\pi, \quad \pi-\alpha \le \theta_S \le \pi, \\
\varphi_{Sl}(\theta) &= \pi + \varphi_{sl}(2\pi-\theta), \quad \pi \le \theta_R \le 2\pi.
\end{aligned} \tag{119}
$$

For $0 \le \theta_R \le 2\pi$ the viewed area extends from $\varphi_{Rl} \le \varphi \le \varphi_{Ru}$: for $0 \le \theta_S \le 2\pi$ the illuminated area extends from $\varphi_{Sl} \le \varphi \le \varphi_{Su}$. The integration area is the intersection of these areas, keeping in mind that one reduces angles φ outside the range $-\pi \le \varphi \le \pi$, by using $\mathrm{Mod}[\varphi, 2\pi, -\pi]$ in the Mathematica language. An illustration of the integration areas is shown in Fig. 22.

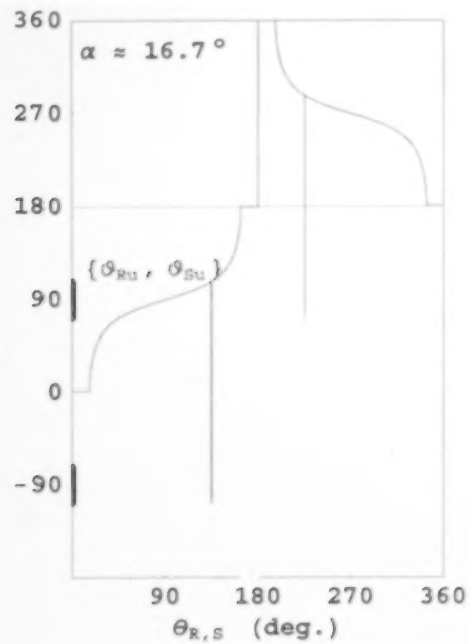

Figure 22: An illustration of the integration regions for the horizontal cone for the in-plane bistatic case. The red lines give $\varphi_{Ru,Su}$, the yellow lines $\varphi_{Rl,Sl}$. For the choices $\theta_R = 3\pi/4$ radians, $\theta_S = 5\pi/4$ radians the viewed/illuminated areas are shown as the black/brown vertical lines. The integration area is the intersection of these ranges shown as the blue lines. In this case the integration regions are two discontinuous blue regions at the top and bottom of the cone, spanning the ranges $\mathrm{Mod}[\varphi_{Su}(5\pi/4), 2\pi, -\pi] = \varphi_{Su}(5\pi/4) - 2\pi \le \varphi \le \varphi_{Rl}(3\pi/4)$ $\varphi_{Ru}(3\pi/4) \le \varphi \le \varphi_{Sl}(5\pi/4)$.

It will prove convenient to define the auxiliary functions:

$$\begin{aligned}
\varphi_{umin}(\theta_R, \theta_S) &= \mathrm{Min}[\varphi_{Ru}(\theta_R), \varphi_{Su}(\theta_S)] \\
\varphi_{umax}(\theta_R, \theta_S) &= \mathrm{Max}[\varphi_{Ru}(\theta_R), \varphi_{Su}(\theta_S)] \\
\varphi_{lmin}(\theta_R, \theta_S) &= \mathrm{Min}[\varphi_{Rl}(\theta_R), \varphi_{Sl}(\theta_S)] \\
\varphi_{lmin}(\theta_R, \theta_S) &= \mathrm{Max}[\varphi_{Rl}(\theta_R), \varphi_{Sl}(\theta_S)]
\end{aligned} \tag{120}$$

For the scattering strength one obtains

$$g = -\frac{1}{4\pi} \int_{\text{illum. area}} (\vec{k}_S + \vec{k}_R) \cdot \vec{n}\, e^{-i(\vec{k}_S + \vec{k}_R)\cdot \vec{R}_a} dS =$$

$$= \frac{k}{4\pi\cos\alpha}\int_{-L/2}^{L/2} dx \int d\varphi(\rho_0 + x\tan\alpha)[-(\cos\theta_R+\cos\theta_S)\sin\alpha + (\sin\theta_R+\sin\theta_S)\cos\alpha\cos\varphi]\times$$
$$e^{ik[x(\cos\theta_R+\cos\theta_S)+(\rho_0+x\tan\alpha)(\sin\theta_R+\sin\theta_S)\cos\varphi]}$$
$$= \frac{ke^{-ik\rho_0(\cos\theta_R+\cos\theta_S)\cot\alpha}}{4\pi\sin\alpha}\int_{\varphi_1}^{\rho 2} d\rho\,\rho \int d\varphi[-(\cos\theta_R+\cos\theta_S)\sin\alpha + (\sin\theta_R+\sin\theta_S)\cos\alpha\cos\varphi]\times$$
$$e^{ik\rho[(\cos\theta_R+\cos\theta_S)\cot\alpha+(\sin\theta_R+\sin\theta_S)\cos\varphi]}. \tag{121}$$

The limits of the $\int d\varphi$ depend on the parameters $\theta_{R/S}$ and are given below:

$$\begin{aligned}
g(\theta_R,\theta_S) &= 0.\quad \mathrm{Or}[0\le\theta_R\le\alpha, 0\le\theta_S\le\alpha],\\
g(\theta_R,\theta_S) &= 0.\quad \mathrm{Or}[2\pi-\alpha\le\theta_R\le 2\pi, 2\pi-\alpha\le\theta_S\le 2\pi].\\
\varphi_{tmax}(\theta_R,\theta_S) \le\ & \varphi \le \varphi_{umin}(\theta_R,\theta_S),\\
& \mathrm{Or}[\mathrm{And}[\alpha<\theta_R\le\pi, \alpha<\theta_S\le\pi], \mathrm{And}[\pi<\theta_R<2\pi-\alpha, \pi<\theta_S<2\pi-\alpha]],\\
\mathrm{Union}[\varphi_{Rl}(\theta_R) \le\ & \varphi \le \varphi_{Su}(\theta_S) - 2\pi, \varphi_{Sl}(\theta_S) \le \varphi \le \varphi_{Ru}(\theta_R)],\\
& \mathrm{And}[\alpha<\theta_R\le\pi, \pi<\theta_S<2\pi-\alpha, \theta_R>\theta_S-\pi],\\
g(\theta_R,\theta_S) &= 0.\\
& \mathrm{And}[\alpha<\theta_R\le\pi, \pi<\theta_S<2\pi-\alpha, \theta_R\le\theta_S-\pi],\ \text{source/receiver shadowed.}\\
\mathrm{Union}[\varphi_{Sl}(\theta_S) \le\ & \varphi \le \varphi_{Ru}(\theta_R) - 2\pi, \varphi_{Rl}(\theta_R) \le \varphi \le \varphi_{Su}(\theta_S)],\\
& \mathrm{And}[\alpha<\theta_S\le\pi, \pi<\theta_R<2\pi-\alpha, \theta_S>\theta_R-\pi],\\
g(\theta_R,\theta_S) &= 0.\quad \mathrm{And}[\alpha<\theta_S\le\pi, \pi<\theta_R<2\pi-\alpha, \theta_S\le\theta_R-\pi],\ \text{source/receiver shadowed.}
\end{aligned} \tag{122}$$

This covers all cases for $0\le\theta_{R,S}<2\pi$, for all other cases just set $g(\theta_R,\theta_S) = g(\mathrm{Mod}[\theta_R,2\pi],\mathrm{Mod}[\theta_S,2\pi])$.

Now consider a comparison between an exact numerical evaluation based on the previous considerations and the Bistatic Theorem version of the HGD model where one substitutes $k\to k\cos(\beta/2)$ into the monostatic expression, where $\theta_R = \theta_b - \beta/2,\quad \theta_S = \theta_b + \beta/2$. One notes that the Bistatic Theorem requires that the viewed/illuminated areas be approximately the same, hence from above bistatic version of HGD should be implemented as

$$\begin{aligned}
g_{bistatic}(k,\theta_b,\beta) &= 0.\\
& \mathrm{Or}[\mathrm{And}[\alpha<\theta_R\le\pi, \pi<\theta_S<2\pi-\alpha, \theta_R\le\theta_S-\pi], \mathrm{And}[\alpha<\theta_S\le\pi, \pi<\theta_R<2\pi-\alpha, \theta_S\le\theta_R-\pi]]\\
g_{bistatic}(k,\theta_b,\beta) &= g_{monostatic}(k\cos(\beta/2),\theta_b),\ \text{otherwise.}
\end{aligned} \tag{123}$$

In other words, when the source/receiver are shadowed, the scattered field is zero. A comparison between this bistatic implementation of the HGD model and an exact numerical evaluation of the Kirchhoff integral is shown in Fig.23.

Now consider our previous approximation for the general side-views where one neglects the effect of the cone half-angle outside the end-views. this gives the following integration areas:

$$\begin{aligned}
-\pi/2 \le\ & \varphi \le \pi/2,\quad \mathrm{And}[\alpha<\theta_R<\pi-\alpha, \alpha<\theta_S<\pi-\alpha],\\
-\pi/2 \le\ & \varphi \le \pi/2,\\
& \mathrm{Or}[\mathrm{And}[\alpha<\theta_R<\pi-\alpha, \pi-\alpha<\theta_S<\pi+\alpha], \mathrm{And}[\alpha<\theta_S<\pi-\alpha, \pi-\alpha<\theta_R<\pi+\alpha]],\\
-\pi \le\ & \varphi \le \pi,\quad \mathrm{And}[\pi-\alpha<\theta_R<\pi+\alpha, \pi-\alpha<\theta_S<\pi+\alpha],\\
\pi/2 \le\ & \varphi \le 3\pi/2\quad \mathrm{And}[\pi+\alpha<\theta_R<2\pi-\alpha, \pi+\alpha<\theta_S<2\pi-\alpha],\\
\pi/2 \le\ & \varphi \le 3\pi/2,\\
& \mathrm{Or}[\mathrm{And}[\pi+\alpha<\theta_R<2\pi-\alpha, \pi-\alpha<\theta_S<\pi+\alpha], \mathrm{And}[\pi+\alpha<\theta_S<2\pi-\alpha, \pi-\alpha<\theta_R<\pi+\alpha]],
\end{aligned}$$

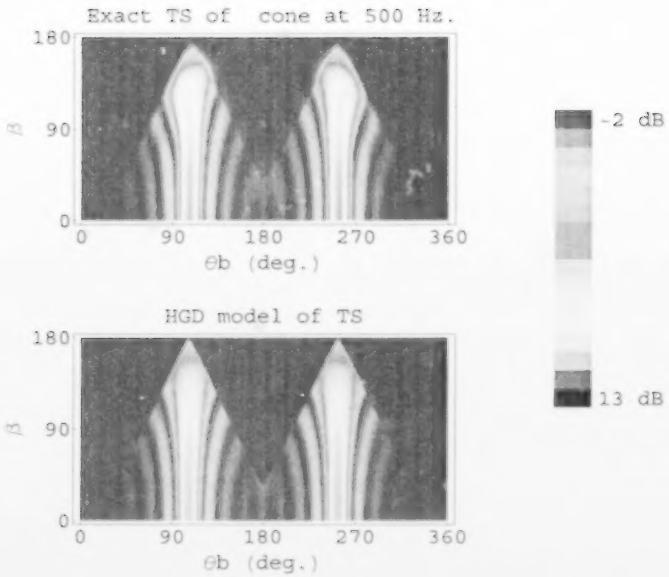

Figure 23: Plots of Target Strength $= 10\log[10^{-2.0} + |g(\theta_B, \beta)|^2]$ for the bistatic HGD model and an exact evaluation of the Kirchhoff integral for the cone. The parameter values are $f = 500$ Hz, $\rho_2 = 2.8$ m, $\rho_1 = 1.0$, $L = 6.0$ m, $\alpha = 16.7$ degrees. The bistatic HGD model loses accuracy as $\beta \to \pi$ since the asymptotic formula for the Bessel functions fails in that case. The exact result also has slightly more structure in the region around the stern view near $\theta_B \approx 180$ degrees and $\beta \approx \alpha$, although these differences are less visible when the -2.0 dB background is added to the scattering strength.

$$
\begin{aligned}
g(\theta_R,\theta_S) &= 0,\quad \mathrm{Or}[0 \le \theta_R \le \alpha, 0 \le \theta_S \le \alpha, 2\pi-\alpha \le \theta_R \le 2\pi, 2\pi-\alpha \le \theta_S \le 2\pi],\ \text{wide-end} \\
g(\theta_R,\theta_S) &= 0,\ \mathrm{Or}[\mathrm{And}[\alpha < \theta_R \le \pi, \pi < \theta_S < 2\pi-\alpha, \theta_R \le \theta_S - \pi], \\
&\qquad \mathrm{And}[\alpha < \theta_S \le \pi, \pi < \theta_R < 2\pi-\alpha, \theta_S \le \theta_R - \pi]],\ \text{source/receiver shadowed.}
\end{aligned} \tag{124}
$$

This gives the scattering strength:

$$
\begin{aligned}
g &= \frac{ke^{-\imath k\rho_0(\cos\theta_R+\cos\theta_S)\cot\alpha}}{4\sin\alpha}\int_{\rho_1}^{\rho_2} d\rho\ \rho\ e^{\imath k\rho(\cos\theta_R+\cos\theta_S)\cot\alpha}\times \\
&\quad [-(\cos\theta_R+\cos\theta_S)\sin\alpha(J_0(k\rho[(\sin\theta_R+\sin\theta_S)) + iE_0(k\rho[(\sin\theta_R+\sin\theta_S))) + \\
&\quad (\sin\theta_R+\sin\theta_S)\cos\alpha(iJ_1(k\rho[(\sin\theta_R+\sin\theta_S)) + E_1(k\rho[(\sin\theta_R+\sin\theta_S)))], \\
&\qquad \mathrm{And}[\alpha < \theta_R < \pi-\alpha, \alpha < \theta_S < \pi-\alpha],\ \text{side-view.}
\end{aligned} \tag{125}
$$

$$
\begin{aligned}
g &= \frac{ke^{-\imath k\rho_0(\cos\theta_R+\cos\theta_S)\cot\alpha}}{2\sin\alpha}\int_{\rho_1}^{\rho_2} d\rho\ \rho\ e^{\imath k\rho(\cos\theta_R+\cos\theta_S)\cot\alpha}\times \\
&\quad [-(\cos\theta_R+\cos\theta_S)\sin\alpha J_0(k\rho[(\sin\theta_R+\sin\theta_S) + i(\sin\theta_R+\sin\theta_S)\cos\alpha J_1(k\rho[(\sin\theta_R+\sin\theta_S))], \\
&\qquad \mathrm{And}[\pi-\alpha < \theta_R < \pi+\alpha, \pi-\alpha < \theta_S < \pi+\alpha] \\
&\approx \frac{e^{-\imath k\rho_0(\cos\theta_R+\cos\theta_S)\cot\alpha}}{2i(\cos\theta_R+\cos\theta_S)\cot\alpha\sin\alpha}\left\{\rho_2\ e^{\imath k\rho_2(\cos\theta_R+\cos\theta_S)\cot\alpha}\times\right. \\
&\quad [-(\cos\theta_R+\cos\theta_S)\sin\alpha J_0(k\rho_2[(\sin\theta_R+\sin\theta_S) + i(\sin\theta_R+\sin\theta_S)\cos\alpha J_1(k\rho_2[(\sin\theta_R+\sin\theta_S))]-, \\
&\quad \rho_2\ e^{\imath k\rho_2(\cos\theta_R+\cos\theta_S)\cot\alpha}\times \\
&\quad \left.[-(\cos\theta_R+\cos\theta_S)\sin\alpha J_0(k\rho_2[(\sin\theta_R+\sin\theta_S) + i(\sin\theta_R+\sin\theta_S)\cos\alpha J_1(k\rho_2[(\sin\theta_R+\sin\theta_S))]\right\} \\
&\qquad \mathrm{And}[\pi-\alpha < \theta_R < \pi+\alpha, \pi-\alpha < \theta_S < \pi+\alpha];,\ \text{source/receiver in the pointy-end-view.}
\end{aligned} \tag{126}
$$

$$
\begin{aligned}
g &= \frac{ke^{-\imath k\rho_0(\cos\theta_R+\cos\theta_S)\cot\alpha}}{4\sin\alpha}\int_{\rho_1}^{\rho_2} d\rho\ \rho\ e^{\imath k\rho(\cos\theta_R+\cos\theta_S)\cot\alpha}\times \\
&\quad [-(\cos\theta_R+\cos\theta_S)\sin\alpha(J_0(k\rho[(\sin\theta_R+\sin\theta_S)) - iE_0(k\rho[(\sin\theta_R+\sin\theta_S))) + \\
&\quad (\sin\theta_R+\sin\theta_S)\cos\alpha(iJ_1(k\rho[(\sin\theta_R+\sin\theta_S)) - E_1(k\rho[(\sin\theta_R+\sin\theta_S)))] \\
&\approx \frac{k\sqrt{2}e^{-\imath k\rho_0(\cos\theta_R+\cos\theta_S)\cot\alpha-\imath\pi/4}}{4\sin\alpha\sqrt{k(\sin\theta_R+\sin\theta_S)}}\left[-(\cos\theta_R+\cos\theta_S)\sin\alpha + (\sin\theta_R+\sin\theta_S)\cos\alpha\right]\times \\
&\quad \int_{\rho_1}^{\rho_2} d\rho\ \sqrt{\rho}e^{\imath k\rho[(\sin\theta_R+\sin\theta_S)+(\cos\theta_R+\cos\theta_S)\cot\alpha]} \\
&\approx \frac{k\sqrt{2}e^{-\imath k\rho_0(\cos\theta_R+\cos\theta_S)\cot\alpha-\imath\pi/4}}{4\sin\alpha\sqrt{k(\sin\theta_R+\sin\theta_S)}}\left[-(\cos\theta_R+\cos\theta_S)\sin\alpha + (\sin\theta_R+\sin\theta_S)\cos\alpha\right]\times \\
&\quad \int_{\rho_1}^{\rho_2} d\rho\ \sqrt{\rho}e^{\imath k\rho[(\sin\theta_R+\sin\theta_S)+(\cos\theta_R+\cos\theta_S)\cot\alpha]}
\end{aligned}
$$

$$
\mathrm{And}[\pi+\alpha < \theta_R < 2\pi-\alpha, \pi+\alpha < \theta_S < 2\pi-\alpha],\ \text{side-view.} \tag{127}
$$

In effect, this gives the Bistatic Theorem result for our previous approximate model, results are shown in Fig. 24.

To summarize, the HGD model works well for the in-plane Bistatic case; a modest improvement can be achieved by substituting Eq. 110 for the end view case in HGD. The side-view case in HGD is the asymptotic expansion of Eq. (114), so not much difference is noticed in the general side-view.

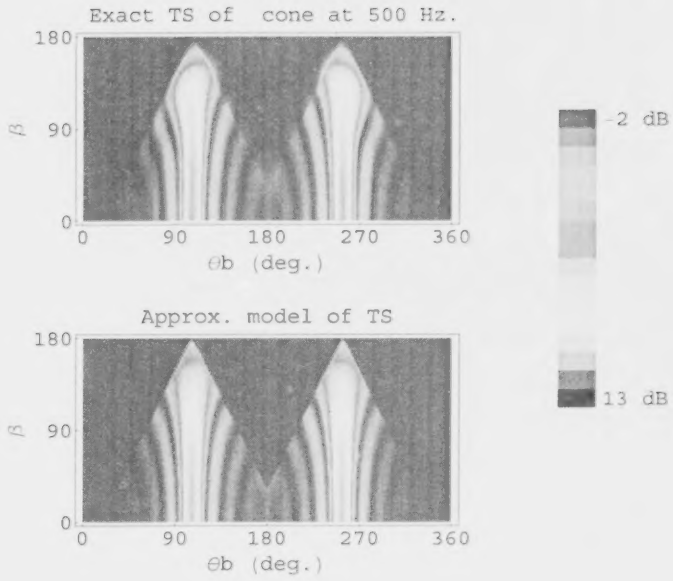

Figure 24: Comparison of the Bistatic approximate model (Eqs. (110), (114)) with an exact evaluation of the Kirchhoff integral for the cone, for the Target Strength $= 10\log[10^{-2.0} + |g(\theta_B, \beta)|^2]$. The parameter values are $f = 500$ Hz, $\rho_2 = 2.8$ m, $\rho_1 = 1.0$, $L = 6.0$ m, $\alpha = 16.7$ degrees. The bistatic approximate model is very similar to the bistatic HGD model, with some additional detail near $\theta_B \approx \pi$.

9.3 The general case: bistatic scattering

Return now to the general bistatic case. For this complicated case, it is more efficient to introduce the idea of interval programming, where in the Mathematica language the interval between the real numbers $x \le y$ is represented as Interval[$\{x, y\}$]. The illumination conditions $\vec{k}_{R/S} \cdot \vec{n} = 0$ give

$$\cos\alpha \sqrt{(\cos\eta_{R/S}\sin\theta_{R/S})^2 + (\sin\eta_{R/S})^2}\cos(\varphi - \omega) = \sin\alpha\cos\eta_{R/S}\cos\theta_{R/S}, \tag{128}$$

where $\omega = \arctan[\sin\eta_{R/S}, \sin\theta_{R/S}\cos\eta_{R/S}]$. To compactly express the formulae in this complicated case consider the shorthand notation:

$$\begin{aligned}
n_{rx} &= -\cos\eta_R\cos\theta_R, \\
n_{ry} &= -\cos\eta_R\sin\theta_R, \\
n_{rz} &= -\sin\eta_R, \\
n_{sx} &= -\cos\eta_S\cos\theta_S, \\
n_{sy} &= -\cos\eta_S\sin\theta_S, \\
n_{sz} &= -\sin\eta_S.
\end{aligned} \tag{129}$$

In terms of these functions the various sub-cases can be defined as

$$\begin{aligned}
\text{source or receiver in the wide-end view,} &\quad \text{Or}[n_{rx} \le -\cos\alpha,\ n_{sx} \le -\cos\alpha]; \\
\text{source and receiver in the pointy-end view,} &\quad \text{And}[n_{rx} \ge \cos\alpha,\ n_{sx} \ge \cos\alpha]; \\
\text{receiver in the pointy-end view, source not in the pointy-end view,} &\quad \text{And}[n_{rx} \ge \cos\alpha,\ n_{sx} < \cos\alpha]; \\
\text{source in the pointy-end view, receiver not in the pointy-end view,} &\quad \text{And}[n_{sx} \ge \cos\alpha,\ n_{rx} < \cos\alpha] \\
\text{source or receiver not in the end views,} &\quad \text{And}[|n_{rx}| < \cos\alpha, |n_{sx}| < \cos\alpha].
\end{aligned} \tag{130}$$

In this notation the viewed/illuminated areas can be written as

$$\begin{aligned}
\varphi_{ru}(\theta_R, \eta_R) &= \arctan(-n_{ry}, -n_{rz}) + \arccos\left(-\frac{n_{rx}\tan\alpha}{(\sqrt{(n_{ry})^2 + (n_{rz})^2}}\right), \\
\varphi_{rl}(\theta_R, \eta_R) &= \arctan(-n_{ry}, -n_{rz}) - \arccos\left(-\frac{n_{rx}\tan\alpha}{(\sqrt{(n_{ry})^2 + (n_{rz})^2}}\right), \\
\varphi_{su}(\theta_S, \eta_S) &= \arctan(-n_{sy}, -n_{sz}) + \arccos\left(-\frac{n_{sx}\tan\alpha}{(\sqrt{(n_{sy})^2 + (n_{sz})^2}}\right), \\
\varphi_{sl}(\theta_S, \eta_S) &= \arctan(-n_{sy}, -n_{sz}) - \arccos\left(-\frac{n_{sx}\tan\alpha}{(\sqrt{(n_{sy})^2 + (n_{sz})^2}}\right),
\end{aligned} \tag{131}$$

provided source and receiver are not in the end-views and where $\arctan(x, y)$ lies in the same quadrant as (x, y). Since $-\pi < \arctan(x, y) \le \pi$ and $0 \le \arccos(x) \le \pi$, then $-\pi < \{\varphi_{ru}, \varphi_{su}\} \le 2\pi$ and $-2\pi < \{\varphi_{rl}, \varphi_{sl}\} \le \pi$. This means that the intervals Interval[$\{\varphi_{rl}, \varphi_{ru}\}$] and Interval[$\{\varphi_{sl}, \varphi_{su}\}$] lie somewhere between -2π and 2π. These intervals can be rewritten as one (or possibly two) interval(s) in the range 0 to 2π , by defining the function

$$\text{interval}[\varphi_l, \varphi_u] = \begin{cases} \text{Interval}[\{\varphi_l, \varphi_u\}], & \text{if } 0 \le \varphi_u,\ 0 \le \varphi_l; \\ \text{Union}[\text{Interval}[\{\text{Mod}[\varphi_l, 2\pi], 2\pi\}], \text{Interval}[\{0, \varphi_u\}]], & \text{if } 0 \le \varphi_u,\ 0 > \varphi_l; \\ \text{Interval}[\{\text{Mod}[\varphi_l, 2\pi], \text{Mod}[\varphi_u, 2\pi]\}], & \text{if } 0 > \varphi_u,\ 0 > \varphi_l. \end{cases} \tag{132}$$

For source and receiver not in the end-views, the integration region for the Kirchhoff integral can then be written very compactly as

IntervalIntersection[interval[$\varphi_{rl}, \varphi_{ru}$], interval[$\varphi_{sl}, \varphi_{su}$]].

This may be a single interval or two discontinuous intervals in the range 0 to 2π. All cases may be summarized by defining the function $0 \le \text{range}[\ldots,] \le 2\pi$. This function is either a single interval or a union of two intervals:

$$\text{range}[\theta_r, \theta_S, \eta_R, \eta_S, \alpha] \quad = \quad \begin{cases} \text{Interval}[\{0,0\}], & \text{Or}[n_{rx} \le -\cos\alpha,\ n_{sx} \le -\cos\alpha]; \\ \text{Interval}[\{0,2\pi\}], & \text{And}[n_{rx} \ge \cos\alpha,\ n_{sx} \ge \cos\alpha]; \\ \text{interval}[\varphi_{sl}, \varphi_{su}], & \text{And}[n_{rx} \ge \cos\alpha,\ n_{sx} < \cos\alpha]; \\ \text{interval}[\varphi_{rl}, \varphi_{ru}], & \text{And}[n_{sx} \ge \cos\alpha,\ n_{rx} < \cos\alpha] \\ \text{IntervalIntersection}[\text{interval}[\varphi_{rl}, \varphi_{ru}], \text{interval}[\varphi_{sl}, \varphi_{su}]], & \text{And}[|n_{rx}| > \cos\alpha, |n_{sx}| > \cos\alpha]. \end{cases} \tag{133}$$

For example to determine the integration region(s) for the parameter case $\{\theta_R, \theta_S, \eta_R, \eta_S, \alpha\} = \{135^o, 45^o, -45^o, 45^o, 16.7^o\}$, just evaluate the range function (details given in the software)

```
In[1]:=
range[135*Degree,45*Degree,-45*Degree,45*Degree,ArcTan[(2.8-1.0)/6.0]]/Degree
Out[1]:=
Interval[{0.,45.2386},{334.71,360.}]
```

Hence mod 2π, the integration region consists of the intervals $0 \le \varphi \le 45.2^0$ and $334.7^o \le \varphi \le 360^o$. The end-points of these regions, appropriate for substitution in the Kirchhoff integral, would be written as

```
((Min[range[[1]]],Max[range[[1]]]),(Min[range[[2]]],Max[range[[2]]])
```

In general, the number of separate integration regions would be expressed as Length[range[$\theta_r, \theta_S, \eta_R, \eta_S, \alpha$]].

As in the monostatic case, the integration areas are still determined by coordinate curves φ constant. This implies that the basic functions determining the scattering strength are from the same family as the monostatic case, but with more complicated arguments. Now introduce the shorthands

$$\begin{aligned} \delta &= \arctan[(\cos\eta_s \sin\theta_s + \cos\eta_r \sin\theta_r), (\sin\eta_s + \sin\eta_r)], \\ \lambda &= \sqrt{(\cos\eta_s \sin\theta_s + \cos\eta_r \sin\theta_r)^2 + (\sin\eta_s + \sin\eta_r)^2}, \\ b &= -k\rho(n_{rx} + n_{sx})\cot\alpha + k\lambda\rho\cos(\varphi). \end{aligned} \tag{134}$$

The function $\arctan[x, y]$ is that branch of the arctan function such that the angle δ lies in the same quadrant as the point (x, y): in Mathematica notation: ArcTan[x,y].

For the general case the scattering strength can be written as

$$\begin{aligned} g &= -\frac{1}{4\pi} \int_{\text{illum. area}} (\vec{k}_s + \vec{k}_s) \cdot \vec{n}\, e^{-i(\vec{k}_s + \vec{k}_r)\cdot\vec{r}} d\vec{S} = \\ &= \frac{k}{4\pi\cos\alpha} \int_{-L/2}^{L/2} d\zeta \int d\varphi (\rho_0 + x\tan\alpha)[-(\cos\eta_s\cos\theta_s + \cos\eta_r\cos\theta_r)\sin\alpha + \\ &\quad (\cos\eta_s \sin\theta_s + \cos\eta_r \sin\theta_r)\cos\alpha\cos\varphi + (\sin\eta_s + \sin\eta_r)\cos\alpha\sin\varphi] \times \\ &\quad e^{ik[(\cos\eta_s\cos\theta_s + \cos\eta_r\cos\theta_r)x + (\cos\eta_s\sin\theta_s + \cos\eta_r\sin\theta_r)(\rho_0 + x\tan\alpha)\cos\varphi + (\sin\eta_s + \sin\eta_r)(\rho_0 + x\tan\alpha)\sin\varphi]} \\ &= \frac{ke^{ik\rho_0(n_{rx}+n_{sx})\cot\alpha}}{4\pi\sin\alpha} \int_{\rho_1}^{\rho_2} d\rho\, \rho\, e^{-ik\rho(n_{rx}+n_{sx})\cot\alpha} \int d\zeta [(n_{rx} + n_{sx})\sin\alpha + \lambda\cos\alpha\cos(\varphi - \delta)] e^{ik\lambda\rho\cos(\varphi-\delta)}. \end{aligned} \tag{135}$$

The integral over φ can be written compactly using the range function as

$$\int d\varphi \equiv \sum_{n=1}^{\text{Length[range]}} \int_{\text{Min[range[[n]]]}}^{\text{Max[range[[n]]]}} d\varphi.$$

If both source and receiver are in the pointy end-view, the scattering strength becomes

$$\begin{aligned}
g &= \frac{k\epsilon^{ik\rho_0(n_{rx}+n_{sx})\cot\alpha}}{4\pi\sin\alpha}\int_{\rho_1}^{\rho_2} d\rho\ \rho\, e^{-ik\rho(n_{rx}+n_{sx})\cot\alpha}\int_{-\pi}^{\pi} d\varphi[(n_{rx}+n_{sx})\sin\alpha+\lambda\cos\alpha\cos\varphi]e^{ik\lambda\rho\cos\varphi} \\
&= \frac{k\epsilon^{ik\rho_0(n_{rx}+n_{sx})\cot\alpha}}{4\pi\sin\alpha}\int_{-\pi}^{\pi} d\varphi[(n_{rx}+n_{sx})\sin\alpha+\lambda\cos\alpha\cos\varphi]\int_{\rho_1}^{\rho_2} d\rho\ \rho\, e^{i\varphi b} \\
&= \frac{k\epsilon^{ik\rho_0(n_{rx}+n_{sx})\cot\alpha}}{2\pi\sin\alpha}\int_{0}^{\pi} d\varphi[(n_{rx}+n_{sx})\sin\alpha+\lambda\cos\alpha\cos\varphi]\left[\frac{e^{i\rho_2 b}(1-ib\rho_2)}{b^2}-\frac{e^{i\rho_1 b}(1-ib\rho_1)}{b^2}\right] \\
&\quad \frac{k\epsilon^{ik\rho_0(n_{rx}+n_{sx})\cot\alpha}}{2\sin\alpha}\int_{\rho_1}^{\rho_2} d\rho\ \rho\, e^{-ik\rho(n_{rx}+n_{sx})\cot\alpha}\times \\
&\qquad [(n_{rx}+n_{sx})\sin\alpha J_0(k\lambda\rho)+i\lambda\cos\alpha J_1(k\lambda\rho)] \\
&\approx \frac{i\epsilon^{ik\rho_0(n_{rx}+n_{sx})\cot\alpha}}{2(n_{rx}+n_{sx})\cos\alpha}\times \\
&\quad \Big[\rho_2\, e^{-ik\rho_2(n_{rx}+n_{sx})\cot\alpha}[(n_{rx}+n_{sx})\sin\alpha J_0(k\lambda\rho_2))+i\lambda\cos\alpha J_1(k\lambda\rho_2)]- \\
&\quad \rho_1\, e^{-ik\rho_1(n_{rx}+n_{sx})\cot\alpha}[(n_{rx}+n_{sx})\sin\alpha J_0(k\lambda\rho_1)+i\lambda\cos\alpha J_1(k\lambda\rho_1)]\Big] \\
&\quad \text{pointy-end-view}
\end{aligned} \tag{136}$$

In the end-view case the integral extended over the range $-\pi \le \varphi \le \pi$ and since the integrand was periodic in 2π it was possible to drop the δ factor in the integration range; the last step above is just an integration by parts.

For the general side-view case

$$\begin{aligned}
g &= \frac{k\epsilon^{ik\rho_0(n_{rx}+n_{sx})\cot\alpha}}{4\pi\sin\alpha}\int_{\rho_1}^{\rho_2} d\rho\ \rho\, e^{-ik\rho(n_{rx}+n_{sx})\cot\alpha}\int d\varphi[(n_{rx}+n_{sx})\sin\alpha+\lambda\cos\alpha\cos(\varphi-\delta)]e^{ik\lambda\rho\cos(\varphi-\delta)} \\
&= \frac{k\epsilon^{ik\rho_0(n_{rx}+n_{sx})\cot\alpha}}{4\pi\sin\alpha}\sum_{n=1}^{\text{Length[range]}}\int_{\text{Min[range[[n]]]}-\delta}^{\text{Max[range[[n]]]}-\delta} d\varphi[(n_{rx}+n_{sx})\sin\alpha+\lambda\cos\alpha\cos\varphi]\int_{\rho_1}^{\rho_2} d\rho\ \rho\, e^{i\varphi b} \\
&= \frac{k\epsilon^{ik\rho_0(n_{rx}+n_{sx})\cot\alpha}}{4\pi\sin\alpha}\sum_{n=1}^{\text{Length[range]}}\int_{\text{Min[range[[n]]]}-\delta}^{\text{Max[range[[n]]]}-\delta} d\varphi[(n_{rx}+n_{sx})\sin\alpha+\lambda\cos\alpha\cos\varphi]\times \\
&\qquad \left[\frac{e^{i\rho_2 b}(1-ib\rho_2)}{b^2}-\frac{e^{i\rho_1 b}(1-ib\rho_1)}{b^2}\right].
\end{aligned} \tag{137}$$

This last form is the one that is used for exact numerical evaluation. Fig. 25 shows some exact calculations based on numerical evaluation of the Kirchhoff integral, using various cases.

Now suppose for the moment that the saddle point $\varphi = 0, 2\pi$ lies in the range of integration. The saddle point approximation for the φ integral gives:

$$\begin{aligned}
g_{\text{saddle point}} &= \frac{k\epsilon^{ik\rho_0(n_{rx}+n_{sx})\cot\alpha}}{4\pi\sin\alpha}[(n_{rx}+n_{sx})\sin\alpha+\lambda\cos\alpha]\times \\
&\quad \epsilon^{-i\pi/4}\sqrt{\frac{2\pi}{\lambda}}\int_{\rho_1}^{\rho_2} d\rho\ \sqrt{\rho}\, e^{ik[-(n_{rx}+n_{sx})\cot\alpha+\lambda]\rho}.
\end{aligned} \tag{138}$$

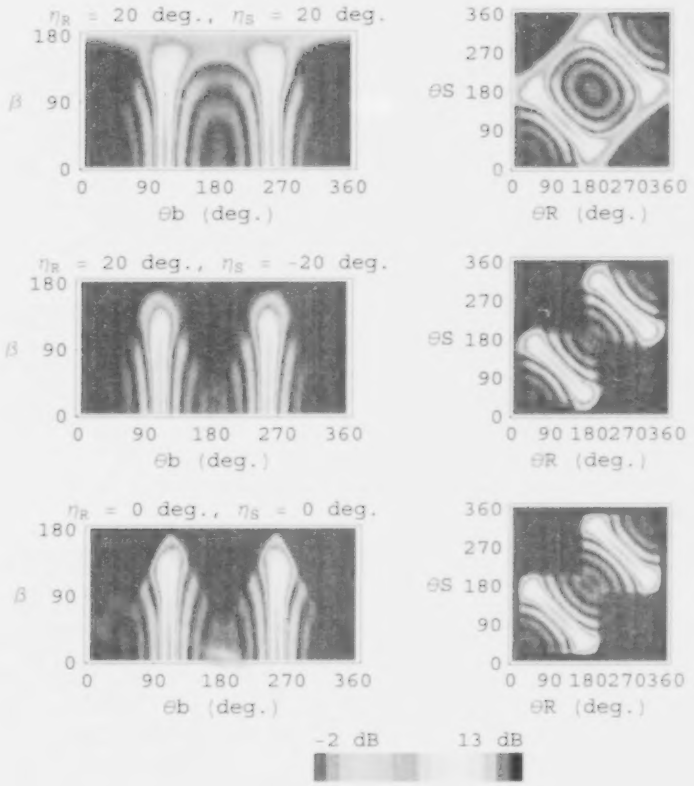

Figure 25: An exact calculation for the Target Strength = $10\log[10^{-2.0} + |g|^2]$, for the out-of-plane case for the cone. The parameter values are $f = 500$ Hz, $\rho_2 = 2.8$ m, $\rho_1 = 1.0$, $L = 6.0$ m, $\alpha = 16.7$ degrees. The column of three plots on the left are with dependent variables θ_B, β, the column of plots on the right are for the same parameter values but wrt θ_R, θ_S, where the aspect angle $\theta_B = (\theta_R + \theta_S)/2$, bistatic angle $\beta = \theta_S - \theta_R$. The top graph, with elevation angles $\eta_R = 20^o$, $\eta_S = 20^o$, contains an extra bright area, which corresonds to the top of the cone being illuminated/viewed when the source/receiver are on opposite sides of the cone. For the two bottom graphs, when the source/receiver are on opposite sides of the cone, they are shadowed. This is the principal feature of out-of-plane scattering of simple shapes, additional bright areas in the θ_R, θ_S plots corresponding to previously shadowed regions being viewed and illuminated when the source/receiver are out-of-plane.

Now consider our result

$$f(a,z) \equiv \int_0^z dt\ \sqrt{t}\ e^{ita} = -i\sqrt{z}\frac{e^{iaz}}{a} - i\frac{(-1)^{\frac{1}{4}}\sqrt{\pi}\ \mathrm{Erf}[(-1)^{\frac{3}{4}}\sqrt{a}\sqrt{z}]}{2a^{\frac{3}{2}}},$$

valid for any real a or z provided one uses principal values for all multiple valued roots and $\mathrm{Erf}[x] = (2/\pi)\int_0^z \exp[-t^2]dt$ is the error function. This gives for the saddle point at $\varphi = 0, 2\pi$

$$g_{\mathrm{sp}} = \frac{ke^{ik\rho_0(n_{rx}+n_{sx})\cot\alpha}}{4\pi\sin\alpha}[(n_{rx}+n_{sx})\sin\alpha + \lambda\cos\alpha] \times$$
$$e^{-i\pi/4}\sqrt{\frac{2\pi}{\lambda}}\{f(k[-(n_{rx}+n_{sx})\cot\alpha + \lambda, \rho_2) - f(k[-(n_{rx}+n_{sx})\cot\alpha + \lambda, \rho_1)\}. \quad (139)$$

To develop a stategy for approximating the scattering strength, consider the generic integral $\int_0^\beta e^{ix\cos\varphi}\,d\varphi$. From Eqs. (9.26) -(9.28) II of Maksimov and Agrest, one may make the general expansion in terms of saddle points and boundary values as:

$$\int_0^\beta e^{ix\cos\varphi}\,d\varphi \approx \frac{1}{2}\sqrt{\frac{2\pi}{x}}e^{i(x-\pi/4)} + \frac{e^{ix\cos\beta}}{-ix\sin\beta}.$$

One asserts that the saddle point term is dominant if

$$\left|\frac{1}{2}\sqrt{\frac{2\pi}{x}}e^{i(x-\pi/4)}\right| >> \left|\frac{e^{ix\cos\beta}}{-ix\sin\beta}\right|, \text{ or } \beta >> \arcsin[\sqrt{\frac{2}{\pi x}}].$$

For an integral of the form $\int_{\beta_1}^{\beta_2} e^{ix\cos\varphi}\,d\varphi$, where the saddle point lies between β_2 and β_1, one picks up a contribution of one-half the saddle point term for each end-point such that $\beta_{1,2} >> \arcsin[\sqrt{\frac{2}{\pi x}}]$. Otherwise or if there is no saddlepoint in the range of integration then there are only boundary value terms present.

In view of these considerations the stategy for the out-of-plane case will be as follows:
(1) for either source or receiver in the wide-end view $g = 0$;
(2) for both source and receiver in the pointy-end view, use integration by parts as shown above;
(3) for the general side-view, if the integation range includes a saddle point, for each end-point such that the end-points $\beta_{1,2} >> \arcsin[\sqrt{\frac{2}{\pi x}}]$, add a contribution of $(1/2)g_{saddlepoint}$.
(4) otherwise or if the integration range does not include a saddle point, use $g \approx 0$.

Hence roughly speaking, our rule for evaluating these scattering functions is as follows: if the width of the integration region surrounding the saddle points is greater than $2\arcsin[1/k\lambda\rho_0]$ then use the saddle point contribution alone to approximate the φ integral; if it is less use $g = 0$.

Fig. 26 shows some calculations based on these saddle point approximations of the Kirchhoff integral. The bright red and green regions are the saddle point contributions from the side-view cases, the faint blue central regions are the integration by parts terms from the pointy end-view cases, the deep blue regions are the -2.0 dB background, which occur in either the wide-end view or when source and receiver are shadowed on opposite sides of the cone. An exact calculation for the Target Strength $= 10\log[10^{-2.0} + |g|^2]$, for the out-of-plane case for the cone. The parameter values are $f = 500$ Hz, $\rho_2 = 2.8$ m, $\rho_1 = 1.0$, $L = 6.0$ m, $\alpha = 16.7$ degrees. The column of three plots on the left are with dependent variables θ_R, β, the column of plots on the right are for the same parameter values but wrt θ_R, θ_S, where the aspect angle $\theta_R = (\theta_R + \theta_S)/2$, bistatic angle $\beta = \theta_S - \theta_R$. The top graph, with elevation angles $\eta_R = 20°$, $\eta_S = 20°$, contains an extra bright area, which corresonds to the top of the cone being illuminated/viewed when the source/receiver are on opposite sides of the cone. For the two bottom graphs, when the source/receiver are on opposite sides of the cone, they are shadowed. This is the principal feature of out-of-plane scattering of simple shapes, additional bright areas in the θ_R, θ_S plots corresponding to previously shadowed regions being viewed and illuminated when the source/receiver are out-of-plane.

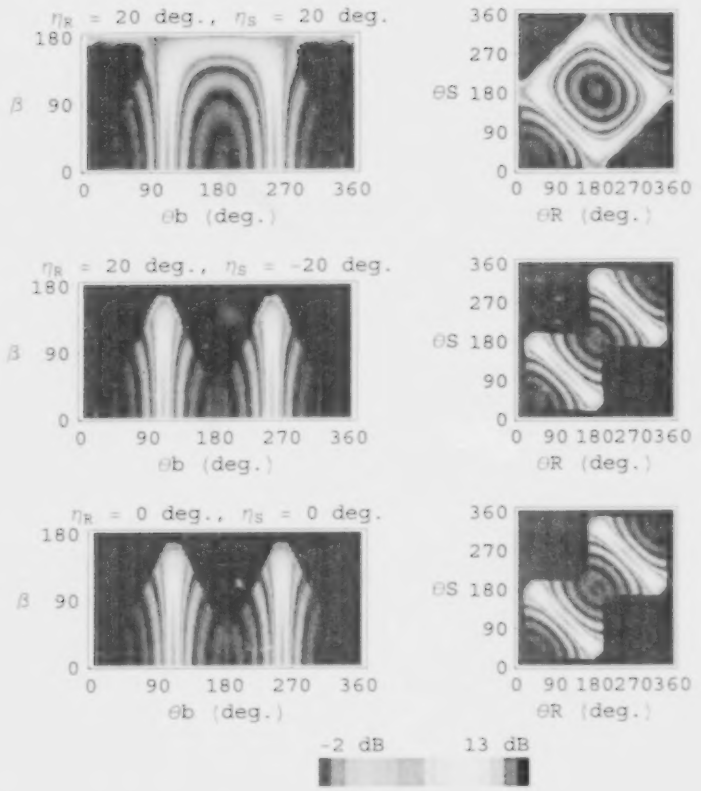

Figure 26: An approximate calculation for the Target Strength $= 10\log[10^{-2.0} + |g|^2]$, for the out-of-plane case for the cone. The parameter values are $f = 500$ Hz, $\rho_2 = 2.8$ m, $\rho_1 = 1.0$, $L = 6.0$ m, $\alpha = 16.7$ degrees. The column of three plots on the left are with dependent variables θ_B, β, the column of plots on the right are for the same parameter values but wrt θ_R, θ_S, where the aspect angle $\theta_B = (\theta_R + \theta_S)/2$, bistatic angle $\beta = \theta_S - \theta_R$. Compared with the exact results in Fig. 25, one can see that the saddle point terms alone give the main features of the scattering plots, but miss the fine detail in the quiet regions. This is not surprising considering the fairly modest values of $k\rho_1 \approx 2$, $k\rho_2 \approx 6$ at 500 Hz. For narrow viewed/illuminated strips, such as the 40° strip on the top of the cone in the top graph, the use of saddle point terms alone, over estimates the scattering.

9.4 Summary

The use of the saddle point approximation, combined with the fairly complicated illumination conditions for the cone, leads to a decent approximation for the main features of out-of-plane scattering for the horizontal cone. Improvements to this model could be made by introducing the incomplete Bessel functions of order 1 and 0 as shown in Appendix C; this would add detail in the quiet regions at a cost in computing time. For higher frequencies, the foregoing results–based on saddle point terms alone, would improve in accuracy. Generally speaking, the modest frequencies 500-1500 Hz ($k \approx 2$–6) of interest in this application, and the small size of the scatterers ($\rho_1 = 1.0$ m, $\rho_2 = 2.8$ m), means that the theory is barely in the asymptotic region, so Fig. 26 can be considered a reasonable approximation to the exact results in Fig. 25.

10 The ellipsoid

10.1 Parametrization of the ellipsoid

Consider the general ellipsoid, whose surface is given in Cartesian coordinates by

$$\frac{x^2}{a^2} + \frac{y^2}{b^2} + \frac{z^2}{c^2} = 1. \tag{140}$$

A sketch of a representative ellipsoid is shown in Fig. 27. A convenient parametrization of the ellipsoid is given by

$$\vec{r} = (a \sin\varphi \sin\phi, b \cos\varphi \sin\phi, c \cos\phi), \tag{141}$$

where $0 \le \varphi \le 2\pi$, $0 \le \phi \le \pi$. The surface area is given by (in a lhs)

$$\begin{aligned} \vec{n} dS &= -\vec{r}_\varphi \times \vec{r}_\phi \, d\varphi \, d\phi \\ &= (bc \sin\varphi \sin^2\phi, ac \cos\varphi \sin^2\phi, ab \cos\phi \sin\phi) \, d\varphi \, d\phi. \end{aligned} \tag{142}$$

11 Source/receiver in the x-y plane–monostatic case

For the moment consider the in-plane monostatic scattering case given by incident/received wavevectors

$$\vec{k}_{R/S} = k(-\cos\theta, -\sin\theta, 0), \tag{143}$$

where $0 \le \theta < 2\pi$.

The viewed/illuminated areas are given formally by the conditions $\vec{k}_{R/S} \cdot \vec{n} = 0$ which gives

$$\tan\varphi = -\frac{a}{b} \tan\theta. \tag{144}$$

This can be solved as

$$\begin{aligned} \varphi_{upper}(\theta) &= \pi - \arctan[b \cos\theta, a \sin\theta], \ 0 \le \theta \le \pi \\ \varphi_{lower}(\theta) &= -\arctan[b \cos\theta, a \sin\theta], \ 0 \le \theta \le \pi, \\ \varphi_{upper}(\theta) &= -\pi - \varphi_{lower}(2\pi - \theta), \ \pi \le \theta \le 2\pi \\ \varphi_{lower}(\theta) &= -\pi - \varphi_{upper}(2\pi - \theta), \ \pi \le \theta \le 2\pi. \end{aligned} \tag{145}$$

These choices give $g(2\pi - \theta) = g(\theta)$ for $\pi \le \theta \le 2\pi$. In the Mathematica convention, the branch of the arctan function such that $\arctan[y/x]$ lies in the same quadrant as (x, y) is denoted as $ArcTan[x, y]$.

For convenience define $\varphi_u = max(\varphi_R, \varphi_S)$, $\varphi_l = min(\varphi_R, \varphi_S)$. In this notation the viewed/illuminated area is given by

$$\int_{\text{illum. area}} d\varphi d\phi \to \int_{\varphi_{lower}}^{\varphi_{upper}} d\varphi \int_0^\pi d\phi.$$

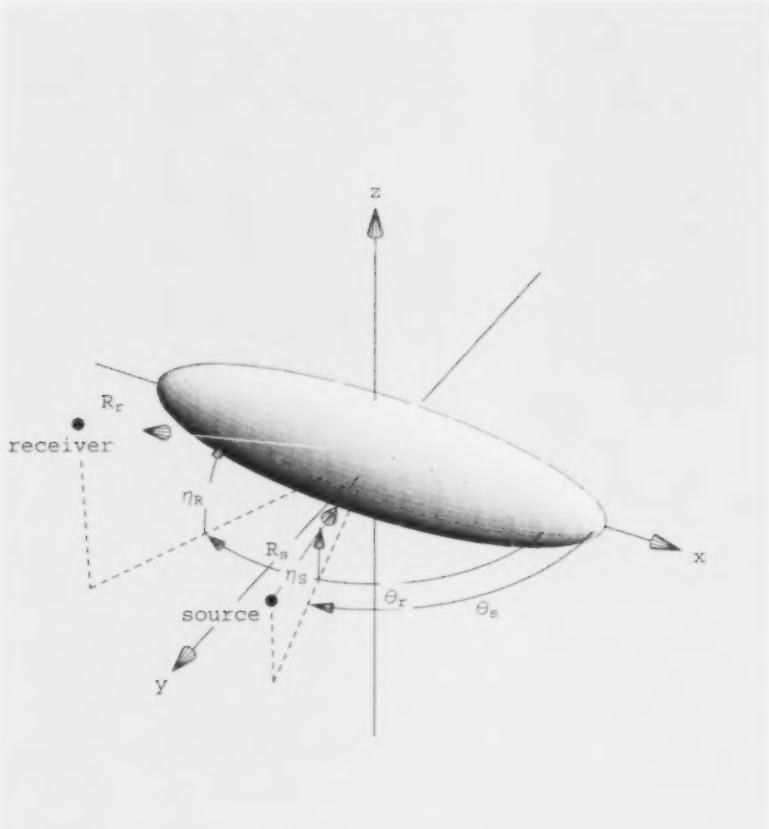

Figure 27: The ellipsoid $x^2/a^2 + y^2/b^2 + z^2/c^2 = 1$ with $a/b = a/c = 4$. The illuminated and viewed areas of the ellipsoid are defined by the red and yellow ellipses.

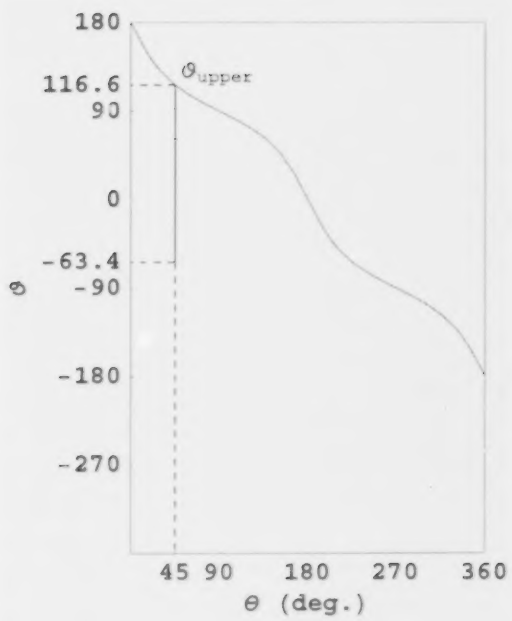

Figure 28: The viewed/illuminated areas for the ellipsoid, $a = 2$, $b = c = 1$ m. For $\theta = 45°$, the viewed/illuminated areas extend from $-63.4° = \varphi_{lower} \leq \varphi \leq \varphi_{upper} = 116.6°$.

An illustration of the viewed/illuminated areas is shown in Fig. 28.

The scattering strength becomes

$$\begin{aligned} g &= -\frac{1}{4\pi}\int_{\text{illum. area}} (\vec{k}_s + \vec{k}_s)\cdot\vec{n}\, e^{-i(\vec{k}_s+\vec{k}_s)\cdot\vec{r}} dS \\ &= \frac{kc}{2\pi}\int_{\varphi_{lower}}^{\varphi_{upper}} d\varphi \int_0^{\pi} d\phi (b\cos\theta\sin\varphi + a\sin\theta\cos\varphi)\sin^2\phi\, e^{i2k(\sin\phi\{a\cos\theta\sin\varphi + b\sin\theta\cos\varphi\})} \end{aligned} \tag{146}$$

Using the result

$$\begin{aligned} \frac{1}{\pi}\int_0^{\pi} d\phi \sin^2\phi\, e^{iA\sin\phi} &= \frac{1}{2}\{J_0(A) - J_2(A)\} - \frac{1}{2}i\{E_0(A) - E_2(A)\} + \frac{2}{\pi A} \\ &= \{J_0(A) + iH_0(A)\} - \frac{1}{A}\{J_1(A) + iH_1(A)\} \\ &= \frac{1}{2}\{J_0(A) - J_2(A)\} + \frac{1}{2}i\{H_0(A) - H_2(A)\} + \frac{iA}{3\pi}, \end{aligned} \tag{147}$$

one obtains the form suitable for exact numerical evaluation:

$$g = \frac{kc}{2}\int_{\varphi_{lower}}^{\varphi_{upper}} d\varphi (b\cos\theta\sin\varphi + a\sin\theta\cos\varphi)\left\{\frac{1}{2}\{J_0(A) - J_2(A)\} + \frac{1}{2}i\{H_0(A) - H_2(A)\} + \frac{iA}{3\pi}\right\}, \tag{148}$$

where $A = 2k\{a\cos\theta\sin\varphi + b\sin\theta\cos\varphi\}$. One notes that the functions $J_n(x)$, $H_n(x)$ are supported in Mathematica, making the previous result appropriate for exact numerical integration.

11.1 Special cases–end-view $\theta = 0$, side-view $\theta = \pi/2$

In the special case $\theta = 0$ one obtains

$$g = \frac{kbc}{2\pi}\int_0^{\pi} d\varphi \int_0^{\pi} d\phi \sin\varphi \sin^2\phi e^{i2ka\sin\phi\sin\varphi} = \frac{ibc}{2a}\left\{\frac{(e^{2iak} - 1)}{2iak} - e^{2iak}\right\}. \tag{149}$$

In the special case $\theta = \pi/2$ one obtains (the same result with a interchanged with b)

$$g = \frac{kac}{2\pi}\int_{-\pi/2}^{\pi/2} d\varphi \int_0^{\pi} d\phi \cos\varphi \sin^2\phi e^{i2kb\sin\phi\cos\varphi} = \frac{iac}{2b}\left\{\frac{(e^{2ibk} - 1)}{2ibk} - e^{2ibk}\right\}. \tag{150}$$

11.2 General in-plane monostatic view

Now define the auxiliary functions

$$\begin{aligned} \varepsilon &= \arctan[b\sin\theta, a\cos\theta], \\ D &= \sqrt{(a\cos\theta)^2 + (b\sin\theta)^2} \\ \varepsilon' &= \arctan[a\sin\theta, b\cos\theta], \\ D' &= \sqrt{(b\cos\theta)^2 + (a\sin\theta)^2}. \end{aligned} \tag{151}$$

$$\begin{aligned} g &= \frac{kcD'}{2\pi}\int_{\varphi_{lower}}^{\varphi_{upper}} d\varphi \int_0^{\pi} d\phi \cos(\varphi - \varepsilon')\sin^2\phi\, e^{i2kD\cos(\varphi-\varepsilon)\sin\phi} \\ &= \frac{kcD'}{2\pi}\int_{\varphi_{lower}-\varepsilon}^{\varphi_{upper}-\varepsilon} d\varphi \int_0^{\pi} d\phi \cos(\varphi + \varepsilon - \varepsilon')\sin^2\phi\, e^{i2kD\cos\varphi\sin\phi}. \end{aligned} \tag{152}$$

Provided the saddle point at $\varphi = 0$ lies in the integration range $\varphi_{lower} - \varepsilon \le \varphi \le \varphi_{upper} - \varepsilon$ then a good appproximation is given by

$$g_{approximate} \approx \frac{cD'\cos(\varepsilon - \varepsilon')}{i2D}\left\{e^{i2kD} - \frac{\sin[kD]}{kD}e^{ikD}\right\}. \tag{153}$$

11.3 Details

Split the integral in Eq. (154) into the two pieces

$$g = -\frac{kcD^{'}\sin(\varepsilon-\varepsilon^{'})}{2\pi}\int_{\varphi_{lower}-\varepsilon}^{\varphi_{upper}-\varepsilon} d\varphi \int_0^{\pi} d\phi \sin\varphi \sin^2\phi\, e^{i2kD\cos\varphi\sin\phi} + \frac{kcD^{'}\cos(\varepsilon-\varepsilon^{'})}{2\pi}\int_{\varphi_{lower}-\varepsilon}^{\varphi_{upper}-\varepsilon} d\varphi \int_0^{\pi} d\phi\, \cos\varphi\, \sin^2\phi\, e^{i2kD\cos\varphi\sin\phi}. \quad (154)$$

The first integral can be performed analytically and it can be neglected for the parameter values considered in this report.

In the second integral, by using Felsen's [22] higher order saddle point result 4.7 (12), the saddle point at $\phi = \pi/2$ gives (to order $1/(kD)^{3/2}$) gives

$$g_{approximate} = \frac{kcD^{'}\cos(\varepsilon-\varepsilon^{'})}{2\pi}\sqrt{\frac{2\pi}{2ikD}}\int_{\varphi_{lower}-\varepsilon}^{\varphi_{upper}-\varepsilon} d\varphi\, (\cos\varphi)^{1/2} e^{i2kD\cos\varphi}\left[1+\frac{(7/8)i}{2kD\cos\varphi}+\cdots\right] \quad (155)$$

Now to apply the saddle point method to this result we deform the contour through the saddle point at $\varphi = 0$ and then to $-\pi/2 + i\infty$ and $\pi/2 - i\infty$. Hence we obtain in addition to the saddle point terms the extra integrals (equivalent to branch line integrals) required to close the contour

$$\begin{aligned}
I_1 &= \frac{kcD^{'}\cos(\varepsilon-\varepsilon^{'})}{2\pi}\left\{-\int_{-\pi/2+i\infty}^{-\pi/2} d\varphi \int_0^{\pi} d\phi\, \cos\varphi\, \sin^2\phi\, e^{i2kD\cos\varphi\sin\phi} - \int_{\pi/2}^{\pi/2-i\infty} d\varphi \int_0^{\pi} d\phi\, \cos\varphi\, \sin^2\phi\, e^{i2kD\cos\varphi\sin\phi}\right\} \\
&= \frac{kcD^{'}\cos(\varepsilon-\varepsilon^{'})}{2\pi}\left\{-2\int_{-\pi/2+i\infty}^{-\pi/2} d\varphi \int_0^{\pi} d\phi\, \cos\varphi\, \sin^2\phi\, e^{i2kD\cos\varphi\sin\phi}\right\} \\
&= \frac{kcD^{'}\cos(\varepsilon-\varepsilon^{'})}{2\pi}\left\{-2\int_0^{\infty} dX \int_0^{\pi} d\phi\, \sinh X\, \sin^2\phi\, e^{-2kD\sinh X\sin\phi}\right\} \\
&\approx \frac{kcD^{'}\cos(\varepsilon-\varepsilon^{'})}{2\pi}\left\{-2\int_0^{\infty} dX \int_0^{\pi} d\phi\, X\, \sin^2\phi\, e^{-2kDX\sin\phi}\right\}, \quad (\sinh X \approx X) \\
&\approx \frac{kcD^{'}\cos(\varepsilon-\varepsilon^{'})}{2\pi}\left\{-\frac{2\pi}{(2kD)^2}\int_0^{\infty} dX\, X\, e^{-X}\right\}, \\
&\approx \frac{kcD^{'}\cos(\varepsilon-\varepsilon^{'})}{2\pi}\left\{-\frac{2\pi}{(2kD)^2}\right\}
\end{aligned} \quad (156)$$

plus the extra finite integrals

$$I_2 = -\frac{kcD^{'}\cos(\varepsilon-\varepsilon^{'})}{2\pi}\sqrt{\frac{2\pi}{2ikD}}\left\{\int_{-\pi/2}^{\varphi_{lower}-\varepsilon} d\varphi\, (\cos\varphi)^{1/2} e^{i2kD\cos\varphi} + \int_{\pi/2}^{\varphi_{upper}-\varepsilon} d\varphi\, (\cos\varphi)^{1/2} e^{i2kD\cos\varphi}\right\}. \quad (157)$$

From 4.7 (12) of Felsen, the first and second order saddle point terms in Eq. (155) give

$$I_{sp} = \frac{kcD^{'}\cos(\varepsilon-\varepsilon^{'})}{2\pi}\sqrt{\frac{2\pi}{2ikD}}\sqrt{\frac{2\pi}{2ikD}}e^{i2kD}\left[1+\frac{(1/8)i}{2kD}+\frac{(7/8)i}{2kD}\right] \quad (158)$$

Neglecting the finite integrals and combining I_{sp} and I_1 gives our approximate results. This is formally identical to the exact result that could have been obtained by integrating $-\pi/2 \le \varphi \le \pi/2$, which occurs in the end and side-view cases, as in Eq. (B-80) of [1].

11.4 Numerical results

A plot of an exact numerical integration of the Kirchhoff integral and this approximate result is shown in Fig. 29. The difference between the exact numeric integration of the Kirchhoff integral and the approximate results is less than 0.7 dB for the parameter values given in Fig. 29. One notes that these results include second order terms in the saddle point approximation: at these modest frequencies including higher order asymptotic terms may decrease accurracy for some parameter values.

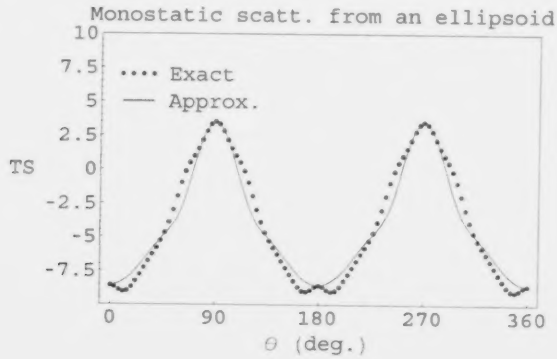

Figure 29: Comparison of exact and approximate scattering formulae for the Target Strength $= 10\log(10, |g|^2)$ for the ellipsoid: $f = 500$ Hz, $a = 2.8$ m, $b = c = 1.4$ m. The data points are given by an exact numerical integration of Eq. (148), the solid line is the asymptotic formula given by Eq. (153). The difference between exact and approximate results is less than 0.7 dB.

11.5 The half-ellipsoid

Now consider the ellipsoid $x^2/a^2 + y^2/b^2 + z^2/c^2 = 1$, truncated for $x < 0$, so one has a half-ellipsoid facing the positive x direction. Define the functions

$$\begin{aligned} \varphi_{halfupper}(\theta) &= \begin{cases} \varphi_{upper}(\theta), & 0 \le \varphi_{upper}(\theta) \le \pi \\ -\pi, & -\pi \le \varphi_{upper}(\theta) \le 0; \end{cases} \\ \varphi_{halflower}(\theta) &= \begin{cases} 0, & -\pi \le \varphi_{lower}(\theta) \le 0 \\ \varphi_{lower}(\theta), & -2\pi \le \varphi_{upper}(\theta) \le -\pi \end{cases} \end{aligned} \tag{159}$$

These functions define the integration area for the truncated ellipsoid, as shown in Fig. 30. These functions $\varphi_{halflower}(\theta)$, $\varphi_{halfupper}(\theta)$ determine the integration limits for the Kirchhoff integral. The exact expression for the scattering strength is given by

$$g = \frac{kc}{2} \int_{\varphi_{halflower}}^{\varphi_{halfupper}} d\varphi (b\cos\theta\sin\varphi + a\sin\theta\cos\varphi) \left\{ \frac{1}{2}\{J_0(A) - J_2(A)\} + \frac{1}{2} i\{H_0(A) - H_2(A)\} + \frac{iA}{3\pi} \right\}, \tag{160}$$

where $A = 2k\{a\cos\theta\sin\varphi + b\sin\theta\cos\varphi\}$. This is the form to use for exact numerical integration of the Kirchhoff integral.

To approximate the scattering strength one observes (by graphical means) that: the saddle point for the φ integral above occurs within the integration range at $\varphi = \varepsilon$ for $0 \le \theta \le \pi/2$, at $\varphi = \varepsilon - 2\pi$ for

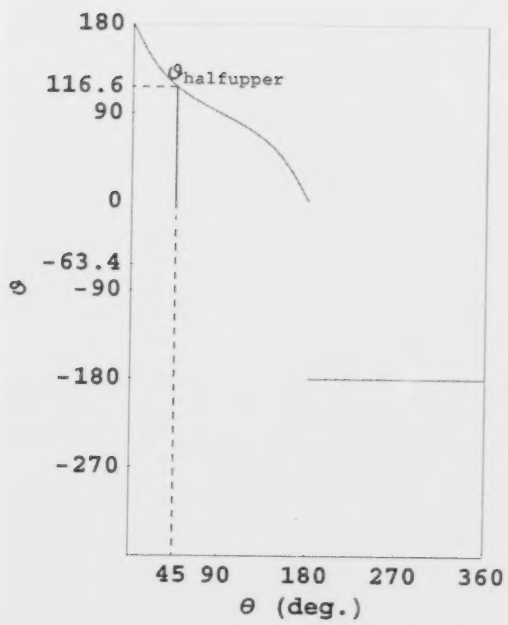

Figure 30: The viewed/illuminated areas for the half-ellipsoid facing the positive x direction, $a = 2$, $b = c = 1$. For $\theta = 45^o$, the viewed/illuminated areas extend from $0 = \varphi_{lower} \leq \varphi \leq \varphi_{halfupper} = 116.6^o$.

$3\pi/2 \le \theta \le 2\pi$, and lies outside the integration range for $\pi/2 < \theta < 3\pi/2$. A crude approximation is to use the full saddle point if the saddle point lies within the integration range and zero otherwise. A slightly more sophisticated approximation, which makes the transition to zero backscattering less abrupt, can be made by comparing the saddle point terms with the end view terms. This gives the following model: for $0 \le \theta \le \pi/2$ or $3\pi/2 \le \theta \le 2\pi$, for each end point that lies within $\arcsin[\sqrt{2/(\pi 2kD(a,b,c.\theta))}]$ of the saddle point, use one-half the saddle point contribution given by Eq. (153), and zero otherwise. Hence

$$g = \begin{cases} g_{approximate}, & |\varphi_{halfupper} - \varepsilon| > \arcsin[\sqrt{\frac{2}{\pi kD}}] \text{ and } |\varphi_{halflower} - \varepsilon| > \arcsin[\sqrt{\frac{2}{\pi kD}}] \\ \frac{1}{2} g_{approximate}, & |\varphi_{halfupper} - \varepsilon| > \arcsin[\sqrt{\frac{2}{\pi kD}}] \text{ and } |\varphi_{halflower} - \varepsilon| < \arcsin[\sqrt{\frac{2}{\pi kD}}] \\ \frac{1}{2} g_{approximate}, & |\varphi_{halfupper} - \varepsilon| < \arcsin[\sqrt{\frac{2}{\pi kD}}] \text{ and } |\varphi_{halflower} - \varepsilon| > \arcsin[\sqrt{\frac{2}{\pi kD}}] \\ 0, & \text{otherwise,} \end{cases}$$

$$\text{for } 0 \le \theta \le \pi/2 \text{ or } 3\pi/2 \le \theta \le 2\pi,$$

$$g = 0, \qquad \text{for } \pi/2 \le \theta \le 3\pi/2. \tag{161}$$

A comparison of exact results in Eq. (160) and our approximation (Eqs. (153), (161)) as shown in Fig. 31, shows that the asymptotic approximation is not as successful for the half-ellipsoid as for the full ellipsoid. To obtain comparable accuracy for the half ellipsoid, one must double the frequency.

12 Source/receiver in the x-y plane

For the moment consider the in-plane scattering case given by incident/received wavevectors

$$\vec{k}_{R/S} = k(-\cos\theta_{R/S}, -\sin\theta_{R/S}, 0), \tag{162}$$

where $0 \le \theta_{R/S} < 2\pi$.

The viewed/illuminated areas are given formally by the conditions $\vec{k}_{R/S} \cdot \vec{n} = 0$ which gives

$$\tan\varphi = -\frac{a}{b}\tan\theta_{R/S}. \tag{163}$$

These equations can be solved as

$$\begin{aligned}
\varphi_{Ru}(\theta_R) &= \pi - \arctan[b\cos\theta_R, a\sin\theta_R],\ 0 \le \theta_R \le \pi \\
\varphi_{Rl}(\theta_R) &= -\arctan[b\cos\theta_R, a\sin\theta_R],\ 0 \le \theta_R \le \pi, \\
\varphi_{RU}(\theta_R) &= -\pi - \varphi_{Rl}(2\pi - \theta_R),\ \pi \le \theta_R \le 2\pi \\
\varphi_{Rl}(\theta_R) &= -\pi - \varphi_{Ru}(2\pi - \theta_R),\ \pi \le \theta_R \le 2\pi, \\
\varphi_{Su}(\theta_S) &= \pi - \arctan[b\cos\theta_S, a\sin\theta_S],\ 0 \le \theta_S \le \pi, \\
\varphi_{Sl}(\theta_S) &= -\arctan[b\cos\theta_S, a\sin\theta_S],\ 0 \le \theta_S \le \pi, \\
\varphi_{SU}(\theta_S) &= -\pi - \varphi_{Sl}(2\pi - \theta_S),\ \pi \le \theta_S \le 2\pi \\
\varphi_{Sl}(\theta_S) &= -\pi - \varphi_{Su}(2\pi - \theta_S),\ \pi \le \theta_S \le 2\pi.
\end{aligned} \tag{164}$$

These choices give $g(2\pi - \theta_R, 2\pi - \theta_S) = g(\theta_R, \theta_S)$ for $0 \le \theta_{R/S} \le 2\pi$. An illustration of the viewed/illuminated areas is shown in Fig. 32.

For convenience define

$$\begin{aligned}
\varphi_{upper} &= Min(\varphi_{Ru}, \varphi_{Su}), \\
\varphi_{lower} &= Max(\varphi_{Rl}, \varphi_{Sl}).
\end{aligned} \tag{165}$$

The integration areas for the Kirchhoff integral can be determined by the following cases:
(1) If both source and receiver lie on the same side of the x-z plane, $0 \le \theta_{R/S} \le \pi$ or $\pi \le \theta_{R/S} \le 2\pi$, then

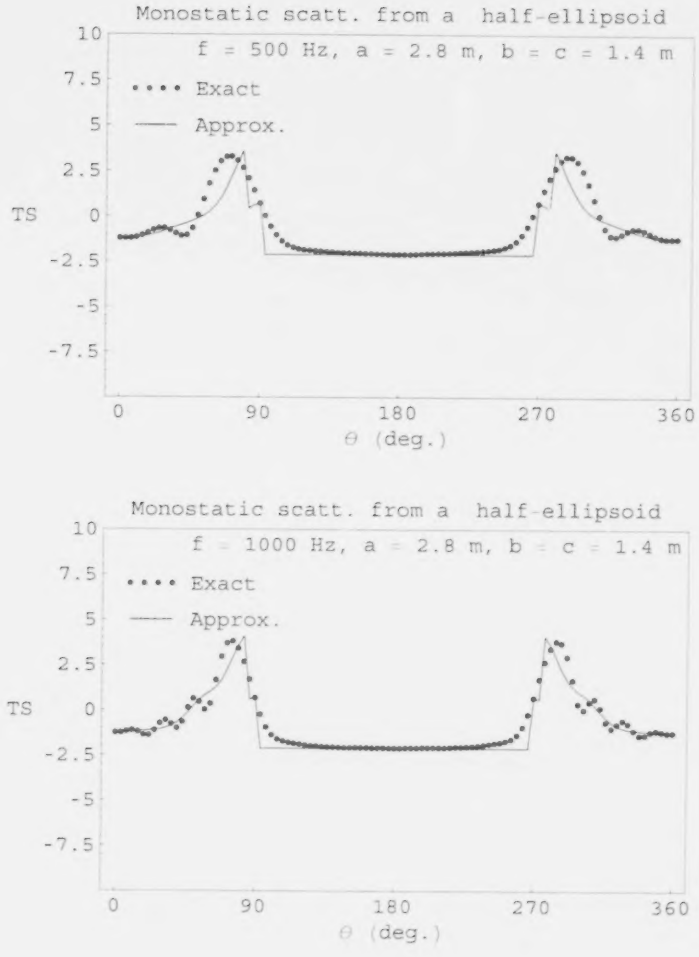

Figure 31: Comparison of exact and approximate scattering formulae for the Target Strength = $10\log(10.|g|^2)$ for the half-ellipsoid facing the positive x direction: $a = 2.8$ m, $b = c = 1.4$ m. The data points are given by an exact numerical integration of Eq. (160), the solid line is the asymptotic formula given by Eq. (161). The top graph has $f = 500$ Hz, the bottom graph $f = 1000$ Hz: as the frequency increases the accuracy of the truncated model improves. For $f = 500$ Hz, the error in the approximate model is less than 2.0 dB, for $f = 1000$ Hz, the error is less than 0.8 dB.

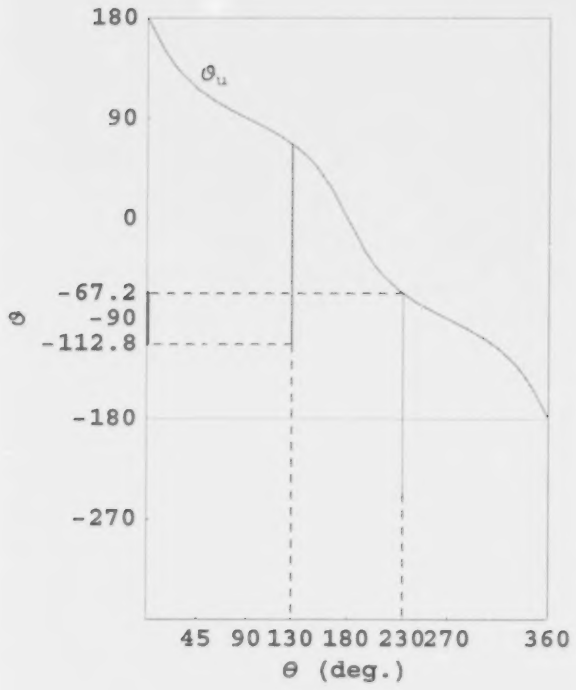

Figure 32: The viewed/illuminated areas for the ellipsoid for the in-plane bistatic case, $a = 2$, $b = c = 1$. For $\theta_R = 130^o$, $\theta_S = 210^o$ the viewed/illuminated areas extend from $-112.8^o \leq \varphi \leq -67.2^o$.

the integration region is given by $\varphi_{lower} \le \varphi \le \varphi_{upper}$;
(2) If $0 \le \theta_R \le \pi$ and $\pi \le \theta_S \le 2\pi$, then the integration region is the intersection of the ranges $Mod[\varphi_{Sl}, 2\pi, -\pi] \le \varphi \le \pi$ and $-\pi \le \varphi \le \varphi_{Su}$ with the range $\varphi_{Rl} \le \varphi \le \varphi_{Ru}$ (if $Mod[\varphi_{Sl}, 2\pi, -\pi] < \varphi_{Ru}$ then the integration range is $Mod[\varphi_{Sl}, 2\pi, -\pi] \le \varphi \le \varphi_{Ru}$, if $\varphi_{Rl} < \varphi_{Su}$ then the integration range is $\varphi_{Rl} \le \varphi \le \varphi_{Su}$);
(3) If $0 \le \theta_S \le \pi$ or $\pi \le \theta_R \le 2\pi$, then the integration region is the intersection of the ranges $Mod[\varphi_{Rl}, 2\pi, -\pi] \le \varphi \le \pi$ and $-\pi \le \varphi \le \varphi_{Ru}$ with the range $\varphi_{Sl} \le \varphi \le \varphi_{Su}$ (if $Mod[\varphi_{Rl}, 2\pi, -\pi] < \varphi_{Su}$ then the integration range is $Mod[\varphi_{Rl}, 2\pi, -\pi] \le \varphi \le \varphi_{Su}$, if $\varphi_{Sl} < \varphi_{Ru}$ then the integration range is $\varphi_{Sl} \le \varphi \le \varphi_{Ru}$).

In case (1) the scattering strength becomes

$$\begin{aligned} g &= -\frac{1}{4\pi}\int_{\text{illum. area}} (\vec{k}_s + \vec{k}_s)\cdot\vec{n}\, e^{-i(\vec{k}_s+\vec{k}_s)\cdot\vec{r}}dS \\ &= \frac{kc}{4\pi}\int_{\varphi_{lower}}^{\varphi_{upper}} d\varphi \int_0^{\pi} d\phi (b[\cos\theta_R + \cos\theta_S]\sin\varphi + a[\sin\theta_R + \sin\theta_S]\cos\varphi)\sin^2\phi \quad \times \\ &\quad e^{ik(\sin\phi\{a[\cos\theta_R+\cos\theta_S]\sin\varphi + b[\sin\theta_R+\sin\theta_S]\cos\varphi\}} \end{aligned} \tag{166}$$

Again using the result

$$\frac{1}{\pi}\int_0^{\pi} d\phi \sin^2\phi\, e^{iA\sin\phi} = \frac{1}{2}\{J_0(A) - J_2(A)\} + \frac{1}{2}i\{H_0(A) - H_2(A)\} + \frac{iA}{3\pi}. \tag{167}$$

one obtains the form suitable for exact numerical evaluation:

$$\begin{aligned} g &= \frac{kc}{4}\int_{\varphi_{lower}}^{\varphi_{upper}} d\varphi\, (b[\cos\theta_R + \cos\theta_S]\sin\varphi + a[\sin\theta_R + \sin\theta_S]\cos\varphi) \quad \times \\ &\quad \left\{\frac{1}{2}\{J_0(A) - J_2(A)\} + \frac{1}{2}i\{H_0(A) - H_2(A)\} + \frac{iA}{3\pi}\right\}. \end{aligned} \tag{168}$$

where $A = k\{a[\cos\theta_R + \cos\theta_S]\sin\varphi + b[\sin\theta_R + \sin\theta_S]\cos\varphi\}$. Cases (2) and (3) are the same with the appropriate limits for the φ integral. An example of an exact bistatic calculation is shown in Fig. 33

To approximate the scattering strength for case (1) define the auxiliary functions:

$$\begin{aligned} \varepsilon &= \arctan[b(\sin\theta_R + \sin\theta_S), a(\cos\theta_R + \cos\theta_S)], \\ D &= \sqrt{(a[\cos\theta_R + \cos\theta_S])^2 + (b[\sin\theta_R + \sin\theta_S])^2} \\ \varepsilon' &= \arctan[a(\sin\theta_R + \sin\theta_S), b(\cos\theta_R + \cos\theta_S)], \\ D' &= \sqrt{(b[\cos\theta_R + \cos\theta_S])^2 + (a[\sin\theta_R + \sin\theta_S])^2}. \end{aligned} \tag{169}$$

Then Eq. (166) becomes

$$\begin{aligned} g &= \frac{kcD'}{4\pi}\int_{\varphi_{lower}}^{\varphi_{upper}} d\varphi \int_0^{\pi} d\phi \cos(\varphi - \varepsilon')\sin^2\phi\, e^{ikD\sin\phi\cos(\varphi-\varepsilon)} \\ &= \frac{kcD'}{4\pi}\int_{\varphi_{lower}-\varepsilon}^{\varphi_{upper}-\varepsilon} d\varphi \int_0^{\pi} d\phi \cos(\varphi + \varepsilon - \varepsilon')\sin^2\phi\, e^{ikD\sin\phi\cos\varphi} \end{aligned} \tag{170}$$

This is formally the same as the monostatic case, with a change in the definitions of the functions auxiliary functions. Hence as in the monostatic case we approximate this function by the form

$$g_{saddlepoint} = \frac{cD'\cos(\varepsilon - \varepsilon')}{2iD}\left\{e^{ikD} - \frac{\sin[kD/2]}{kD/2}e^{ikD/2}\right\}. \tag{171}$$

Our rule for handling this integral is the same as in the monostatic case: if there is no saddle point in the range of integration use $g \approx 0$, if there is a saddle point in the range of integration, for each end-point

such that $|\varphi_{lower} - \varepsilon| > \arcsin[\sqrt{2/(\pi kD)}]$ or $|\varphi_{lower} - \varepsilon| > \arcsin[\sqrt{2/(\pi kD)}]$, count one-half the saddle point contribution, otherwise count zero. Then the scattering strength is approximated as

$$g \approx \begin{cases} g_{saddlepoint}, & \text{if } |\varphi_{lower} - \varepsilon| > \arcsin[\sqrt{2/(\pi kD)}] \text{ and } |\varphi_{lower} - \varepsilon| > \arcsin[\sqrt{2/(\pi kD)}], \\ \frac{1}{2} g_{saddlepoint}, & \text{if } |\varphi_{lower} - \varepsilon| > \arcsin[\sqrt{2/(\pi kD)}] \text{ and } |\varphi_{lower} - \varepsilon| < \arcsin[\sqrt{2/(\pi kD)}], \\ \frac{1}{2} g_{saddlepoint}, & \text{if } |\varphi_{lower} - \varepsilon| < \arcsin[\sqrt{2/(\pi kD)}] \text{ and } |\varphi_{lower} - \varepsilon| > \arcsin[\sqrt{2/(\pi kD)}], \end{cases}$$
$$\text{if } \varphi_{lower} \le \varepsilon \le \varphi_{upper} \text{ and } 0 \le \theta_{R/S} \le \pi \text{ or } \pi \le \theta_{R/S} \le 2\pi; \tag{172}$$

Cases (2) and (3) are evaluated in a similar fashion using the appropriate integration limits for those cases to determine the position of the saddle points. Details are implemented in the software.

Note that we have assumed that $kD >> 1$ in using the asymptotic results. In the case $kD << 1$, approximate the scattering strength by expanding the exponential; the following model will be sufficient:

$$g \approx \frac{kcD'}{8}[\sin(\varphi_{upper} - \varepsilon') - \sin(\varphi_{lower} - \varepsilon')], \quad kD << 1. \tag{173}$$

A comparison of the approximate model and the exact calculation is shown in Fig. 33. This plot shows that the asymptotic approximation is quite successful for the in-plane bistatic case. One notes that it is the higher order terms in the saddle point expansion (and branch line integrals) that gives the subtle bow-tie type detail in the approximate scattering results that so closely match the exact results. If the higher order terms in Eq. (171) were dropped, the areas of high scattering in the approximate results would reduce to uniform diagonal bars, and the bow-tie effect would be lost.

12.1 The in-plane bistatic case for the half-ellipsoid

Now consider the half-ellipsoid discussed previously.

For the full ellipsoid the viewed/illuminated areas were defined by

$$\begin{aligned}
\varphi_{Ru}(\theta_R) &= \pi - \arctan[b\cos\theta_R, a\sin\theta_R],\ 0 \le \theta_R \le \pi \\
\varphi_{Rl}(\theta_R) &= -\arctan[b\cos\theta_R, a\sin\theta_R],\ 0 \le \theta_R \le \pi, \\
\varphi_{RU}(\theta_R) &= -\pi - \varphi_{Rl}(2\pi - \theta_R),\ \pi \le \theta_R \le 2\pi \\
\varphi_{Rl}(\theta_R) &= -\pi - \varphi_{Ru}(2\pi - \theta_R),\ \pi \le \theta_R \le 2\pi, \\
\varphi_{Su}(\theta_S) &= \pi - \arctan[b\cos\theta_S, a\sin\theta_S],\ 0 \le \theta_S \le \pi, \\
\varphi_{Sl}(\theta_S) &= -\arctan[b\cos\theta_S, a\sin\theta_S],\ 0 \le \theta_S \le \pi, \\
\varphi_{SU}(\theta_S) &= -\pi - \varphi_{Sl}(2\pi - \theta_S),\ \pi \le \theta_S \le 2\pi \\
\varphi_{Sl}(\theta_S) &= -\pi - \varphi_{Su}(2\pi - \theta_S),\ \pi \le \theta_S \le 2\pi.
\end{aligned} \tag{174}$$

Now to define the viewed/illuminated areas for the half-ellipsoid, proceed exactly as in the monostatic case; namely define the functions

$$\begin{aligned}
\varphi_{halfRu}(\theta_R) &= \begin{cases} \varphi_{Ru}(\theta_R), & 0 \le \varphi_{Ru}(\theta_R) \le \pi \\ -\pi, & -\pi \le \varphi_{Ru}(\theta_R) \le 0; \end{cases} \\
\varphi_{halfRl}(\theta_R) &= \begin{cases} 0, & -\pi \le \varphi_{Rl}(\theta_R) \le 0 \\ \varphi_{Rl}(\theta_R), & -2\pi \le \varphi_{Ru}(\theta_R) \le -\pi \end{cases} \\
\varphi_{halfSu}(\theta_S) &= \begin{cases} \varphi_{Su}(\theta_S), & 0 \le \varphi_{Su}(\theta_S) \le \pi \\ -\pi, & -\pi \le \varphi_{Su}(\theta_S) \le 0; \end{cases} \\
\varphi_{halfSl}(\theta_S) &= \begin{cases} 0, & -\pi \le \varphi_{Sl}(\theta_S) \le 0 \\ \varphi_{Sl}(\theta_S), & -2\pi \le \varphi_{Su}(\theta_S) \le -\pi \end{cases}
\end{aligned} \tag{175}$$

Now formally everything else is unchanged in our exact expression and in our approximation, provided one makes the substitutions $\{\varphi_{Ru}, \varphi_{Rl}, \varphi_{Su}, \varphi_{Sl}\} \to \{\varphi_{halfRu}, \varphi_{halfRl}, \varphi_{halfSu}, \varphi_{halfSl}\}$

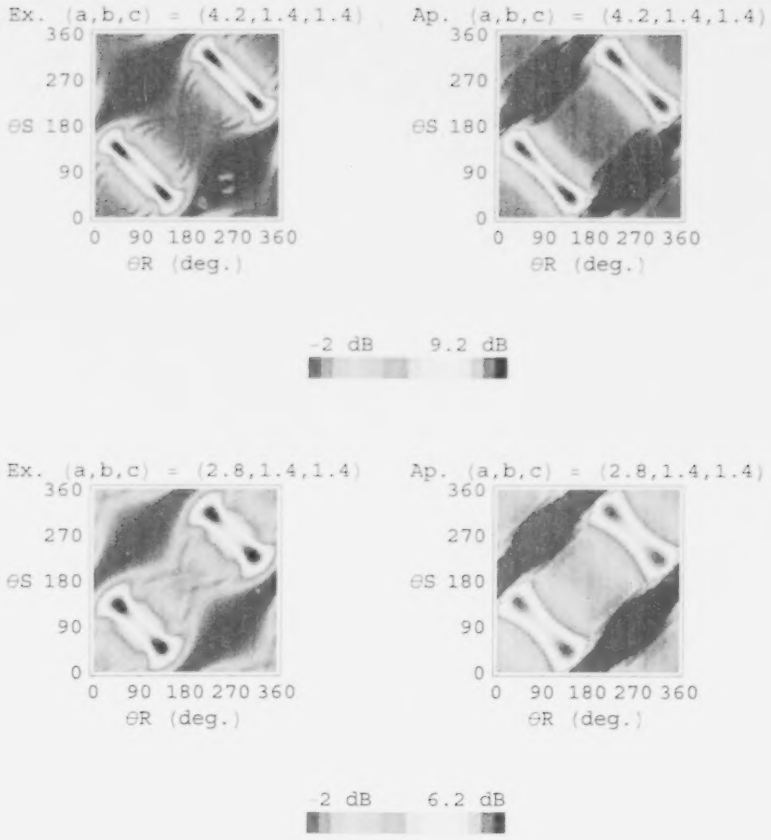

Figure 33: The in-plane bistatic case for the ellipsoid. This shows a comparison between an exact calculation and an approximate result using saddle point terms for the ellipsoid. For the top row, the parameters are $f = 500$ Hz, $a = 4.2$ m, $b = c = 1.4$ m; for the bottom row $f = 500$ Hz, $a = 2.8$ m, $b = c = 1.4$ m.

A comparison between an exact calculation and the saddle point approximation is shown in Fig 34. Generally speaking, the model for these truncated surfaces is not as successful as the full surface, simply because the truncated surface is half the size. Equivalently one would have to double the frequency to obtain comparable accuracy with the full surface results.

13 The out-of-plane case

Now return to the general case shown in Fig. 27, where

$$\vec{k}_{R/S} = k\{-\cos\eta_{R/S}\cos\theta_{R/S}, -\cos\eta_{R/S}\sin\theta_{R/S}, -\sin\eta_{R/S}\}. \tag{176}$$

In performing surface integrals, one possible strategy is to choose a surface parametrization such that the coordinate curves map out the integration area. The integration area for Kirchhoff integral is determined by imposing the constraints $\vec{k}_{R/S}\cdot\vec{n} = 0$. Each of these constraints defines an ellipse on the surface of the ellipsoid. The integration area is shown in Fg. 27 as the area between the red and yellow ellipses. It is possible to choose a parametrization of the ellipsoid such that coordinates curves match these ellipses. The details to support this procedure are shown below.

Instead of the parametrization given by Eq. (141), choose a more general representation

$$\begin{aligned}\vec{r}(\varphi,\phi) &= \{x(\varphi,\phi), y(\varphi,\phi), z(\varphi,\phi)\}\\ &= \{a[\cos\varphi_1\sin\varphi\sin\phi + \cos\phi_1\sin\varphi_1\cos\varphi\sin\phi + \sin\varphi_1\sin\phi_1\cos\phi],\\ &\quad b[\cos\varphi_1\cos\phi_1\cos\varphi\sin\phi - \sin\varphi_1\sin\varphi\sin\phi + \cos\varphi_1\sin\phi_1\cos\phi],\\ &\quad c[\cos\phi_1\cos\phi - \sin\phi_1\cos\varphi\sin\phi]\},\end{aligned} \tag{177}$$

where $0 \le \varphi \le 2\pi$, $0 \le \phi \le \pi$. In terms of Euler angles, this is a rotation ϕ_1 around the x-axis followed by a rotation φ_1 around the z-axis. The origin $(0,0,c)$ gets rotated to

$$\{x_1, y_1, z_1\} = \{a\sin\varphi_1\sin\phi_1, b\cos\varphi_1\sin\phi_1, c\cos\phi_1\}. \tag{178}$$

The representation could be rewritten as

$$\begin{aligned}\vec{r}(\varphi,\phi) &= \sin\phi\{a[\cos\varphi_1\sin\varphi + \cos\phi_1\sin\varphi_1\cos\varphi], b[\cos\varphi_1\cos\phi_1\cos\varphi - \sin\varphi_1\sin\varphi], c[-\sin\phi_1\cos\varphi]\} +\\ &\quad \cos\phi\{x_1, y_1, z_1\}.\end{aligned} \tag{179}$$

Hence $\vec{r}(\varphi,0) = \{x_1, y_1, z_1\}$ and $\vec{r}(\varphi,\pi) = -\{x_1, y_1, z_1\}$. This representation allows one to arbitrarily choose the origin of coordinates to lie anywhere on the surface of the ellipsoid, as illustrated in Fig. 35.

Choose $\varphi_1 = \varphi_1(\vec{k}_R, \vec{k}_S)$, $\phi_1 = \phi_1(\vec{k}_R, \vec{k}_S)$ such that the origin coincides with the intersection of the red and yellow ellipses shown in Fig. 27.

One may note that in Cartesian coordinates the normal to the ellipsoid may be written as

$$\vec{n}(\varphi,\phi) = (\frac{x}{a^2}, \frac{y}{b^2}, \frac{z}{c^2})/\sqrt{\frac{x^2}{a^4} + \frac{y^2}{b^4} + \frac{z^2}{c^4}}. \tag{180}$$

The conditions $\vec{k}_{R/S}\cdot\vec{n} = 0$ give the planes

$$(\frac{\cos\eta_{R/S}\cos\theta_{R/S}}{a^2})x + (\frac{\cos\eta_{R/S}\sin\theta_{R/S}}{b^2})y + (\frac{\sin\eta_{R/S}}{c^2})z = 0, \tag{181}$$

intersecting the ellipsoid, yielding the red and yellow ellipses. Explicit parametrizations of these ellipses may be constructed if desired.

These ellipses intersect at the points on the ellipsoid given by the simultaneous solution of Eqs.(181) i.e.

$$\begin{aligned}(\frac{\cos\eta_R\cos\theta_R}{a^2})x + (\frac{\cos\eta_R\sin\theta_R}{b^2})y + (\frac{\sin\eta_R}{c^2})z &= 0,\\ (\frac{\cos\eta_S\cos\theta_S}{a^2})x + (\frac{\cos\eta_S\sin\theta_S}{b^2})y + (\frac{\sin\eta_S}{c^2})z &= 0,\\ \frac{x^2}{a^2} + \frac{y^2}{b^2} + \frac{z^2}{c^2} &= 1.\end{aligned} \tag{182}$$

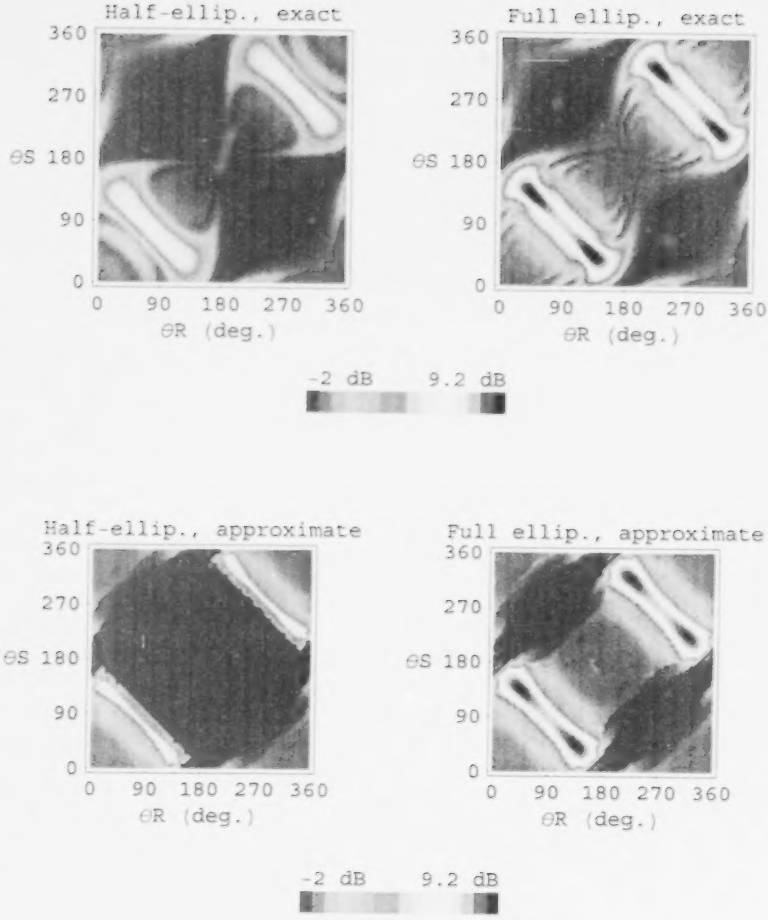

Figure 34: The in-plane bistatic case for the half-ellipsoid. This shows a comparison between an exact calculation and an approximate result using saddle point terms for the half-ellipsoid and the full ellipsoid. The parameters are $f = 500$ Hz, $a = 4.2$ m, $b = c = 1.4$ m.

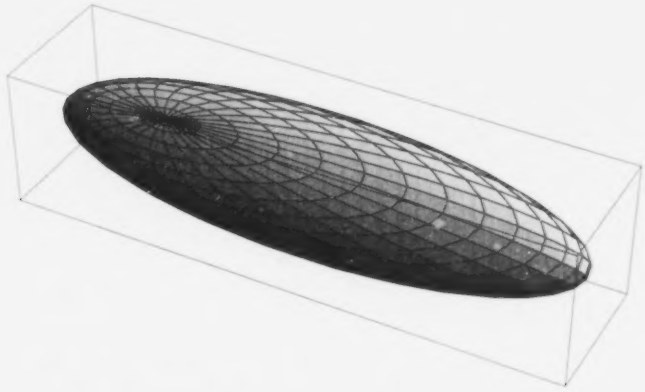

Figure 35: The ellipsoid $x^2/a^2 + y^2/b^2 + z^2/c^2 = 1$ with $a/b = a/c = 4$. The illuminated and viewed areas of the ellipsoid are now defined by coordinates curves in the rotated coordinate system.

This gives the two solutions $(x_1, y_1, z_1) = (x_1(\vec{k}_R, \vec{k}_S), y_1(\vec{k}_R, \vec{k}_S), z_1(\vec{k}_R, \vec{k}_S))$ and $(-x_1, -y_1, -z_1)$.

Explicit expressions for the coordinates are given by

$$\begin{aligned}
\frac{x_1}{a} &= \frac{[n_{rz}n_{sy} - n_{ry}n_{sz}]}{\sqrt{[n_{rz}n_{sy} - n_{ry}n_{sz}]^2 + [-n_{rz}n_{sx} + n_{rx}n_{sz}]^2 + [n_{ry}n_{sx} - n_{rx}n_{sy}]^2}}, \\
\frac{y_1}{b} &= \frac{[-n_{rz}n_{sx} + n_{rx}n_{sz}]}{\sqrt{[n_{rz}n_{sy} - n_{ry}n_{sz}]^2 + [-n_{rz}n_{sx} + n_{rx}n_{sz}]^2 + [n_{ry}n_{sx} - n_{rx}n_{sy}]^2}}, \\
\frac{z_1}{c} &= \frac{[n_{ry}n_{sx} - n_{rx}n_{sy}]}{\sqrt{[n_{rz}n_{sy} - n_{ry}n_{sz}]^2 + [-n_{rz}n_{sx} + n_{rx}n_{sz}]^2 + [n_{ry}n_{sx} - n_{rx}n_{sy}]^2}},
\end{aligned} \tag{183}$$

where for shorthand

$$\begin{aligned}
\{n_{rx}, n_{ry}, n_{rz}\} &= \{\frac{\cos\eta_R \cos\theta_R}{a}, \frac{\cos\eta_R \sin\theta_R}{b}, \frac{\sin\eta_R}{c}\}, \\
\{n_{sx}, n_{sy}, n_{sz}\} &= \{\frac{\cos\eta_S \cos\theta_S}{a}, \frac{\cos\eta_S \sin\theta_S}{b}, \frac{\sin\eta_S}{c}\}.
\end{aligned} \tag{184}$$

The Cartesian coordinates of the origin $\{x_1, y_1, z_1\} = \{a\sin\varphi_1 \sin\phi_1, b\cos\varphi_1 \sin\phi_1, c\cos\phi_1\}$ then yield

$$\begin{aligned}
\varphi_1 &= \arctan[y_1, x_1] \\
\phi_1 &= \arccos[z_1/c],
\end{aligned} \tag{185}$$

where arccos is the principal value and the branch of arctan has been defined in the previous subsection.

13.1 Special case: out-of-plane monostatic case

In the out-of-plane monostatic case, the viewed/illuminated area is defined by $\{\cos\theta\cos\eta, \sin\theta\cos\eta, \sin\eta\} \cdot \vec{n} = 0$: in terms of the parametric representation introduced previously this can be written as:

$$\sin\phi \left\{ \sin\varphi [\frac{\cos\eta\cos\theta}{a}\cos\varphi_1 - \frac{\cos\eta\sin\theta}{b}\sin\varphi_1] +\right.$$

$$\cos\varphi[\frac{\cos\eta\cos\theta}{a}\cos\phi_1\sin\varphi_1+\frac{\cos\eta\sin\theta}{b}\cos\varphi_1\cos\phi_1-\frac{\sin\eta}{c}\sin\phi_1]\Big\}+$$
$$\cos\phi\left\{-\frac{1}{k}\vec{k}\cdot\{\frac{x_1}{a^2},\frac{y_1}{b^2},\frac{z_1}{c^2}\}\right\}=0. \tag{186}$$

If one chooses the new origin such that it lies on the ellipse defining the viewed/illuminated area then

$$\vec{k}\cdot\vec{n}(0,0)\propto\vec{k}\cdot\{\frac{x_1}{a^2},\frac{y_1}{b^2},\frac{z_1}{c^2}\}=0$$

then this gives the constraint

$$\frac{\cos\eta\cos\theta}{a}\sin\varphi_1\sin\phi_1+\frac{\cos\eta\sin\theta}{b}\cos\varphi_1\sin\phi_1+\frac{\sin\eta}{c}\cos\phi_1=0. \tag{187}$$

If we choose $\varphi_1=\arctan[\frac{\sin\theta}{b},\frac{\cos\theta}{a}]$, then $\phi_1=\arctan[c\sqrt{(\frac{\sin\theta}{b})^2+(\frac{\cos\theta}{a})^2},-\tan\eta]$.

Then the former equation becomes

$$\sin\varphi[\frac{\cos\eta\cos\theta}{a}\cos\varphi_1-\frac{\cos\eta\sin\theta}{b}\sin\varphi_1]+$$
$$\cos\varphi[\frac{\cos\eta\cos\theta}{a}\cos\phi_1\sin\varphi_1+\frac{\cos\eta\sin\theta}{b}\cos\varphi_1\cos\phi_1-\frac{\sin\eta}{c}\sin\phi_1]=0. \tag{188}$$

This is easily recognized as the equation for an ellipse and it can be rewritten as

$$\tan\varphi=\frac{[-\frac{\cos\eta\cos\theta}{a}\cos\phi_1\sin\varphi_1-\frac{\cos\eta\sin\theta}{b}\cos\varphi_1\cos\phi_1+\frac{\sin\eta}{c}\sin\phi_1]}{[\frac{\cos\eta\cos\theta}{a}\cos\varphi_1-\frac{\cos\eta\sin\theta}{b}\sin\varphi_1]}. \tag{189}$$

If $\eta=0$ then $\phi_1=0$ and one can choose $\varphi_1=0$ this reduces to Eq. (144). This equation can be solved as

$$\begin{aligned}\varphi_{upper} &= \pi-\arctan[\frac{\cos\eta\cos\theta}{a}\cos\varphi_1-\frac{\cos\eta\sin\theta}{b}\sin\varphi_1,\\ &\quad -\frac{\cos\eta\cos\theta}{a}\cos\phi_1\sin\varphi_1-\frac{\cos\eta\sin\theta}{b}\cos\varphi_1\cos\phi_1+\frac{\sin\eta}{c}\sin\phi_1],\\ \varphi_{lower} &= -\arctan[\frac{\cos\eta\cos\theta}{a}\cos\varphi_1-\frac{\cos\eta\sin\theta}{b}\sin\varphi_1,\\ &\quad -\frac{\cos\eta\cos\theta}{a}\cos\phi_1\sin\varphi_1-\frac{\cos\eta\sin\theta}{b}\cos\varphi_1\cos\phi_1+\frac{\sin\eta}{c}\sin\phi_1].\end{aligned} \tag{190}$$

The integration limits are given by

$$\int_{\text{illum. area}}d\varphi d\phi\rightarrow\int_{\varphi_{lower}}^{\varphi_{upper}}d\varphi\int_0^{\pi}d\phi,$$

so the scattering strength is given by

$$\begin{aligned}g &= \frac{k}{2\pi}\int_{\varphi_{lower}}^{\varphi_{upper}}d\varphi\int_0^{\pi}d\phi\sin\phi\times\\ &\quad\{bc[\sin\varphi\sin\phi\cos\varphi_1+\sin\varphi_1(\cos\varphi\cos\phi_1\sin\phi+\cos\phi\sin\phi_1)]\cos\eta\cos\theta+\\ &\quad ac[\cos\varphi\cos\varphi_1\cos\phi_1\sin\phi-\sin\varphi\sin\varphi_1\sin\phi+\cos\varphi_1\cos\phi\sin\phi_1]\cos\eta\sin\theta+\\ &\quad ab[\cos\phi\cos\phi_1-\cos\varphi\sin\phi\sin\phi_1]\sin\eta\}\times\\ &\quad\exp[2ik\{a[\cos\varphi_1\sin\varphi\sin\phi+\cos\phi_1\sin\varphi_1\cos\varphi\sin\phi+\sin\varphi_1\sin\phi_1\cos\phi]\cos\eta\cos\theta+\\ &\quad b[\cos\varphi_1\cos\phi_1\cos\varphi\sin\phi-\sin\varphi_1\sin\varphi\sin\phi+\cos\varphi_1\sin\varphi_1\cos\phi]\cos\eta\sin\theta+\\ &\quad c[\cos\phi_1\cos\phi-\sin\phi_1\cos\varphi\sin\phi]\sin\eta\})]\end{aligned} \tag{191}$$

This simplifies to

$$
\begin{aligned}
g &= \frac{k}{2\pi}\int_{\varphi_{lower}}^{\varphi_{upper}} d\varphi\,\{bc[\sin\varphi\cos\varphi_1+\sin\varphi_1\cos\varphi\cos\phi_1]\cos\eta\cos\theta+ \\
&\quad ac[\cos\varphi\cos\varphi_1\cos\phi_1-\sin\varphi\sin\varphi_1]\cos\eta\sin\theta+ab[-\cos\varphi\sin\phi_1]\sin\eta\}\times \\
&\quad \int_0^{\pi} d\phi\sin^2\phi\times\exp[2ik\{a[\cos\varphi_1\sin\varphi\sin\phi+\cos\phi_1\sin\varphi_1\cos\varphi\sin\phi+\sin\varphi_1\sin\phi_1\cos\phi]\cos\eta\cos\theta+ \\
&\quad b[\cos\varphi_1\cos\phi_1\cos\varphi\sin\phi-\sin\varphi_1\sin\varphi\sin\phi+\cos\varphi_1\sin\phi_1\cos\phi]\cos\eta\sin\theta+ \\
&\quad c[\cos\phi_1\cos\phi-\sin\phi_1\cos\varphi\sin\phi]\sin\eta]\})]. \qquad (192)
\end{aligned}
$$

This is in a form appropriate for exact numerical evaluation, provided one does the double integral numerically.

$$
\begin{aligned}
g &= \frac{k}{2\pi}\int_{\varphi_{lower}}^{\varphi_{upper}} d\varphi\{A\cos\varphi+B\sin\varphi\}\int_0^{\pi} d\phi\sin^2\phi\, e^{2ik\{C\cos\phi+(D\sin\varphi+E\cos\varphi)\sin\phi\}} \\
&= \frac{k\sqrt{A^2+B^2}}{2\pi}\int_{\varphi_{lower}}^{\varphi_{upper}} d\varphi\cos(\varphi-\varepsilon')\int_0^{\pi} d\phi\sin^2\phi\, e^{2ik\{C\cos\phi+\sqrt{D^2+E^2}\cos(\varphi-\varepsilon)\sin\phi\}} \\
&= \frac{k\sqrt{A^2+B^2}}{2\pi}\int_{\varphi_{lower}-\varepsilon}^{\varphi_{upper}-\varepsilon} d\varphi\cos(\varphi+\varepsilon-\varepsilon')\int_0^{\pi} d\phi\sin^2\phi\, e^{2ik\{C\cos\phi+\sqrt{D^2+E^2}\cos\varphi\sin\phi\}} \\
&= \frac{k\sqrt{A^2+B^2}\sin(\varepsilon-\varepsilon')}{2\pi}\int_{\varphi_{lower}-\varepsilon}^{\varphi_{upper}-\varepsilon} d\varphi\sin\varphi\int_0^{\pi} d\phi\sin^2\phi\, e^{2ik\{C\cos\phi+\sqrt{D^2+E^2}\cos\varphi\sin\phi\}}+ \\
&\quad \frac{k\sqrt{A^2+B^2}\cos(\varepsilon-\varepsilon')}{2\pi}\int_{\varphi_{lower}-\varepsilon}^{\varphi_{upper}-\varepsilon} d\varphi\cos\varphi\int_0^{\pi} d\phi\sin^2\phi\, e^{2ik\{C\cos\phi+\sqrt{D^2+E^2}\cos\varphi\sin\phi\}}, \qquad (193)
\end{aligned}
$$

where

$$
\begin{aligned}
A &= \{bc[\sin\varphi_1\cos\phi_1]\cos\eta\cos\theta+ac[\cos\varphi_1\cos\phi_1]\cos\eta\sin\theta+ \\
&\quad ab[-\sin\phi_1]\sin\eta\}, \\
B &= \{bc[\cos\varphi_1]\cos\eta\cos\theta+ac[-\sin\varphi_1]\cos\eta\sin\theta\}, \\
C &= \{a[\sin\varphi_1\sin\phi_1]\cos\eta\cos\theta+b[\cos\varphi_1\sin\phi_1]\cos\eta\sin\theta+ \\
&\quad c[\cos\phi_1]\sin\eta\}, \\
D &= \{a[\cos\varphi_1]\cos\eta\cos\theta+b[-\sin\varphi_1]\cos\eta\sin\theta\} \\
E &= \{a[\cos\phi_1\sin\varphi_1]\cos\eta\cos\theta+b[\cos\varphi_1\cos\phi_1]\cos\eta\sin\theta+ \\
&\quad c[-\sin\phi_1]\sin\eta\}, \\
D' &= \sqrt{C^2+D^2+E^2}, \\
\varepsilon &= \arctan[E,D], \\
\varepsilon' &= \arctan[A,B]. \qquad (194)
\end{aligned}
$$

The term involving $\sin(\varepsilon-\varepsilon')$ can be performed analytically and it is small and will be neglected. This gives

$$
g \approx \frac{k\sqrt{A^2+B^2}\cos(\varepsilon-\varepsilon')}{2\pi}\int_{\varphi_{lower}-\varepsilon}^{\varphi_{upper}-\varepsilon} d\varphi\cos\varphi\int_0^{\pi} d\phi\sin^2\phi\, e^{2ik\{C\cos\phi+\sqrt{D^2+E^2}\cos\varphi\sin\phi\}}. \qquad (195)
$$

A saddle point approximation for this integral will be developed in the following more general bistatic case.

13.2 General bistatic case

Now return to the bistatic case. The viewed area is defined by the ellipse

$$\sin\varphi[\frac{\cos\eta_R\cos\theta_R}{a}\cos\varphi_1-\frac{\cos\eta_R\sin\theta_R}{b}\sin\varphi_1]+$$
$$\cos\varphi[\frac{\cos\eta_R\cos\theta_R}{a}\cos\phi_1\sin\varphi_1+\frac{\cos\eta_R\sin\theta_R}{b}\cos\varphi_1\cos\phi_1-\frac{\sin\eta_R}{c}\sin\phi_1]=0, \tag{196}$$

or equivalently one may define the angles

$$\begin{aligned}
\varphi_{Ru} &= \pi-\arctan[[\frac{\cos\eta_R\cos\theta_R}{a}\cos\varphi_1-\frac{\cos\eta_R\sin\theta_R}{b}\sin\varphi_1],\\
&\quad [\frac{\cos\eta_R\cos\theta_R}{a}\cos\phi_1\sin\varphi_1+\frac{\cos\eta_R\sin\theta_R}{b}\cos\varphi_1\cos\phi_1-\frac{\sin\eta_R}{c}\sin\phi_1]]\\
\varphi_{Rl} &= -\arctan[[\frac{\cos\eta_R\cos\theta_R}{a}\cos\varphi_1-\frac{\cos\eta_R\sin\theta_R}{b}\sin\varphi_1],\\
&\quad [\frac{\cos\eta_R\cos\theta_R}{a}\cos\phi_1\sin\varphi_1+\frac{\cos\eta_R\sin\theta_R}{b}\cos\varphi_1\cos\phi_1-\frac{\sin\eta_R}{c}\sin\phi_1]],\\
\varphi_{Su} &= \pi-\arctan[[\frac{\cos\eta_S\cos\theta_S}{a}\cos\varphi_1-\frac{\cos\eta_S\sin\theta_S}{b}\sin\varphi_1],\\
&\quad [\frac{\cos\eta_S\cos\theta_S}{a}\cos\phi_1\sin\varphi_1+\frac{\cos\eta_S\sin\theta_S}{b}\cos\varphi_1\cos\phi_1-\frac{\sin\eta_S}{c}\sin\phi_1]]\\
\varphi_{Sl} &= -\arctan[[\frac{\cos\eta_S\cos\theta_S}{a}\cos\varphi_1-\frac{\cos\eta_S\sin\theta_S}{b}\sin\varphi_1],\\
&\quad [\frac{\cos\eta_S\cos\theta_S}{a}\cos\phi_1\sin\varphi_1+\frac{\cos\eta_S\sin\theta_S}{b}\cos\varphi_1\cos\phi_1-\frac{\sin\eta_S}{c}\sin\phi_1]],
\end{aligned} \tag{197}$$

and hence the viewed area is defined by the coordinate range $\varphi_{Rl}\le\varphi\le\varphi_{Ru}$ and the illuminated area by the range $\varphi_{Sl}\le\varphi\le\varphi_{Su}$. Again, for convenience define $\varphi_{upper}=Min(\varphi_{Ru},\varphi_{Su})$, $\varphi_{lower}=Max(\varphi_{Rl},\varphi_{Sl})$. In this notation, the viewed/illuminated area is given by

$$\int_{\text{illum. area}}d\varphi d\phi\to\int_{\varphi_{lower}}^{\varphi_{upper}}d\varphi\int_0^{\pi}d\phi.$$

Formally this is the same as the in-plane case except the expressions for $\varphi_{R/S}$ are more complicated.

The surface area is given by (in a lhs)

$$\begin{aligned}
\vec{n}dS &= -\vec{r}_\varphi\times\vec{r}_\phi\,d\varphi\,d\phi\\
&= \sin\phi(bc[\sin\varphi\sin\phi\cos\varphi_1+\sin\varphi_1(\cos\varphi\cos\phi_1\sin\phi+\cos\phi\sin\phi_1),\\
&\quad ac[\cos\varphi\cos\varphi_1\cos\phi_1\sin\phi-\sin\varphi\sin\varphi_1\sin\phi+\cos\varphi_1\cos\phi\sin\phi_1],\\
&\quad ab[\cos\phi\cos\phi_1-\cos\varphi\sin\phi\sin\phi_1])\,d\varphi\,d\phi.
\end{aligned} \tag{198}$$

This gives the bistatic scattering strength as

$$\begin{aligned}
g &= -\frac{1}{4\pi}\int_{\text{illum. area}}(\vec{k}_s+\vec{k}_s)\cdot\vec{n}\,e^{-i(\vec{k}_s+\vec{k}_s)\cdot\vec{r}}dS\\
&= \frac{k}{4\pi}\int_{\varphi_{lower}}^{\varphi_{upper}}d\varphi\int_0^{\pi}d\phi\sin\phi\times\\
&\quad \{bc[\sin\varphi\sin\phi\cos\varphi_1+\sin\varphi_1(\cos\varphi\cos\phi_1\sin\phi+\cos\phi\sin\phi_1)(\cos\eta_R\cos\theta_R+\cos\eta_S\cos\theta_S)+\\
&\quad ac[\cos\varphi\cos\varphi_1\cos\phi_1\sin\phi-\sin\varphi\sin\varphi_1\sin\phi+\cos\varphi_1\cos\phi\sin\phi_1](\cos\eta_R\sin\theta_R+\cos\eta_S\sin\theta_S)+\\
&\quad ab[\cos\phi\cos\phi_1-\cos\varphi\sin\phi\sin\phi_1](\sin\eta_R+\sin\eta_S)\}\times\\
&\quad \exp[ik\{a[\cos\varphi_1\sin\varphi\sin\phi+\cos\phi_1\sin\varphi_1\cos\varphi\sin\phi+\sin\varphi_1\sin\phi_1\cos\phi](\cos\eta_R\cos\theta_R+\cos\eta_S\cos\theta_S)+\\
&\quad b[\cos\varphi_1\cos\phi_1\cos\varphi\sin\phi-\sin\varphi_1\sin\varphi\sin\phi+\cos\varphi_1\sin\phi_1\cos\phi](\cos\eta_R\sin\theta_R+\cos\eta_S\sin\theta_S)+\\
&\quad c[\cos\phi_1\cos\phi-\sin\phi_1\cos\varphi\sin\phi](\sin\eta_R+\sin\eta_S)\})].
\end{aligned} \tag{199}$$

This simplifies to

$$
\begin{aligned}
g &= \frac{k}{4\pi}\int_{\varphi_{lower}}^{\varphi_{upper}} d\varphi \int_0^{\pi} d\phi \sin^2\phi \times \\
&\{bc[\sin\varphi\cos\varphi_1 + \sin\varphi_1\cos\varphi\cos\phi_1](\cos\eta_R\cos\theta_R + \cos\eta_S\cos\theta_S) + \\
&ac[\cos\varphi\cos\varphi_1\cos\phi_1 - \sin\varphi_1\sin\varphi](\cos\eta_R\sin\theta_R + \cos\eta_S\sin\theta_S) + \\
&ab[-\cos\varphi\sin\phi_1](\sin\eta_R + \sin\eta_S)\} \times \\
&\exp[ik\{a[\cos\varphi_1\sin\varphi\sin\phi + \cos\phi_1\sin\varphi_1\cos\varphi\sin\phi + \sin\varphi_1\sin\phi_1\cos\phi](\cos\eta_R\cos\theta_R + \cos\eta_S\cos\theta_S) + \\
&b[\cos\varphi_1\cos\phi_1\cos\varphi\sin\phi - \sin\varphi_1\sin\varphi\sin\phi + \cos\varphi_1\sin\phi_1\cos\phi](\cos\eta_R\sin\theta_R + \cos\eta_S\sin\theta_S) + \\
&c[\cos\phi_1\cos\phi - \sin\phi_1\cos\varphi\sin\phi](\sin\eta_R + \sin\eta_S)\})]. \qquad (200)
\end{aligned}
$$

This further simplifies to

$$
\begin{aligned}
g &= \frac{k}{4\pi}\int_{-\varphi_\ell}^{\pi-\varphi_u} \{bc[\sin\varphi\cos\varphi_1 + \sin\varphi_1\cos\varphi\cos\phi_1](\cos\eta_R\cos\theta_R + \cos\eta_S\cos\theta_S) + \\
&ac[\cos\varphi\cos\varphi_1\cos\phi_1 - \sin\varphi_1\sin\varphi](\cos\eta_R\sin\theta_R + \cos\eta_S\sin\theta_S) + \\
&ab[-\cos\varphi\sin\phi_1](\sin\eta_R + \sin\eta_S)\} d\varphi \int_0^{\pi} d\phi \sin^2\phi \times \\
&\times \\
&\exp[ik\{a[\cos\varphi_1\sin\varphi\sin\phi + \cos\phi_1\sin\varphi_1\cos\varphi\sin\phi + \sin\varphi_1\sin\phi_1\cos\phi](\cos\eta_R\cos\theta_R + \cos\eta_S\cos\theta_S) + \\
&b[\cos\varphi_1\cos\phi_1\cos\varphi\sin\phi - \sin\varphi_1\sin\varphi\sin\phi + \cos\varphi_1\sin\phi_1\cos\phi](\cos\eta_R\sin\theta_R + \cos\eta_S\sin\theta_S) + \\
&c[\cos\phi_1\cos\phi - \sin\phi_1\cos\varphi\sin\phi](\sin\eta_R + \sin\eta_S)\})]. \qquad (201)
\end{aligned}
$$

Using various abbreviations this reduces to

$$
g = \frac{k}{4\pi}\int_{\varphi_{lower}}^{\varphi_{upper}} d\varphi\{A\cos\varphi + B\sin\varphi\} \int_0^{\pi} d\phi \sin^2\phi\, e^{ik\{C\cos\phi + (D\sin\varphi + E\cos\varphi)\sin\phi\}}, \qquad (202)
$$

where

$$
\begin{aligned}
A &= \{bc[\sin\varphi_1\cos\phi_1](\cos\eta_R\cos\theta_R + \cos\eta_S\cos\theta_S) + ac[\cos\varphi_1\cos\phi_1](\cos\eta_R\sin\theta_R + \cos\eta_S\sin\theta_S) + \\
&\quad ab[-\sin\phi_1](\sin\eta_R + \sin\eta_S)\}, \\
B &= \{bc[\cos\varphi_1](\cos\eta_R\cos\theta_R + \cos\eta_S\cos\theta_S) + ac[-\sin\varphi_1](\cos\eta_R\sin\theta_R + \cos\eta_S\sin\theta_S)\}, \\
C &= \{a[\sin\varphi_1\sin\phi_1](\cos\eta_R\cos\theta_R + \cos\eta_S\cos\theta_S) + b[\cos\varphi_1\sin\phi_1](\cos\eta_R\sin\theta_R + \cos\eta_S\sin\theta_S) + \\
&\quad c[\cos\phi_1](\sin\eta_R + \sin\eta_S)\}, \\
D &= \{a[\cos\varphi_1](\cos\eta_R\cos\theta_R + \cos\eta_S\cos\theta_S) + b[-\sin\varphi_1](\cos\eta_R\sin\theta_R + \cos\eta_S\sin\theta_S)\} \\
E &= \{a[\cos\phi_1\sin\varphi_1](\cos\eta_R\cos\theta_R + \cos\eta_S\cos\theta_S) + b[\cos\varphi_1\cos\phi_1](\cos\eta_R\sin\theta_R + \cos\eta_S\sin\theta_S) + \\
&\quad c[-\sin\phi_1](\sin\eta_R + \sin\eta_S)\} \\
D' &= \sqrt{C^2 + D^2 + E^2}, \\
\varepsilon &= \arctan[E, D], \\
\varepsilon' &= \arctan[A, B]. \qquad (203)
\end{aligned}
$$

This can be rewritten as

$$
\begin{aligned}
g &= \frac{k\sqrt{A^2+B^2}}{4\pi}\int_{\varphi_{lower}}^{\varphi_{upper}} d\varphi\cos(\varphi - \varepsilon') \int_0^{\pi} d\phi \sin^2\phi\, e^{ik\{C\cos\phi + \sqrt{D^2+E^2}\cos(\varphi-\varepsilon)\sin\phi\}} \\
&\approx \frac{k\cos(\varepsilon-\varepsilon')\sqrt{A^2+B^2}}{4\pi}\int_{\varphi_{lower}-\varepsilon}^{\varphi_{upper}-\varepsilon} d\varphi\cos\varphi \int_0^{\pi} d\phi \sin^2\phi\, e^{ik\{C\cos\phi + \sqrt{D^2+E^2}\cos\varphi\sin\phi\}}. \qquad (204)
\end{aligned}
$$

Using Felsen's second order saddle point results gives

$$g \approx \frac{k\cos^2\omega\cos(\varepsilon-\varepsilon')\sqrt{A^2+B^2}}{4\pi}\int_{\varphi_{lower}-\varepsilon}^{\varphi_{upper}-\varepsilon} d\varphi\cos\varphi\sqrt{\frac{2\pi}{ik\sqrt{C^2+(D^2+E^2)\cos^2\varphi}}}e^{ik\sqrt{C^2+(D^2+E^2)\cos^2\varphi}}\times \left\{1-\frac{(7/8)}{ik\sqrt{C^2+(D^2+E^2)\cos^2\varphi}}\right\}, \tag{205}$$

where $\omega = \arctan[\sqrt{D^2+E^2}\cos\varphi, C] \approx \arctan[\sqrt{D^2+E^2}, C]$. Since most of the value of the integral occurs near $\varphi \approx 0$, one can make the following further approximation

$$g \approx \frac{k\cos^2\omega\cos(\varepsilon-\varepsilon')\sqrt{A^2+B^2}}{4\pi}\sqrt{\frac{2\pi}{ik\sqrt{C^2+(D^2+E^2)}}}\int_{\varphi_{lower}-\varepsilon}^{\varphi_{upper}-\varepsilon} d\varphi\sqrt{\cos\varphi}\,e^{ik\sqrt{C^2+(D^2+E^2)}\cos\varphi}\times \left\{1-\frac{(7/8)}{ik\sqrt{C^2+(D^2+E^2)}}\right\}. \tag{206}$$

By evaluating this integral numerically one can verify that this is a good approximation, even in the out-of-plane case; this is shown in Fig. 36.

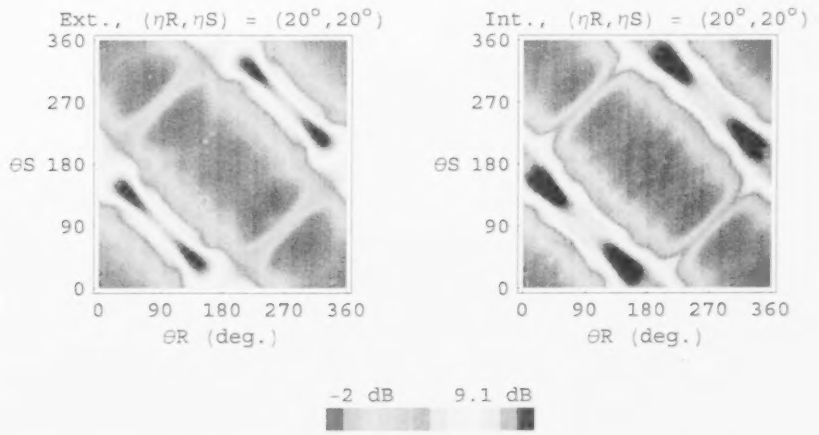

Figure 36: Comparison of the exact double integral form, Eq. (204), with the approximate integral form given by Eq. (206). The approximate form gives good results even for the forward scattering case, $\theta_R = \theta_S \pm \pi$, shown as the diagonal faint green lines above. The parameters are $f = 500$ Hz, $a = 4.2$ m, $b = c = 1.4$ m.

This is similar in form to the in-plane monostatic case; to second order, saddle point terms in the φ integral gives

$$g_{saddlepoint2} \approx \frac{k\cos^2\omega\cos(\varepsilon-\varepsilon')\sqrt{A^2+B^2}}{2\sqrt{C^2+(D^2+E^2)}}\times$$

$$\left\{ e^{ik\sqrt{C^2+(D^2+E^2)}\}} - \frac{\sin[\frac{1}{2}k\sqrt{C^2+(D^2+E^2)}]}{\frac{1}{2}k\sqrt{C^2+(D^2+E^2)}} e^{i\frac{1}{2}k\sqrt{C^2+(D^2+E^2)}} \right\}. \tag{207}$$

To lowest order

$$g_{saddlepoint1} \approx \frac{k\cos^2\omega\cos(\varepsilon-\varepsilon')\sqrt{A^2+B^2}}{2\sqrt{C^2+(D^2+E^2)}} e^{ik\sqrt{C^2+(D^2+E^2)}}. \tag{208}$$

Our rule for handling this integral is as follows: if there is no saddle point in the range of integration use $g \approx 0$, if there is a saddle point in the range of integration, for each end-point such that $|\varphi_{lower} - \varepsilon| > \arcsin[\sqrt{2/(\pi kD')}]$ or $|\varphi_{lower} - \varepsilon| > \arcsin[\sqrt{2/(\pi kD')}]$, count one-half the saddle point contribution, otherwise count zero. Then the scattering strength is approximated as

$$g \approx \begin{cases} g_{saddlepoint}, & \text{if } |\varphi_{lower}-\varepsilon| > \arcsin[\sqrt{2/(\pi kD')}] \text{ and } |\varphi_{lower}-\varepsilon| > \arcsin[\sqrt{2/(\pi kD')}], \\ \frac{1}{2}g_{saddlepoint}, & \text{if } |\varphi_{lower}-\varepsilon| > \arcsin[\sqrt{2/(\pi kD')}] \text{ and } |\varphi_{lower}-\varepsilon| < \arcsin[\sqrt{2/(\pi kD')}], \\ \frac{1}{2}g_{saddlepoint}, & \text{if } |\varphi_{lower}-\varepsilon| < \arcsin[\sqrt{2/(\pi kD')}] \text{ and } |\varphi_{lower}-\varepsilon| > \arcsin[\sqrt{2/(\pi kD')}], \\ \text{if } \varphi_{lower} \le \varepsilon \le \varphi_{upper}. \end{cases} \tag{209}$$

A comparison between the exact results (numerical integration of Eq. (202)) and the approximate results (Eqs. (207), (209)) for the ellipsoid is shown in Fig. 37. The parameters are $f = 500$ Hz, $a = 4.2$ m, $b = c = 1.4$ m. For the case of source and receiver 20 degrees above and 20 degrees below the x-y plane, the saddlepoint approximation gives good results throughout the $\theta_R - \theta_S$ plane. The difficult case is the source and receiver 20 degrees above the x-y plane, $\eta_R = \eta_S = 20^o$. The main feature of this out-of-plane case is the appearance of additional viewed/illuminated areas on the scattering surface; a 40^o wide strip on the top of the ellipsoid when the source and receiver are on opposite sides. This gives rise to the additional diagonal high scattering areas, corresponding to forward reflection from the top of the ellipsoid. The saddle point results are not as accurate as the scattering results from the side views. This is the general feature of out of plane scattering; there are additional high scattering areas in the $\theta_R - \theta_S$ plane corresponding to additional viewed/illuminated areas. For source/receiver slightly out of plane, the size of the extra viewed/illuminated areas is small; hence the saddle point approximation for these areas is not as accurate as for the in-plane side views, where approximately half the surface is viewed/illuminated. As the frequency increases, the saddle point description of these smaller viewed/illuminated areas will improve. On a mathematical level, this area of the $\theta_R - \theta_S$ plane corresponds to the forward scattering case $\theta_R = \theta_S \pm \pi$, where the argument of the exponential kD', takes on its smallest values. Hence one expects an asymptotic approximation to fare the worst.

14 The out-of-plane half ellipsoid

In the previous sections, the in-plane half-ellipsoid case was easily treated by a slight change in the definitions of the functions φ_{Ru} etc. This does not seem possible for the out-of-plane half-ellipsoid case. The coordinate curves of the general parametrization given in Eq. (177), chosen to coincide with the viewed/illuminated areas, do not coincide with the truncated areas. For this case one might as well return to the parametrization given by Eq. (141), and formulate the problem as a double integral, where the coordinate curves do not map out the integration area. One could then treat the problem using Felsen's formula for multiple integrals (see 4.7 (5) of [22]) and use the results of Jones and Kline [23] for higher order terms. This was not possible to achieve in the time span of this contract. The alternate is to proceed in the same manner as the hemisphere case and multitply the result for the full ellipsoid by a windowing function. For the half-ellipsoid facing the positive x-axis this means multiplying by the factor:

$$\text{If}[\cos\eta_s\cos\theta_s + \cos\eta_r\cos\theta_r > 0, 1, 0] = \begin{cases} 1, & \text{if } \cos\eta_s\cos\theta_s + \cos\eta_r\cos\theta_r \ge 0, \\ 0, & \text{if } \cos\eta_s\cos\theta_s + \cos\eta_r\cos\theta_r \le 0. \end{cases} \tag{210}$$

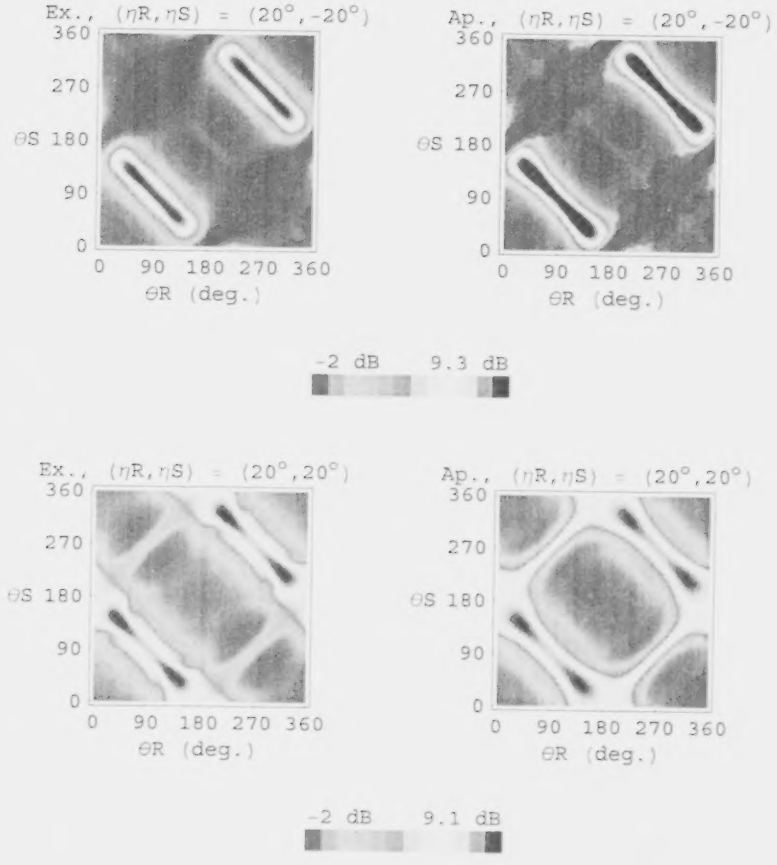

Figure 37: The out-of-plane bistatic case for the ellipsoid. This shows a comparison between an exact calculation (Eq. (202) and an approximate result using saddle point terms for the ellipsoid (Eqs. (207), (209)). The parameters are $f = 500$ Hz, $a = 4.2$ m, $b = c = 1.4$ m.
(a) In the top graphs the source and receiver are 20 degrees above and below the $x - y$ plane, the saddle point terms give a good approximation throughout the $\theta_R - \theta_S$ plane.
(b) In the bottom graphs, the source and receiver are 20 degrees above the x-y plane, $\eta_R = \eta_S = 20^o$. The main feature of this out-of-plane case is the appearance of additional viewed/illuminated areas on the scattering surface: in this case a 40^o wide strip on the top of the ellipsoid. This gives rise to the additional diagonal high scattering areas, corresponding to forward reflection from the top of the ellipsoid. Because of the smaller size of the viewed/illuminated strip on the top of the ellipsoid, the saddle point results are not as accurate as the scattering results from the side views.

This is equivalent to simply cutting (a diagonal square from the center of) the full ellipsoid results (in the $\theta_R - \theta_S$ plane). As one can see by looking at the half-vertical cylinder results there are some considerable edge effects obtained by a more accurate treatment of truncated surfaces, so this is a fairly crude treatment of truncation.

15 Scattering strength for the composite surface

For a surface composed of a collection of the simple surfaces analyzed in the preceding sections, the scattering strength is just the sum of the individual scattering strengths, provided the phase factors $e^{-i(\vec{k}_s+\vec{k}_r)\cdot\vec{x}_{surface}}$ have been included to account for the change in coordinate origin. To test this addition of out-of-plane scattering strengths, the surface is chosen to consist of a horizontal cylinder of radius R_1 and length L, joined to the bow hemispheres of radius R_1, along with the port and starboard sail plates, and the vertical elliptical sail front, the stern cone and stern hemisphere of radius R_2 as shown in Fig. 38 (b). A background of -2.0 dB is added to account for random contributions. The full set of physical parameters are taken from pages 52 and 53 of [1] and are given in the software. The hull length $L = 55.0$ m and radius $R_1 = 5.0$ m, the stern hemisphere radius $R_2 = 1.0$ m, the height of the sail plates $S_L = 5.7$ m, the x and y radii of the elliptical sail are $a = SB = 5.0$ m, $b = S_W \tan[\alpha]$ width of the sail plates $S_W/\cos(\alpha) = 7.0\,\mathrm{m}/\cos(\alpha)$, angle of the sail plates from the centerline $\alpha = 11$ degrees, the distance from the end of the cylinder to back of the sail plates $S_L = 22.9$ m and the length of the stern cone is $T_W = 20.0$ m. This gives the model of the target

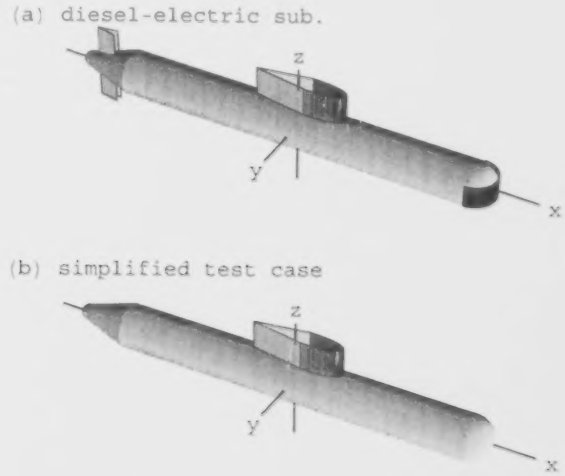

Figure 38: (a) The generic diesel-electric submarine hull consisting of the horizontal cylinder for the hull, hemispherical bow and stern caps, truncated stern cone, vertical bow half-cylinder, vertical elliptical half-cylinder sail front, port and starboard sail and fantail plates.
(b) Simplified generic submarine hull consisting of the horizontal cylinder for the hull, hemispherical bow and stern caps, stern cone, vertical elliptical half-cylinder sail front, and port and starboard sail plates.

strength for the composite surface as

$$\text{Target Strength}(\eta_r, \eta_s, \theta_r, \theta_s) = 10^{\frac{2.0}{10}} + |g_{ssail} + g_{psail} + g_{hcylinder} + g_{bowhemisphere} + g_{sternhemisphere} + g_{sail} + g_{cone}|^2, \quad (211)$$

where the formulae for the various terms are given respectively by Eqs. (17), (18), (38), (97), (98), (72), (73) and (139).

Some numerical examples are shown in the Figs. 39, 40 for the simplified generic submarine model. As the angles $\{\eta_r, \eta_s\}$ shift from the in-plane case $\{\eta_r, \eta_s\} = \{0, 0\}$ to 20 degrees out-of-plane, $\{\eta_r, \eta_s\} = \{20^o, 20^o\}$, the top graph smoothly makes the transition to the bottom graph. The main difference between the in-plane and out-of-plane cases is that the horizontal cylinder and stern cone now make a contribution in the regions $0 \leq \theta_s \leq \pi$, $\pi \leq \theta_r \leq 2\pi$ and $0 \leq \theta_r \leq \pi$, $\pi \leq \theta_s \leq 2\pi$, previously dominated by the hemispheres and sail front. In effect, one is now looking down on the horizontal cylinder and stern cone, so the cylinder and cone are no longer completely shadowed when the source and receiver lie on opposite sides. For $\{\eta_r, \eta_s, \theta_r, \theta_s\} = \{20^o, 20^o, 270^o, 90^o\}$, one now sees an approximately 40^o wide viewed/illuminated strip on the top of the sub. One should also note that these graphs do not have any contributions from forward scattering, which is not treated in this report.

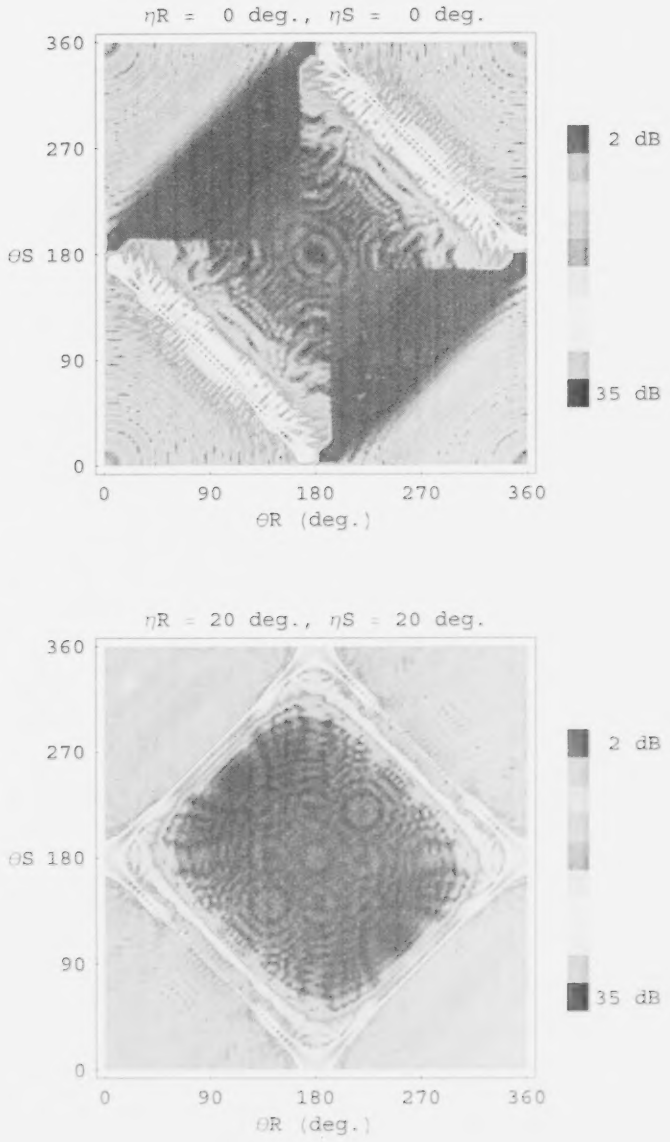

Figure 39: Target strength for the simplified case shown in Fig. 38 (b) with frequency $f = 500$ Hz. The graph gives the full Kirchhoff result Target Strength $= 10\log[10^{2.0/10}+|g(\eta_r,\eta_s,\theta_r,\theta_s)|^2]$, given by Eq. (211). The top graph is the in-plane case $\{\eta_r,\eta_s,\theta_r,\theta_s\} = \{0,0,\theta_r,\theta_s\}$; the bottom graph is the out-of-plane case $\{\eta_r,\eta_s,\theta_r,\theta_s\} = \{20^o,20^o,\theta_r,\theta_s\}$. The main difference between these cases is the appearance of additional high scattering regions (along $\theta_R \approx \theta_S \pm \pi$), corresponding to scattering from a thin viewed/illuminated strip on the top of the horizontal cylinder and the stern cone.

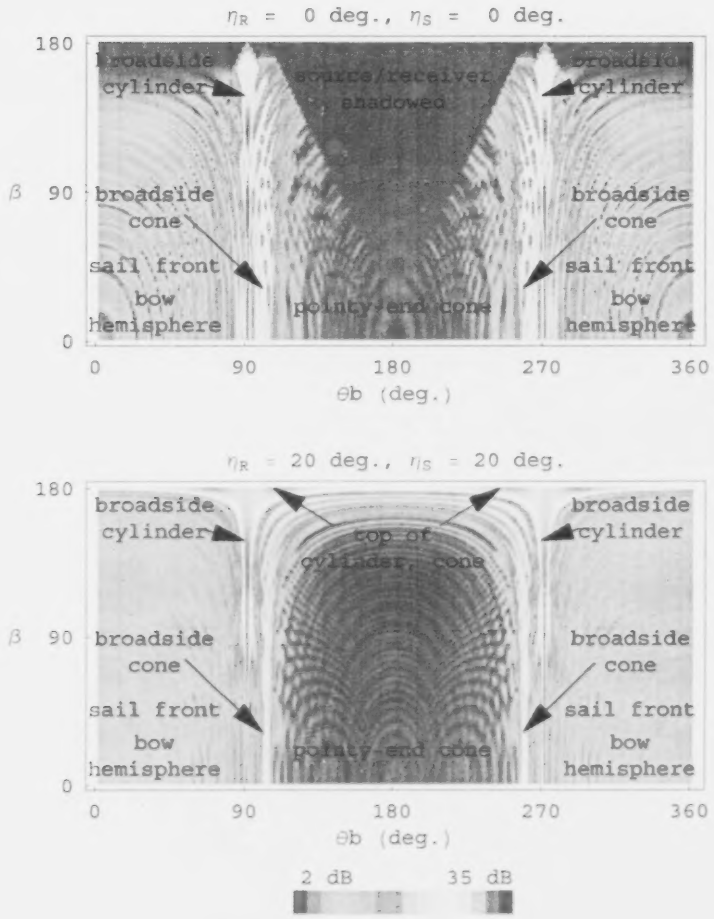

Figure 40: Same parameters as in the previous figure, but plotted with respect to the bistatic angle and aspect angle, along with some annotated comments giving the source of the main features of the composite model. Most notable are the broadside cylinder and (offset by α) cone contributions, along with an additional contribution from the top of the cylinder and cone in the out-of-plane case. For this particular out-of-plane case there is no shadow zone, since the source/receiver are are never shadowed.

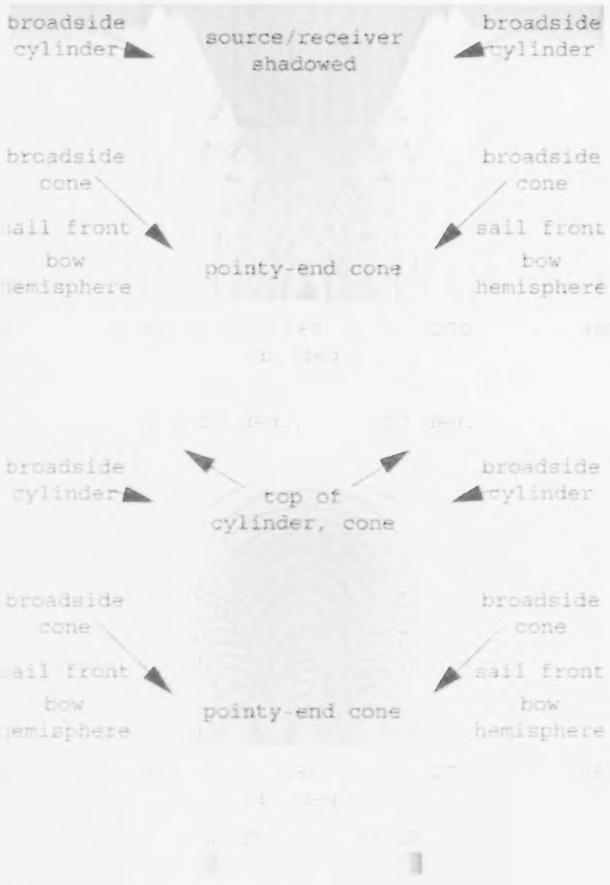
broadside
cylinder
source/receiver
shadowed
broadside
cylinder
broadside
cone
sail front
bow
hemisphere
pointy-end cone
broadside
cone
sail front
bow
hemisphere
broadside
cylinder
top of
cylinder, cone
broadside
cylinder
broadside
cone
sail front
bow
hemisphere
pointy-end cone
broadside
cone
sail front
bow
hemisphere

16 Summary

A key point to glean from the figures, is the success of the Bistatic Theorem predictions even in the out-of-plane scattering cases. The reason for this comes from the fact that as the source/receiver plane shifts from the symmetry plane of the scatterer, a certain portion of the integration region is omitted. However, the contribution of the omitted region is alternately positive or negative depending on the phase of the factor $e^{-i(\vec{k}_s+\vec{k}_r)\cdot\vec{r}}$ in the integrand of the Kirchhoff integral. Hence the full Kirchhoff result oscillates around the Bistatic Theorem result, until the bistatic angle is decreased to the point that $2kr_c\cos(\beta/2) \leq 1$. From that point onward the Bistatic Theorem result always overestimates the scattering strength. In the parameter cases applicable to the diesel-electric sub model, for values $2kr_c\cos(\beta/2) \geq 1$, the errors incurred by using the Bistatic Theorem results for out-of-plane scattering are typically less than 5.0 dB. For bistatic angles near the forward direction such that $2kr_c\cos(\beta/2) \leq 1$, the Bistatic Theorem result can overestimate the scattering strength by over 15.0 dB. An important effect of out-of-plane scattering will come in the regions $0 \leq \theta_s \leq \pi,\ \pi \leq \theta_r \leq 2\pi$ and $0 \leq \theta_r \leq \pi,\ \pi \leq \theta_s \leq 2\pi$, where the horizontal cylinder will now make a contribution in addition to the bow, stern and sail front structures.

A conclusion to draw from the all the foregoing, is that the out-of-plane case for all the cylinders (horizontal, vertical, or vertical elliptical) is completely solved in terms of the incomplete cylinder functions of Agrest and Maksimov[2]. It would have been a daunting task to reproduce their asymptotic results for the incomplete cylinder functions in the modest time span allotted for this contract. In addition the techniques used by Agrest and Maksimov in their asymptotic analysis of the incomplete Bessel type integrals (essentially an integration by parts) are adaptable to the other basic surfaces such as the sphere, although not in as elegant a fashion. One notes that Agrest and Maksimov have already applied their results to a circular section (a pie shaped flat surface) and to a right triangle ((see Eq. (5.18), (5.21) of [2]). It would therefore be a very useful project to polish the accompanying software (for this contract) for the incomplete functions $A_1(\beta, z)$, $B_1(\beta, z)$ to the same degree as for the Bessel/Weber/Struve functions, whose programs are commercially available. It does not seem possible to express the incomplete functions $A_1(\beta, z)$, $B_1(\beta, z)$ in terms of any other generalized functions (Meijer's's G functions etc.) so this would be very useful software in the calculation of scattering strengths.

Another interesting observation to make generally for simple shapes, is that the maximum target strength does not necessarily occur in the monostatic case $\theta_r = \theta_s$. The maximum target strength can occur well away from the monostatic source/receiver configuration. Even though the illuminated/viewed region in the Kirchhoff/Fraunhofer integral (Eq. (1)) may decrease as $|\theta_r - \theta_s|$ increases, the neglected portion of the surface integral may make a negative contribution, causing an increase in the target strength as one moves away from the monostatic view. For the shapes examined in this contract the potential increase in target strength is modest, a few dB at most.

From Fig. 38 it is visually apparent that shadowing of the hull by the sail and fantail plates will become a factor as the source/receiver moves out of the x-y plane. The problem of self-shadowing of a composite object of simple shapes is not treated in this report. One possible solution is to solve for the viewed/illuminated areas numerically, then apply this result to the saddle point expressions for each individual simple shape. If the saddle point for that simple shape is viewed/illuminated, then add in that saddle point expression. The key element would be finding an efficient numerical scheme to numerically solve the illumination problem, $\vec{k}_{S/R}\cdot\vec{n} = 0$, for the composite surface. However one would still make use of the saddle point expressions for each individual shape, supplemented with some numerical rule for adding them.

By plotting the scattering strength for the exact solutions for the infinite cylinder and the sphere, the following picture emerges for the forward scattering case. The Babinet's principle result for the scattering strength $g = -kA_P/(2\pi)$ in the case $\beta = \pi$ is remarkably accurate even for modestly large values of $kr_c \geq 1$. However, the width of the forward scattering lobes in the region around $\beta = \pi$, is a very slowly decreasing function of kr_c. Hence, even for very large values of kr_c one does not obtain the simple scattering picture of a single scattering spike $g = -kA_P/(2\pi)$ at $\beta = \pi$, with the angles $|\beta| < \pi$ described by the Kirchhoff approximation. Rather, the forward scattering is given by an oscillatory series of peaks around $\beta = \pi$, whose width decreases very slowly as a function of frequency. The heuristic model given in Eq. (22) of the NRL

report will give realistic peak values for the forward scattering at $\beta = \pi$, but would not be expected to give the correct detailed interference patterns near $\beta = \pi$. The width of the forward scattering model in Eq. (22) of the NRL report is given by the factor $W(\beta) = (1 - \cos(\beta/2))^2$. For a cylinder, one would expect this factor to be a slowly decreasing function of frequency. This suggests the heuristic model in Eq. (22) of the NRL report may overestimate the forward scatter for angles near $\beta = \pi$, as the frequency increases; this point is also made in [1]. It would seem that the analysis of the Watson transform for the infinite cylinder and the sphere (see Siegel[13] for details) could be used to find a more realistic model for forward scatter in the region away from $\beta = \pi$, which in turn could be used as a starting point for the out-of-plane case for forward scatter. Within the time span of this current contract there was insufficient time to pursue this idea in sufficient detail to extract a simple formula. however an initial investigation by the contractor suggests progress can be made along this line. The questions of modelling forward scatter in the out-of-plane case, will require additional time beyond the scope of this exploratory contract.

Another point to consider is the question of generalizing the boundary conditions for the simple objects from a rigid surface to more general conditions. Certainly, the Kirchhoff integral may be easily generalized to allow for an arbitrary plane wave reflection coefficient as is done in Chapters 7 and 9 of Bass and Fuks[6]. As observed by Bass and Fuks, for a sufficiently slowly varying reflection coefficient this would just introduce an additional multiplicative factor for the scattering strength. For incident plane waves, which are assumed in this analysis, more complicated situations such as surface waves would not occur: hence this sort of generalization could be attempted in a simple manner.

Finally, the truncated cone and the ellipsoid cases were treated using saddle point terms alone. Compared to the cylinder cases, the results for parameter values that correspond to small viewed/illuminated areas, are not as accurate. As a general observation, one may note that the accuracy of the saddle point approximation will decrease as the viewed/illuminated area decreases and as end-point contributions become increasingly important. The results in the appendices suggest that it may be possible to treat the truncated cone in terms of incomplete cylinder functions; this could be used to improve the accuracy of the cone scattering results.

ACKNOWLEDGEMENTS

The author would like to thank Mark Hazen and Layton Gilroy of DRDC Atlantic for their assistance. This work was funded by the DRDC Atlantic under contract number W7707-032345/001/HAL.

A The incomplete Jacobi-Anger and Weber functions

The incomplete Jacobi-Anger functions and incomplete Weber functions have studied carefully by M.M. Agrest and M.S. Maksimov[2] in *Theory of Incomplete Cylindrical Functions and their Applications*. From Eqs. (1.12) and (1.13) of Chapter III of Agrest and Maksimov the incomplete Bessel and Weber functions are given by

$$\begin{aligned} A_n(\beta, z) &\equiv \frac{1}{\pi}\int_0^\beta d\varphi \cos(n\varphi - z\sin\varphi), \\ B_n(\beta, z) &\equiv \frac{1}{\pi}\int_0^\beta d\varphi \sin(n\varphi - z\sin\varphi). \end{aligned} \tag{212}$$

Some useful special case of these formulae include

$$\begin{aligned} \frac{2}{\pi}\int_0^\beta d\varphi \cos\varphi\cos(z\sin\varphi) &\equiv A_1(\beta, z) + A_{-1}(\beta, z), \\ \frac{2}{\pi}\int_0^\beta d\varphi \sin\varphi\sin(z\sin\varphi) &\equiv A_1(\beta, z) - A_{-1}(\beta, z), \end{aligned}$$

$$\frac{2}{\pi}\int_0^\beta d\varphi \sin\varphi\cos(z\sin\varphi) \equiv B_1(\beta,z) - B_{-1}(\beta,z),$$
$$\frac{2}{\pi}\int_0^\beta d\varphi \cos\varphi\sin(z\sin\varphi) \equiv -B_1(\beta,z) - B_{-1}(\beta,z), \tag{213}$$

For $\beta = \pi$, $A_n(\pi,z) = J_n(z)$ and $B_n(\pi,z) = E_n(z)$. Many of the properties of the standard Bessel and Weber functions can be developed for their incomplete counterparts; see Chapter III in Agrest and Maksimov. The recursion relations become (Eqs. (2.2) and (2.3) of III in [2]))

$$\begin{aligned}
A_{n-1}(\beta,z) - A_{n+1}(\beta,z) - 2\frac{\partial}{\partial z}A_n(\beta,z) &= 0,\\
B_{n-1}(\beta,z) - B_{n+1}(\beta,z) - 2\frac{\partial}{\partial z}B_n(\beta,z) &= 0,\\
A_{n-1}(\beta,z) + A_{n+1}(\beta,z) - \frac{2n}{z}A_n(\beta,z) &= \frac{2\sin(z\sin\beta - n\beta)}{\pi z},\\
B_{n-1}(\beta,z) + B_{n+1}(\beta,z) - \frac{2n}{z}B_n(\beta,z) &= -\frac{2[1-\cos(z\sin\beta - n\beta)]}{\pi z}.
\end{aligned} \tag{214}$$

Important special cases include

$$\begin{aligned}
A_{-1}(\beta,z) + A_1(\beta,z) &= \frac{2\sin(z\sin\beta)}{\pi z},\\
B_{-1}(\beta,z) + B_1(\beta,z) &= -\frac{2[1-\cos(z\sin\beta)]}{\pi z}.
\end{aligned} \tag{215}$$

The asymptotic properties of these functions are given in Eqs. (7.10)–(7.13) of Chapter III in Agrest and Maksimov valid for $z\cos\beta >> 1$;

$$A_n(\beta,z) \approx \frac{1}{\pi z}\frac{\sin(z\sin\beta - n\beta)}{\cos\beta} + \begin{cases} J_n(z) & \pi/2 < \beta < 3\pi/2,\\ 0 & -\pi/2 < \beta < \pi/2,\\ -J_n(z) & -3\pi/2 < \beta < -\pi/2. \end{cases} \tag{216}$$

$$A_n(\pm\pi/2,z) \approx \pm\left[\frac{n}{\pi z}\cos(z - n\pi/2) + \frac{1}{2}J_n(z)\right], \tag{217}$$

$$B_n(\beta,z) \approx \frac{1}{\pi z}\left[\frac{\cos(z\sin\beta - n\beta)}{\cos\beta} - 1\right] + \begin{cases} 0 & |\beta| < \pi/2,\\ -Y_n(z) & \pi/2 < |\beta| < 3\pi/2. \end{cases} \tag{218}$$

$$B_n(\pm\pi/2,z) \approx -\frac{1}{\pi z}\left[1 \pm n\sin(z - n\pi/2) - \frac{1}{2}Y_n(z)\right]. \tag{219}$$

The Neumann function is denoted $Y_n(z)$ by Watson. It is important to observe that there are typographical errors in Eqs. (7.11) and (7.12) of Maksimov (corrected above). The higher order asymptotic expansions which are used in the accompanying software (to order $1/(z\cos\beta)^3$) are easily deduced from Eqs. (7.4) and (7.5) of Maksimov. In particular define the function $\varepsilon_\nu(w,z) = A_\nu(\beta,z) - iB_\nu(\beta,z)$ where $w = i\beta$. Now set

$$\begin{aligned}
\varepsilon_\nu(w,z) \approx\ & \frac{1}{\pi i z}\left(\frac{e^{z\sinh w - \nu w}}{\cosh w} - 1\right) + \frac{1}{\pi i z^2}\left[\frac{e^{z\sinh w - \nu w}}{\cosh^2 w}(\nu + \tanh w)) - \nu\right] +\\
& \frac{1}{\pi i z^3}\left[\frac{e^{z\sinh w - \nu w}}{\cosh^3 w}(\nu^2 - 1 + 3\nu\tanh w - 3\tanh^2 w)) - (\nu^2 - 1)\right].
\end{aligned} \tag{220}$$

Now substitute $w = i\beta$ above , assume that β, ν and z are real and set $\mathrm{Real}[\varepsilon_\nu(i\beta,z)] = A_\nu(\beta,z)$ and $\mathrm{Imaginary}[\varepsilon_\nu(i\beta,z)] = -B_\nu(\beta,z)$ to obtain the higher order versions of Eqs. (216) and (218), which are used in the software.

A very useful observation is that the following special cases can be computed exactly from elementary definitions in Watson:

$$A_1(\pi/2,z) \equiv \frac{\sin z}{\pi z} + J_1(z)/2, \tag{221}$$

$$A_1(-\pi/2,z) \equiv -\frac{\sin z}{\pi z} - J_1(z)/2, \tag{222}$$

$$A_{-1}(\pi/2,z) \equiv \frac{\sin z}{\pi z} - J_1(z)/2, \tag{223}$$

$$A_{-1}(-\pi/2,z) \equiv -\frac{\sin z}{\pi z} + J_1(z)/2, \tag{224}$$

$$B_1(\pi/2,z) \equiv -\frac{(1-\cos z)}{z\pi} + \frac{H_{-1}(z)}{2}, \tag{225}$$

$$B_1(-\pi/2,z) \equiv -\frac{(1-\cos z)}{z\pi} + \frac{H_{-1}(z)}{2}, \tag{226}$$

$$B_{-1}(\pi/2,z) \equiv -\frac{(1-\cos z)}{z\pi} - \frac{H_{-1}(z)}{2}, \tag{227}$$

$$B_{-1}(-\pi/2,z) \equiv -\frac{(1-\cos z)}{z\pi} - \frac{H_{-1}(z)}{2}. \tag{228}$$

This means that it is not necessary to use the asymptotic expressions given by Eqs. (217), (219); instead one may use Eqs. (221) -(228). This will give very accurate results at $\beta = \pm\pi/2$, in what will amount to the forward scattering limit for certain geometrical shapes.

One may further observe that the expansions in Eqs. (216), (218) fail for $z\cos\beta \leq 1$. Unfortunately, Maksimov does not give an expansion valid in the vicinity of $\beta = \pi/2, -\pi/2$ for $z\cos\beta \leq 1$. This would severely limit the asymptotic results from the important limit $|\beta| \to \pi/2$.

However, consider the following approximation for $A_1(\beta,x)$ where $\beta = \pi/2+\epsilon$, $\epsilon << 1$: from the integral definition Eq. (212) one obtains

$$\begin{aligned}
A_1(\beta,z) &= \frac{1}{\pi}\int_0^{\frac{\pi}{2}+\epsilon} d\theta \cos(\theta - z\sin\theta) \\
&= \frac{1}{\pi}\int_0^{\frac{\pi}{2}} d\theta \cos(\theta - z\sin\theta) + \frac{1}{\pi}\int_{\pi/2}^{\frac{\pi}{2}-\epsilon} d\theta \cos(\theta - z\sin\theta) \\
&= \frac{1}{\pi}\int_0^{\frac{\pi}{2}} d\theta \cos(\theta - z\sin\theta) - \frac{1}{\pi}\int_0^{\epsilon} d\theta \sin(\theta - z\cos\theta) \\
&= \frac{1}{\pi}\int_0^{\frac{\pi}{2}} d\theta \cos(\theta - z\sin\theta) - \frac{1}{\pi}\int_0^{\epsilon} d\theta \sin\theta\cos(z\cos\theta) + \frac{1}{\pi}\int_0^{\epsilon} d\theta \cos\theta\sin(z\cos\theta).
\end{aligned} \tag{229}$$

The first two integrals above can be performed exactly: in the third integral make the expansion $\sin(z\cos\theta) \approx \sin(z[1-\frac{1}{2}\sin^2(\theta)])$ to yield

$$A_1(\beta,z) = \frac{1}{\pi}\int_0^{\frac{\pi}{2}} d\theta \cos(\theta - z\sin\theta) - \frac{1}{\pi}\int_0^{\epsilon} d\theta \sin\theta\cos(z\cos\theta) + \frac{1}{\pi}\int_0^{\epsilon} d\theta \cos\theta\sin(z[1-\frac{1}{2}\sin^2(\theta)]). \tag{230}$$

Now all three integrals above can be performed exactly in terms of Bessel, Struve and Fresnel functions: from Mathematical library

$$A_1(\beta = \frac{\pi}{2}+\epsilon, z) = \frac{1}{2}J_1(x) + \frac{\sin(z\sin\beta)}{\pi z} - \frac{\cos z}{\sqrt{\pi z}}\text{FresnelS}\left[-\frac{\sqrt{z}\cos\beta}{\sqrt{\pi}}\right] + \frac{\sin z}{\sqrt{\pi z}}\text{FresnelC}\left[-\frac{\sqrt{z}\cos\beta}{\sqrt{\pi}}\right],$$

$$A_{-1}(\beta=\frac{\pi}{2}+\epsilon,z) = -\frac{1}{2}J_1(x)+\frac{\sin(z\sin\beta)}{\pi z}-\frac{\cos z}{\sqrt{\pi z}}\text{FresnelS}\left[-\frac{\sqrt{z}\cos\beta}{\sqrt{\pi}}\right]+\frac{\sin z}{\sqrt{\pi z}}\text{FresnelC}\left[-\frac{\sqrt{z}\cos\beta}{\sqrt{\pi}}\right], \tag{231}$$

$$A_1(\beta=-\frac{\pi}{2}+\epsilon,z) = -\frac{1}{2}J_1(x)+\frac{\sin(z\sin\beta)}{\pi z}-\frac{\cos z}{\sqrt{\pi z}}\text{FresnelS}\left[-\frac{\sqrt{z}\cos\beta}{\sqrt{\pi}}\right]+\frac{\sin z}{\sqrt{\pi z}}\text{FresnelC}\left[-\frac{\sqrt{z}\cos\beta}{\sqrt{\pi}}\right], \tag{232}$$

$$A_{-1}(\beta=-\frac{\pi}{2}+\epsilon,z) = \frac{1}{2}J_1(x)+\frac{\sin(z\sin\beta)}{\pi z}+\frac{\cos z}{\sqrt{\pi z}}\text{FresnelS}\left[-\frac{\sqrt{z}\cos\beta}{\sqrt{\pi}}\right]-\frac{\sin z}{\sqrt{\pi z}}\text{FresnelC}\left[-\frac{\sqrt{z}\cos\beta}{\sqrt{\pi}}\right], \tag{233}$$

$$B_1(\beta=\frac{\pi}{2}+\epsilon,z) = \frac{1}{2}H_{-1}(x)-\frac{(1-\cos(z\sin\beta)}{\pi z}-\frac{\cos z}{\sqrt{\pi z}}\text{FresnelC}\left[\frac{\sqrt{z}\cos\beta}{\sqrt{\pi}}\right]-\frac{\sin z}{\sqrt{\pi z}}\text{FresnelS}\left[\frac{\sqrt{z}\cos\beta}{\sqrt{\pi}}\right], \tag{234}$$

$$B_{-1}(\beta=\frac{\pi}{2}+\epsilon,z) = -\frac{1}{2}H_{-1}(x)-\frac{(1-\cos(z\sin\beta)}{\pi z}+\frac{\cos z}{\sqrt{\pi z}}\text{FresnelC}\left[\frac{\sqrt{z}\cos\beta}{\sqrt{\pi}}\right]+\frac{\sin z}{\sqrt{\pi z}}\text{FresnelS}\left[\frac{\sqrt{z}\cos\beta}{\sqrt{\pi}}\right], \tag{235}$$

$$B_1(\beta=-\frac{\pi}{2}+\epsilon,z) = \frac{1}{2}H_{-1}(x)-\frac{(1-\cos(z\sin\beta)}{\pi z}-\frac{\cos z}{\sqrt{\pi z}}\text{FresnelC}\left[\frac{\sqrt{z}\cos\beta}{\sqrt{\pi}}\right]-\frac{\sin z}{\sqrt{\pi z}}\text{FresnelS}\left[\frac{\sqrt{z}\cos\beta}{\sqrt{\pi}}\right], \tag{236}$$

$$B_{-1}(\beta=-\frac{\pi}{2}+\epsilon,z) = -\frac{1}{2}H_{-1}(x)-\frac{(1-\cos(z\sin\beta)}{\pi z}+\frac{\cos z}{\sqrt{\pi z}}\text{FresnelC}\left[\frac{\sqrt{z}\cos\beta}{\sqrt{\pi}}\right]+\frac{\sin z}{\sqrt{\pi z}}\text{FresnelS}\left[\frac{\sqrt{z}\cos\beta}{\sqrt{\pi}}\right], \tag{237}$$

$$\text{valid for}\sqrt{z}\sin\epsilon/\sqrt{\pi}<<1. \tag{238}$$

One can then join Eqs. (216), (218) and Eqs. (231)-(238) to form an asymptotic representation valid for all angles β, as is done in the accompanying software.

The following special case will prove useful:

$$B_n(\beta,z)+iA_n(\beta,z) \approx \frac{1}{\pi z}\left[\frac{e^{i(z\sin\beta-n\beta)}}{\cos\beta}-1\right], \quad -\frac{\pi}{2}+\arcsin(\frac{1}{z})\le\beta\le\frac{\pi}{2}-\arcsin(\frac{1}{z}). \tag{239}$$

In the numerical evaluation of the functions A, B the following results will prove useful:

$$\varepsilon_1(w,x) = \frac{1}{i\pi}\sum_{m=0}^{\infty}\frac{a_m x^m}{m!}, \tag{240}$$

where the coefficients

$$a_m \equiv \int_0^w d\varphi\sinh^m\varphi e^{-\varphi}, \tag{241}$$

satisfy the recurrence relation

$$a_m = -\frac{m}{m+1}a_{m-2}+\frac{1}{m^2-1}\left\{\sinh^m we^{-w}+m\sinh^{m-1}w\cosh we^{-w}\right\}. \tag{242}$$

In the special case $-\pi/2\le\beta\le\pi/2$, $z>>1$ and $z\cos\beta>>1$ then

$$B_1(\beta,z)+iA_1(\beta,z) \approx \frac{1}{\pi z}\left\{\frac{e^{(iz\sin\beta-\beta)}}{\cos\beta}-1\right\} \tag{243}$$

Obviously, access to the results of Agrest and Maksimov represents a huge labor saving in efforts to analyze the asymptotic properties of various incomplete Bessel type integrals which will occur in the bistatic analysis of various simple shapes.

B Some elementary properties of Bessel, Weber and Struve functions

From **2.2** (8) and **10.11** (3) of Watson From **2.2** (8) and **10.11** (3) of Watson

$$J_0(z) = \frac{2}{\pi}\int_0^{\pi/2} d\varphi \cos(z\cos\varphi), \tag{244}$$

$$J_1(z) = \frac{2}{\pi}\int_0^{\pi/2} d\varphi \cos\varphi \sin(z\cos\varphi), \tag{245}$$

$$J_2(z) = -\frac{2}{\pi}\int_0^{\pi/2} d\varphi \cos(2\varphi)\cos(z\cos\varphi), \tag{246}$$

$$E_0(z) = -\frac{2}{\pi}\int_0^{\pi/2} d\varphi \sin(z\cos\varphi). \tag{247}$$

$$E_1(z) = \frac{2}{\pi}\int_0^{\pi/2} d\varphi \cos\varphi \cos(z\cos\varphi). \tag{248}$$

$$E_2(z) = \frac{2}{\pi}\int_0^{\pi/2} d\varphi \cos(2\varphi)\sin(z\cos\varphi). \tag{249}$$

where $J_{-1}(x) = -J_1(x)$ and $E_{-1}(x) = -E_1(x)$. It will prove useful to introduce the compact notation

$$J_0(z) - iE_0(z) = \frac{2}{\pi}\int_0^{\pi/2} d\varphi e^{iz\cos\varphi}, \tag{250}$$

$$i(J_1(z) - iE_1(z) = \frac{2}{\pi}\int_0^{\pi/2} d\varphi \cos\varphi e^{iz\cos\varphi}, \tag{251}$$

$$J_0(z) = \frac{1}{\pi}\int_0^{\pi} d\varphi e^{iz\cos\varphi}, \tag{252}$$

$$iJ_1(z) = \frac{1}{\pi}\int_0^{\pi} d\varphi \cos\varphi e^{iz\cos\varphi}. \tag{253}$$

The Weber functions can be related to the Struve functions by the relations

$$E_0(x) = -H_0(x), \tag{254}$$

$$E_1(x) = \frac{2}{\pi} - H_1(x), \tag{255}$$

$$E_2(x) = \frac{2x}{3\pi} - H_2(x), \tag{256}$$

$$E_1(x) = H_{-1}(x), \tag{257}$$

$$E_n(x) = -H_n(x) + \sum_{m=0}^{\leq (n-1)/2} \frac{\Gamma[m+1/2](x/2)^{(n-2m-1)}}{\pi\Gamma[n+1/2-m]}, \quad n > 0 \tag{258}$$

$$E_n(x) = -H_n(x) + (-1)^{n+1}\sum_{m=0}^{\leq (-n-1)/2} \frac{\Gamma[-n-m-1/2](x/2)^{(n+2m+1)}}{\pi\Gamma[m+3/2]}, \quad n < 0. \tag{259}$$

The Struve functions are supported in Mathematica through the functions $StruveH[n,x]$ (note the special case $StruveH[-1,0] = 2/\pi$ is not rendered correctly in Mathematica 4.1). From **10.14** (2) and **7.21** (1), (2) of Watson

$$\begin{aligned} J_0(x) &\approx \sqrt{\frac{2}{\pi x}}\cos[x-\pi/4], \\ E_0(x) &\approx -Y_0(x) - \frac{2}{\pi x} \approx -\sqrt{\frac{2}{\pi x}}\sin[x-\pi/4] - \frac{2}{\pi x} \\ E_1(x) &\approx -Y_1(x) \approx -\sqrt{\frac{2}{\pi x}}\sin[x-3\pi/4], \qquad (260) \\ J_1(x) &\approx \sqrt{\frac{2}{\pi x}}\cos[x-3\pi/4]. \qquad (261) \end{aligned}$$

This is equivalent to

$$\begin{aligned} J_0(x) - iE_0(x) &\approx \sqrt{\frac{2}{\pi x}}e^{i(x-\pi/4)} + \frac{2i}{\pi x} + O(z^{-3/2}) \\ E_1(x) + iJ_1(x) &\approx \sqrt{\frac{2}{\pi x}}e^{i(x-\pi/4)} + O(z^{-3/2}), \qquad (262) \end{aligned}$$

C Some integrals of Bessel, Weber and Struve functions related to scattering from a cone

For in-plane scattering from the cone, certain integrals of the complete Bessel functions are required. Consider initially the the asymptotic approximations

$$\begin{aligned} J_0(x) - iE_0(x) &\approx \sqrt{\frac{2}{\pi x}}e^{i(x-\pi/4)} + \frac{2i}{\pi x} + O(z^{-3/2}) \\ E_1(x) + iJ_1(x) &\approx \sqrt{\frac{2}{\pi x}}e^{i(x-\pi/4)} + O(z^{-3/2}), \\ J_0(x) + iY_0(x) \approx i\{J_1(x) + iY_1(x)\} &\approx \sqrt{\frac{2}{\pi x}}e^{i(x-\pi/4)} + O(z^{-3/2}), \text{valid for } |x| >> 1, x > 0. \qquad (263) \end{aligned}$$

These results are also true for negative x, provided the principal branch of the square root is used. This suggest the following approximations

$$\begin{aligned} \int_0^z dt\, te^{iat}\{J_0(bt) - iE_0(bt)\} &\approx \sqrt{\frac{2}{\pi b}}e^{-i\pi/4}\int_0^z \sqrt{t}e^{i(a+b)t} + \frac{2i}{\pi b}\int_0^z dt\, e^{iat} \\ &\approx \sqrt{\frac{2}{\pi b}}e^{-i\pi/4}\left\{-i\sqrt{z}\frac{e^{i(a+b)z}}{(a+b)} - i\frac{(-1)^{\frac{1}{4}}\sqrt{\pi}\,\mathrm{Erf}[(-1)^{\frac{3}{4}}\sqrt{(a+b)}\sqrt{z}]}{2(a+b)^{\frac{3}{2}}}\right\} + \frac{2}{\pi b}\frac{[e^{iaz}-1]}{a} \\ &\equiv f(a,b,z) + \frac{2}{\pi b}\frac{[e^{iaz}-1]}{a}, \qquad (264) \end{aligned}$$

and

$$\begin{aligned} \int_0^z dt\, te^{iat}\{E_1(bt) + iJ_1(bt)\} &\approx \sqrt{\frac{2}{\pi b}}e^{-i\pi/4}\left\{-i\sqrt{z}\frac{e^{i(a+b)z}}{(a+b)} - i\frac{(-1)^{\frac{1}{4}}\sqrt{\pi}\,\mathrm{Erf}[(-1)^{\frac{3}{4}}\sqrt{(a+b)}\sqrt{z}]}{2(a+b)^{\frac{3}{2}}}\right\} \\ &\equiv f(a,b,z), \qquad (265) \end{aligned}$$

In the previous formulae principal values are used for all multiple-valued roots so $(-1)^{1/4} = (1+i)/\sqrt{2}$, $(-1)^{3/4} = -(1-i)/\sqrt{2}$. Furthermore, provided principal values are used, the previous results are true for a and b positive or negative.

In addition, for the out-of-plane case, integrals over the incomplete Bessel functions, $J_0(\beta,x)-iB_0(\beta,x)$, $B_1(\beta,x)+iJ_1(\beta,x)$ are needed as well, where the angular parameter $-\pi\le\beta\le\pi$. From the previous section, the fairly complicated asymptotic behavior, depending on both saddle point and boundary contributions, may be summarized as follows. For $x>>1$:

$$J_0(\beta,x)-iB_0(\beta,x) \approx \begin{cases} -\{J_0(x)-iY_0(x)\}-\frac{i}{\pi x}\left[\frac{e^{ix\sin\beta}}{\cos\beta}-1\right], & -\frac{3\pi}{2}+\arcsin[\frac{1}{x}]<\beta<-\frac{\pi}{2}-\arcsin[\frac{1}{x}]; \\ -\frac{1}{2}\{J_0(x)-iY_0(x)\}+\frac{i}{\pi x}+\frac{(\beta+\frac{\pi}{2})}{\pi}e^{-ix}, & -\frac{\pi}{2}-\arcsin[\frac{1}{x}]\le\beta\le-\frac{\pi}{2}+\arcsin[\frac{1}{x}]; \\ -\frac{i}{\pi x}\left[\frac{e^{ix\sin\beta}}{\cos\beta}-1\right], & -\frac{\pi}{2}+\arcsin[\frac{1}{x}]<\beta<\frac{\pi}{2}-\arcsin[\frac{1}{x}] \\ \frac{1}{2}\{J_0(x)+iY_0(x)\}+\frac{i}{\pi x}+\frac{(\beta-\frac{\pi}{2})}{\pi}e^{ix}, & \frac{\pi}{2}-\arcsin[\frac{1}{x}]\le\beta\le\frac{\pi}{2}+\arcsin[\frac{1}{x}]; \\ \{J_0(x)+iY_0(x)\}-\frac{i}{\pi x}\left[\frac{e^{ix\sin\beta}}{\cos\beta}-1\right], & \frac{\pi}{2}+\arcsin[\frac{1}{x}]<\beta<\frac{3\pi}{2}-\arcsin[\frac{1}{x}]. \end{cases} \tag{266}$$

Roughly speaking, if β is within $\arcsin[1/x]$ of a saddle point or includes a saddle point then use just the saddle point result, otherwise use just the boundary value contributions. Also keep in mind that for asymptotic representations, adding higher order terms can decrease accuracy for smaller values of the argument. Hence when both saddle point and boundary values are present, the best accuracy may be obtained by using the dominant saddle point terms alone.

$$J_0(\beta,x)-iB_0(\beta,x) \approx \begin{cases} -\sqrt{\frac{2}{\pi x}}e^{-i(x-\pi/4)}-\frac{i}{\pi x}\left[\frac{e^{ix\sin\beta}}{\cos\beta}-1\right], & -\frac{3\pi}{2}<\beta<-\frac{\pi}{2}; \\ -\frac{1}{2}\sqrt{\frac{2}{\pi x}}e^{-i(x-\pi/4)}+\frac{i}{\pi x}, & \beta=-\frac{\pi}{2}; \\ -\frac{i}{\pi x}\left[\frac{e^{ix\sin\beta}}{\cos\beta}-1\right], & -\frac{\pi}{2}+\arcsin[\frac{1}{x}]<\beta<\frac{\pi}{2}-\arcsin[\frac{1}{x}] \\ \frac{1}{2}\sqrt{\frac{2}{\pi x}}e^{i(x-\pi/4)}+\frac{i}{\pi x}, & \beta=\frac{\pi}{2}; \\ \sqrt{\frac{2}{\pi x}}e^{i(x-\pi/4)}-\frac{i}{\pi x}\left[\frac{e^{ix\sin\beta}}{\cos\beta}-1\right], & \frac{\pi}{2}<\beta<\frac{3\pi}{2}. \end{cases} \tag{267}$$

This gives the results

$$\int_{z_1}^{z_2} dt\, te^{iat}\{J_0(\beta,bt)-iE_0(\beta,bt)\}$$

$$\approx \begin{cases} \int_{z_1}^{z_2} dt\, te^{iat}\left\{-\sqrt{\frac{2}{\pi bt}}e^{-i(bt-\pi/4)}-\frac{i}{\pi bt}\left[\frac{e^{ibt\sin\beta}}{\cos\beta}-1\right]\right\}, & -\frac{3\pi}{2}<\beta<-\frac{\pi}{2}; \\ \int_{z_1}^{z_2} dt\, te^{iat}\left\{-\frac{1}{2}\sqrt{\frac{2}{\pi bt}}e^{-i(bt-\pi/4)}+\frac{i}{\pi bt}\right\}, & \beta=-\frac{\pi}{2}; \\ \int_{z_1}^{z_2} dt\, te^{iat}\left\{-\frac{i}{\pi bt}\left[\frac{e^{ibt\sin\beta}}{\cos\beta}-1\right]\right\}, & -\frac{\pi}{2}<\beta<\frac{\pi}{2} \\ \int_{z_1}^{z_2} dt\, te^{iat}\left\{\frac{1}{2}\sqrt{\frac{2}{\pi bt}}e^{i(bt-\pi/4)}+\frac{i}{\pi bt}\right\}, & \beta=\frac{\pi}{2}; \\ \int_{z_1}^{z_2} dt\, te^{iat}\left\{\sqrt{\frac{2}{\pi bt}}e^{i(bt-\pi/4)}-\frac{i}{\pi bt}\left[\frac{e^{ibt\sin\beta}}{\cos\beta}-1\right]\right\}, & \frac{\pi}{2}<\beta<\frac{3\pi}{2}; \end{cases}$$

$$\approx \begin{cases} -\sqrt{\frac{2}{\pi b}}e^{i\pi/4}\int_{z_1}^{z_2} dt\sqrt{t}e^{i(a-b)t}-\frac{i}{\pi b}\int_{z_1}^{z_2} dt\left[\frac{e^{i(a+b\sin\beta)t}}{\cos\beta}-e^{iat}\right], & -\frac{3\pi}{2}<\beta<-\frac{\pi}{2}; \\ -\frac{1}{2}\sqrt{\frac{2}{\pi b}}e^{i\pi/4}\int_{z_1}^{z_2} dt\sqrt{t}e^{i(a-b)t}+\frac{i}{\pi b}\int_{z_1}^{z_2} dt\, e^{iat}, & \beta=-\frac{\pi}{2}; \\ -\frac{i}{\pi b}\int_{z_1}^{z_2} dt\left[\frac{e^{i(a+b\sin\beta)t}}{\cos\beta}-e^{iat}\right], & -\frac{\pi}{2}<\beta<\frac{\pi}{2} \\ \frac{1}{2}\sqrt{\frac{2}{\pi b}}e^{-i\pi/4}\int_{z_1}^{z_2} dt\sqrt{t}e^{i(a+b)t}+\frac{i}{\pi b}\int_{z_1}^{z_2} dt\, e^{iat}, & \beta=\frac{\pi}{2}; \\ \sqrt{\frac{2}{\pi b}}e^{-i\pi/4}\int_{z_1}^{z_2} dt\sqrt{t}e^{i(a+b)t}-\frac{i}{\pi b}\int_{z_1}^{z_2} dt\left[\frac{e^{i(a+b\sin\beta)t}}{\cos\beta}-e^{iat}\right], & \frac{\pi}{2}<\beta<\frac{3\pi}{2}; \end{cases}$$

$$\approx \begin{cases} f(a,-b,z_2)-f(a,-b,z_1)-\frac{i}{\pi b}\left[\frac{e^{i(a+b\sin\beta)z_2}-e^{i(a+b\sin\beta)x_1}}{i(a+b\sin\beta)\cos\beta}-\frac{e^{iaz_2}-e^{iaz_1}}{ia}\right], & -\frac{3\pi}{2}<\beta<-\frac{\pi}{2}; \\ -\frac{1}{2}[f(a,-b,z_2)-f(a,-b,z_1)]+\frac{e^{iaz_2}-e^{iaz_1}}{ia}, & \beta=-\frac{\pi}{2}; \\ -\frac{i}{\pi b}\left[\frac{e^{i(a+b\sin\beta)z_2}-e^{i(a+b\sin\beta)z_1}}{i(a+b\sin\beta)\cos\beta}-\frac{e^{iaz_2}-e^{iaz_1}}{ia}\right], & -\frac{\pi}{2}<\beta<\frac{\pi}{2} \\ \frac{1}{2}[f(a,b,z_2)-f(a,b,z_1)]+\frac{e^{iaz_2}-e^{iaz_1}}{ia}, & \beta=\frac{\pi}{2}; \\ f(a,b,z_2)-f(a,b,z_1)-\frac{i}{\pi b}\left[\frac{e^{i(a+b\sin\beta)z_2}-e^{i(a+b\sin\beta)z_1}}{i(a+b\sin\beta)\cos\beta}-\frac{e^{iaz_2}-e^{iaz_1}}{ia}\right], & \frac{\pi}{2}<\beta<\frac{3\pi}{2}. \end{cases} \tag{268}$$

For the incomplete functions of order one:

$$B_1(\beta,x)+iJ_1(\beta,x) \approx \begin{cases} -\{Y_1(x)+iJ_1(x)\}+\frac{1}{\pi x}\left[\frac{e^{i(x\sin\beta-\beta)}}{\cos\beta}-1\right], & -\frac{3\pi}{2}<\beta<-\frac{\pi}{2}; \\ -\frac{1}{2}\{Y_1(x)+iJ_1(x)\}-\frac{1}{\pi x}\left[e^{ix}+1\right], & \beta=-\frac{\pi}{2}; \\ \frac{1}{\pi x}\left[\frac{e^{i(x\sin\beta-\beta)}}{\cos\beta}-1\right], & -\frac{\pi}{2}<\beta<\frac{\pi}{2} \\ -\frac{1}{2}\{Y_1(x)-iJ_1(x)\}+\frac{1}{\pi x}\left[e^{ix}-1\right], & \beta=\frac{\pi}{2}; \\ -\{Y_1(x)-iJ_1(x)\}+\frac{1}{\pi x}\left[\frac{e^{i(x\sin\beta-\beta)}}{\cos\beta}-1\right], & \frac{\pi}{2}<\beta<\frac{3\pi}{2}. \end{cases} \tag{269}$$

D Integrals of Bessel, Weber and Struve functions in terms of incomplete Bessel functions

It is possible to formulate in-plane scattering from the cone in terms of incomplete Bessel functions. Although these results will not be used in this report, they may be useful for future, more rigorous treatments of scattering from the cone.

D.1 Results

It will prove convenient to introduce the incomplete Bessel function of Poisson's type (see Eqs. (2.1), (2.16) of Chapter II of [AM])

$$E_\nu^+(w,z)=\frac{2z^\nu}{A_\nu}\int_0^w e^{iz\cos t}\sin^{2\nu}t\,dt, \quad \text{where } A_\nu=2^\nu\Gamma[\nu+1/2]\Gamma[1/2], \tag{270}$$

and w and z are arbitrary complex variables ($A_{0,1,2}=\pi,\pi,3\pi$). One has the special cases

$$\begin{aligned} E_0^+(\pi,z) &= 2J_0(z), \\ E_1^+(\pi,z) &= 2J_1(z), \\ E_0^+(\pi/2,z) &= J_0(z)-iE_0(z)=J_0(z)+iH_0(z), \\ E_1^+(\pi/2,z) &= J_1(z)-iE_1(z)+\frac{2i}{\pi}=J_1(z)+iH_1(z). \end{aligned} \tag{271}$$

$$\int_0^z dt\, e^{it\cos\beta}t\,J_0(t) = \sin^{-2}\beta\, e^{iz\cos\beta}z\,J_1(z)+\cos\beta\sin^{-3}\beta\frac{\pi z}{2}\left[E_0^+(\beta,z)J_1(z)-J_0(z)E_1^+(\beta,z)\right] \tag{272}$$

$$\int_0^z dt\, e^{it\cos\beta}t\,J_1(t) = i\cos\beta\sin^{-2}\beta\, e^{iz\cos\beta}z\,J_1(z)+\sin^{-3}\beta\frac{\pi z}{2i}\left[J_1(z)E_0^+(\beta,z)-E_1^+(\beta,z)J_0(z)\right]. \tag{273}$$

$$\int_{z_1}^{z_2} dt\, e^{it\cos\beta}\, t\, E_0(t) \;\approx$$
$$-\left\{\sin^{-2}\beta\, e^{iz_2\cos\beta}\, z_2\, Y_1(z_2) + \cos\beta\sin^{-3}\beta\frac{\pi z_2}{2}\left[E_0^+(\beta,z_2)Y_1(z_2) - Y_0(z_2)E_1^+(\beta,z_2)\right]\right\} +$$
$$\left\{\sin^{-2}\beta\, e^{iz_1\cos\beta}\, z_1\, Y_1(z_1) + \cos\beta\sin^{-3}\beta\frac{\pi z_1}{2}\left[E_0^+(\beta,z_1)Y_1(z_1) - Y_0(z_1)E_1^+(\beta,z_1)\right]\right\} +$$
$$\frac{2\cos^{-1}\beta}{i\pi}(e^{iz_2\cos\beta} - e^{iz_1\cos\beta}), \quad z_{1,2} >> 1. \tag{274}$$

$$\int_{z_1}^{z_2} dt\, e^{it\cos\beta}\, t\, E_1(t) \;\approx$$
$$-\left\{i\cos\beta\,\sin^{-2}\beta\, e^{iz_2\cos\beta}\, z_2\, Y_1(z_2) + \sin^{-3}\beta\,\frac{\pi z_2}{2i}\left[Y_1(z_2)E_0^+(\beta,z_2) - E_1^+(\beta,z_2)Y_0(z_2)\right]\right\} +$$
$$\left\{i\cos\beta\,\sin^{-2}\beta\, e^{iz_1\cos\beta}\, z_1\, Y_1(z_1) + \sin^{-3}\beta\,\frac{\pi z_1}{2i}\left[Y_1(z_1)E_0^+(\beta,z_1) - E_1^+(\beta,z_1)Y_0(z_1)\right]\right\} -$$
$$\frac{2}{\pi}\left\{\text{ExpIntegralEi}(iz_2\cos\beta) - \text{ExpIntegralEi}(iz_1\cos\beta)\right\}, \quad z_{1,2} >> 1. \tag{275}$$

The special cases $\cos\beta \to 0$ or $\sin\beta \to 0$ can be obtained as limiting cases: for convenience:

$$\int_0^z dt\; t\, J_0(t) \;=\; z\, J_1(z). \tag{276}$$

$$\int_0^z dt\, t\, J_1(t) \;=\; \frac{\pi z}{2}\left[J_1(z)H_0(z) - H_1(z)J_0(z)\right]. \tag{277}$$

$$\int_{z_1}^{z_2} dt\, t\, E_0(t) \;\approx\; -z_2 Y_1(z_2) + z_1 Y_1(z_1) + \frac{2}{\pi}(z_2 - z_1), \quad z_{1,2} >> 1. \tag{278}$$

$$\int_{z_1}^{z_2} dt\, t\, E_1(t) \;\approx\; -\left\{\frac{\pi z_2}{2}\left[Y_1(z_2)H_0(z_2) - H_1(z_2)Y_0(z_2)\right]\right\} + \left\{\frac{\pi z_1}{2}\left[Y_1(z_1)H_0(z_1) - H_1(z_1)Y_0(z_1)\right]\right\} -$$
$$\frac{2}{\pi}\log[z_2/z_1], \quad z_{1,2} >> 1, \tag{279}$$

where one keeps in mind 3.63 (12) of Watson: $J_0(z)Y_1(z) - J_1(z)Y_0(z) = -2/(\pi z)$.

$$\int_0^z dt\, e^{it}\, t\, J_0(t) \;=\; \frac{1}{3}ze^{iz}\left[z\, J_0(z) + J_1(z) - iz J_0(z)\right]. \tag{280}$$

$$\int_0^z dt\, e^{it}\, t\, J_1(t) \;=\; \frac{1}{3}ze^{iz}\left[izJ_0 - 2iJ_1(z) + zJ_1(z)\right] \tag{281}$$

$$\int_{z_1}^{z_2} dt\, e^{it}\, t\, E_0(t) = -\left\{\frac{1}{3} z_2 e^{iz_2}\left[z_2\, Y_0(z_2) + Y_1(z_2) - i z_2 Y_0(z_2)\right]\right\} + \left\{\frac{1}{3} z_2 e^{iz_2}\left[z_2\, Y_0(z_2) + Y_1(z_2) - i z_2 Y_0(z_2)\right]\right\} - \frac{2}{\pi}(e^{iz_2} - e^{iz_1}), \quad z_{1,2} >> 1. \tag{282}$$

$$\int_{z_1}^{z_2} dt\, e^{it}\, t\, E_1(t) = -\left\{\frac{1}{3} z_2 e^{iz_2}\left[i z_2 Y_0(z_2) - 2i Y_1(z_2) + z_2 Y_1(z_2)\right]\right\} + \left\{\frac{1}{3} z_1 e^{iz_1}\left[i z_1 Y_0(z_1) - 2i Y_1(z_1) + z_1 Y_1(z_1)\right]\right\} - \frac{2}{\pi}\left\{\text{ExpIntegralEi}(iz_2) - \text{ExpIntegralEi}(iz_1)\right\}, \quad z_{1,2} >> 1. \tag{283}$$

D.2 Proofs

By differentiation and use of Eqs. (4.2), (2.22), (2.23) of II of [AM] one obtains the definite integrals

$$\int_0^z dt\, \left[\sin^{2\nu+1}\beta\, e^{it\cos\beta}\, t^\nu\, E_\nu^+(w,t) - \sin^{2\nu+1} w\, e^{it\cos w}\, t^\nu\, E_\nu^+(\beta,t)\right] = \left[i\cos\beta\, \sin^{2\nu-1}\beta\, e^{iz\cos\beta}\, z^\nu\, E_\nu^+(w,z) - i\cos w\, \sin^{2\nu-1} w\, e^{iz\cos w}\, z^\nu\, E_\nu^+(\beta,z)\right] + (A_\nu/(2i)) z\left[E_\nu^+(w,z) E_{\nu-1}^+(\beta,z) - E_\nu^+(\beta,z) E_{\nu-1}^+(w,z)\right]. \tag{284}$$

An alternate form is given by

$$\int_0^z dt\, \left[\sin^{2\nu+1}\beta\, e^{it\cos\beta}\, t^\nu\, E_\nu^+(w,t) - \sin^{2\nu+1} w\, e^{it\cos w}\, t^\nu\, E_\nu^+(\beta,t)\right] = (A_\nu/A_{\nu+1})\left[\sin^{2\nu+1}\beta\, e^{iz\cos\beta}\, z^{\nu+1}\, E_\nu^+(w,z) - \sin^{2\nu+1} w\, e^{iz\cos w}\, z^{\nu+1}\, E_\nu^+(\beta,z)\right] + (A_\nu/(2i)) z\left[E_\nu^+(\beta,z) E_{\nu+1}^+(w,z) - E_\nu^+(w,z) E_{\nu+1}^+(\beta,z)\right]. \tag{285}$$

Special cases of these integrals are given on p.50 of [AM].

In Eq. (285), set $\nu = 0$ and $w = \pi$ to obtain

$$\int_0^z dt\, \sin\beta\, e^{it\cos\beta} J_0(t) = \sin\beta\, e^{iz\cos\beta}\, z\, J_0(z) + \frac{\pi z}{2i}\left[E_0^+(\beta,z) J_1(z) - J_0(z) E_1^+(\beta,z)\right]. \tag{286}$$

In Eq. (284), set $\nu = 1$ and $w = \pi$ to obtain

$$\int_0^z dt\, \sin^3\beta\, e^{it\cos\beta}\, t\, J_1(t) = i\cos\beta\, \sin\beta\, e^{iz\cos\beta}\, z\, J_1(z) + \frac{\pi z}{2i}\left[J_1(z) E_0^+(\beta,z) - E_1^+(\beta,z) J_0(z)\right]. \tag{287}$$

Differentiation wrt β of Eq. (286) gives

$$\int_0^z dt\, \sin\beta\, e^{it\cos\beta}\, t\, J_0(t) = \sin^{-1}\beta\, e^{iz\cos\beta}\, z\, J_1(z) + \cos\beta \sin^{-2}\beta \frac{\pi z}{2}\left[E_0^+(\beta,z) J_1(z) - J_0(z) E_1^+(\beta,z)\right]. \tag{288}$$

A single integration by parts shows that Eqs. (287) and (288) are equivalent.

Now in Eq. (285), set $\nu = 0$, $w = \pi/2$ and subtract Eq. (288) to obtain

$$\int_0^z dt\, \left[\sin\beta\, e^{it\cos\beta} E_0(t) - i E_0^+(\beta,t)\right] = \sin\beta\, e^{iz\cos\beta}\, z\, E_0(z) + \frac{\pi z}{2i}\left[E_0^+(\beta,z) E_1(z) - E_0(z) E_1^+(\beta,z)\right]. \tag{289}$$

In Eq. (284), set $\nu = 1$ and $w = \pi/2$ to obtain

$$\int_0^z dt\ \left[\sin^3\beta\, e^{it\cos\beta}\, t\, E_1(t) - it\, E_1^+(\beta,t)\right] \quad = \quad (2/\pi)\sin^3\beta\cos^{-2}\beta((e^{iz\cos\beta}-1) - \frac{2iz}{\pi}\cos^{-1}\beta\sin\beta\, e^{iz\cos\beta} + iz E_0^+(\beta,z) + i\cos\beta\sin\beta e^{iz\cos\beta}\, z\, E_1(z) + \frac{\pi z}{2i}\left[E_1(z)E_0^+(\beta,z) - E_1^+(\beta,z)E_0(z)\right]. \tag{290}$$

From (2.24) II of [AM]

$$E_1^+(\beta,t) = -\frac{d}{dt}E_0^+(\beta,t) + (2i/\pi)\sin\beta e^{it\cos\beta}. \tag{291}$$

By using the previous result one may show that differentiation of Eq. (289) wrt β also leads to Eq. (290). Hence this is all the information that one may extract with this approach. Therefore it does not seem possible to obtain the results corresponding to Eq. (286) with $E_0(t)$ substituting for $J_0(t)$ because of the presence of the extra $\int_0^z dt\ E_0^+(\beta,t)$ term in Eq. (289).

However, from Eq. (6.10) of Chapter II of [AM]

$$\int_0^z dt\ \sin\beta\, e^{it\cos\beta} Y_0(t) \quad = \quad \frac{2\beta}{i\pi} + \sin\beta\, e^{iz\cos\beta}\, z\, Y_0(z) + \frac{\pi z}{2i}\left[E_0^+(\beta,z)Y_1(z) - Y_0(z)E_1^+(\beta,z)\right], \tag{292}$$

$$\int_0^z dt\ \sin^3\beta\, e^{it\cos\beta}\, t\, Y_1(t) \quad = \quad \frac{2\beta}{i\pi} + \frac{2i}{\pi}\cos\beta\sin\beta + i\cos\beta\,\sin\beta\, e^{iz\cos\beta}\, z\, Y_1(z) + \frac{\pi z}{2i}\left[Y_1(z)E_0^+(\beta,z) - E_1^+(\beta,z)Y_0(z)\right], \tag{293}$$

$$\int_0^z dt\ \sin\beta\, e^{it\cos\beta}\, t\, Y_0(t) \quad = \quad \frac{2}{\pi}\sin^{-1}\beta + \frac{2\beta\cos\beta}{\pi\sin^2\beta} + + \sin^{-1}\beta\, e^{iz\cos\beta}\, z\, Y_1(z) + \cos\beta\sin^{-2}\beta\frac{\pi z}{2}\left[E_0^+(\beta,z)Y_1(z) - Y_0(z)E_1^+(\beta,z)\right]. \tag{294}$$

Now from 10.42 (2) of Watson, the Struve (or equivalently Weber) function is related to the Bessel Y function by

$$\begin{aligned} E_0(t) &= -Y_0(t) - \frac{2}{\pi t} + O(1/t^3), \\ E_1(t) &= -Y_1(t) - \frac{2}{\pi t^2} + O(1/t^4). \end{aligned} \tag{295}$$

This yields the following approximations:

$$\int_{z_1}^{z_2} dt\ \sin\beta\, e^{it\cos\beta} E_0(t) \quad \approx \quad -\left\{\sin\beta\, e^{iz_2\cos\beta}\, z_2\, Y_0(z_2) + \frac{\pi z_2}{2i}\left[E_0^+(\beta,z_2)Y_1(z_2) - Y_0(z_2)E_1^+(\beta,z_2)\right]\right\} + \left\{\sin\beta\, e^{iz_1\cos\beta}\, z_1\, Y_0(z_1) + \frac{\pi z_1}{2i}\left[E_0^+(\beta,z_1)Y_1(z_1) - Y_0(z_1)E_1^+(\beta,z_1)\right]\right\} - \frac{2\sin\beta}{\pi}\int_{z_1}^{z_2} dt\ \frac{e^{it\cos\beta}}{t}, \quad z_{1,2} >> 1. \tag{296}$$

$$\int_{z_1}^{z_2} dt\ \sin^3\beta\, e^{it\cos\beta}\, t\, E_1(t) \approx$$
$$-\left\{ i\cos\beta\,\sin\beta\, e^{iz_2\cos\beta}\, z_2\, Y_1(z_2) + \frac{\pi z_2}{2i}\left[Y_1(z_2)E_0^+(\beta,z_2) - E_1^+(\beta,z_2)Y_0(z_2)\right]\right\} +$$
$$\left\{ i\cos\beta\,\sin\beta\, e^{iz_1\cos\beta}\, z_1\, Y_1(z_1) + \frac{\pi z_1}{2i}\left[Y_1(z_1)E_0^+(\beta,z_1) - E_1^+(\beta,z_1)Y_0(z_1)\right]\right\} -$$
$$\frac{2\sin^3\beta}{\pi}\int_{z_1}^{z_2} dt\ \frac{e^{it\cos\beta}}{t}, \quad z_{1,2} >> 1. \tag{297}$$

$$\int_{z_1}^{z_2} dt\ \sin\beta\, e^{it\cos\beta}\, t\, E_0(t) \approx$$
$$-\left\{ \sin^{-1}\beta\, e^{iz_2\cos\beta}\, z_2\, Y_1(z_2) + \cos\beta\sin^{-2}\beta\frac{\pi z_2}{2}\left[E_0^+(\beta,z_2)Y_1(z_2) - Y_0(z_2)E_1^+(\beta,z_2)\right]\right\} +$$
$$\left\{ \sin^{-1}\beta\, e^{iz_1\cos\beta}\, z_1\, Y_1(z_1) + \cos\beta\sin^{-2}\beta\frac{\pi z_1}{2}\left[E_0^+(\beta,z_1)Y_1(z_1) - Y_0(z_1)E_1^+(\beta,z_1)\right]\right\} -$$
$$\frac{2\sin\beta}{\pi}\int_{z_1}^{z_2} dt\ e^{it\cos\beta}, \quad z_{1,2} >> 1. \tag{298}$$

References

[1] Drumheller, D.M., Hazen, M.G., and Gilroy, L.E., "The Bistatic Acoustic Simple Integrated Structure (BASIS) Target Strength Model", NRL/FR-MM/7140-02-10019, April 2002.

[2] M.M. Agrest and M.S. Maksimov, *Theory of Incomplete Cylindrical Functions and their Applications*,(Springer-Verlag, Berlin, Heidelberg, New York, 1971).

[3] S. Wolfram, *The Mathematica Book, 3rd ed.*, (Wolfram Media/Cambridge University Press, 1996).

[4] M. Born and E. Wolf., *Principles of Optics*, (Pergamon Press, Fourth Edition, 1970), Chapter 8.

[5] C.S. Clay and H. Medwin, *Acoustical Oceanography: Principles and Applications*, (John Wiley and Sons, New York, NY, 1977).

[6] F.G. Bass and I.M. Fuks, *Wave Scattering From Statistically rough Surfaces*, (Pergamon Press, Oxford, 1979).

[7] R.E. Kell, "On the derivation of bistatic RCS from Monostatic Measurements," Proceedings of the IEEE,**53**, August 1965, pp. 983-988.

[8] J.W. Crispin and A.L. Maffett, "Radar Cross-Section Estimation for Simple Shapes," Proceedings of the IEEE,**53**, August 1965, pp. 833–848.

[9] D.G. Falconer, "Extrapolation of Near-Field RCS Measurements to the Far Zone," IEEE Transactions on Antennas and Propagation, June 1988, pp. 822-829.

[10] K.M. Siegel, H.A. Alperin, R.R. Bonkowski, J.W. Crispin, A.L. Maffert, C.E. Schensted, and I.V. Schensted, "Bistatic Radar Cross Sections of Surfaces of Revolution," Journal of Applied Physics, Vol. **26**, No. 3, pp. 297–305 (1955).

[11] J.I. Glaser, "Some results in the Bistatic Radar Cross Section (RCS) of Complex Objects," Proceedings of the IEEE,**77**, No. 5, May 1989, pp. 639-648.

[12] S.J. Gabig, P.J. Collins, and G. Nesti, "Bistatic Scattering Characterization of Complex Objects," IEEE Transactions on Geoscience and Remote Sensing, Vol. **38**, No. 5, September 2000, pp. 2078–2092.

[13] J.W. Crispin and K.M. Siegel, *Methods of Radar Cross-Section Analysis*, (Academic Press, New york and London, 1968).

[14] J.J. Bowman, *Electromagnetic and Acoustic Scattering by simple Shapes*, (North Holland, Amsterdam, The Netherlands, 1969).

[15] G.T. Ruck, D.E. Barrick, W.D. Stuart, and C.K. Krichbaum, *Radar Cross Handbook*, (Plenum Press, New York, NY, 1970).

[16] R.J. Urick, *Principals of underwater sound*, (McGraw-Hill, 1983).

[17] E.F. Knott, J.F. Scheffer, and M.T. Tulley, *Radar Cross Section: Its Prediction, Measurement and Reduction*, (Artech House, Dedham, MA, 1985).

[18] D.K. Barton, *Modern Radar Analysis*, (Artech House, Dedham, MA, 1988).

[19] J.W. Nicholas, *Bistatic Radar*, (Artech House, Norwood, MA, 1991).

[20] N.J. Willis, *Bistatic Radar*, (Artech House, Norwood, MA, 1991).

[21] G.N. Watson, *A Treatise on the Theory of Bessel Functions, 2nd Ed.* (Cambridge University Press, New York, 1980).

[22] L.B. Felsen and N. Marcuvitz, *Radiation and Scattering of Waves* (Prentice Hall, NJ, 1973).

[23] D.S. Jones and M. Kline, Journal of Mathematics and Physics **37**, (1958), pp. 1-28.

Distribution List

DRDC Atlantic

5	M. Hazen, Scientific Authority (1 hard copy and 4 soft copies)
1	L. Gilroy, GL/Acoustic Signatures
1	J. Osler, GL/Ocean Sensing and Modelling
1	D. Ellis
1	J. Theriault
1	M. LeFrancois, GL/Underwater Warfare Data Fusion
1	G. Heard, GL/Rapidly Deployable Systems
1	D. Chapman
6	Library (3 hard copies and 3 soft copies)

DND

1	DRDKIM

Outside Canada Address(es)

1	Dr. David Drumheller, ONR Code 333, 800 North Quincy St, Arlington, VA 22217-5660, USA
1	Mr. Chris Gillard, MOD, DSTO Edinburgh, PO Box 1500, Edinburgh, SA, 5111, Australia

DOCUMENT CONTROL DATA SHEET		
1a. PERFORMING AGENCY Anthony Purcell Consultants, PO Box 1388, Lunenburg, NS, B0J 2C0		2. SECURITY CLASSIFICATION UNCLASSIFIED –
1b. PUBLISHING AGENCY DRDC Atlantic		
3. TITLE (U) 3D Acoustic Target Strength of Combinations of Geometric Shapes / Force cible acoustique 3D de combinaisons de formes génométrique		
4. AUTHORS Anthony Purcell		
5. DATE OF PUBLICATION January, 2005		6. NO. OF PAGES 102
7. DESCRIPTIVE NOTES		
8. SPONSORING/MONITORING/CONTRACTING/TASKING AGENCY Sponsoring Agency: Monitoring Agency: Contracting Agency : DRDC Atlantic Tasking Agency:		
9. ORIGINATORS DOCUMENT NO. Contract Report CR 2003-150	10. CONTRACT GRANT AND/OR PROJECT NO. 11bk	11. OTHER DOCUMENT NOS.
13. DOCUMENT ANNOUNCEMENT Unlimited announcement		

14. ABSTRACT

(U) This report is an investigation of the Kirchhoff approximation for the 3D acoustic target strength of simple geometric shapes and their combinations. In particular, it gives expressions for the out−of−plane bistatic scattering strengths of a variety of simple shapes, including the cylinder, the truncated cone and the ellipsoid. Previous investigations have given similar results for the in−plane bistatic case using the Bistatic Theorem to deduce bistatic formulae from monostatic results. The out−of−plane results given here do not depend upon the Bistatic Theorem, but require a detailed analysis of the viewed/illuminated area for each simple shape.

(U) Le présent rapport est une recherche sur l'approximation de Kirchhoff pour l'intensité des cibles acoustiques 3D constituées de formes géométriques simples et de leurs combinaisons. Plus précisément, il donne des expressions pour des forces de diffusion bistatiques et hors plan de diverses formes simples, y compris le cylindre, le cône tronqué et l'ellipsoïde. Des recherches antérieures ont donné des résultats similaires au moyen du théorème bistatique dans le cas de forces bistatiques dans le plan, afin de déduire des formules bistatiques à partir de résultats monostatiques. Les valeurs hors−plan résultantes données ici ne dépendent pas du théorème bistatique, mais nécessitent une analyse détaillée de la surface vue/illuminée pour chaque forme simple.

15. KEYWORDS, DESCRIPTORS or IDENTIFIERS

(U) Acoustic Target Strength
3D
Kirchhoff scattering
Modelling